

ANALYSIS AND CONTROL OF INDUCTION GENERATOR

A DISSERTATION

*Submitted in partial fulfillment of the
requirements for the award of the degree*

of

MASTER OF TECHNOLOGY

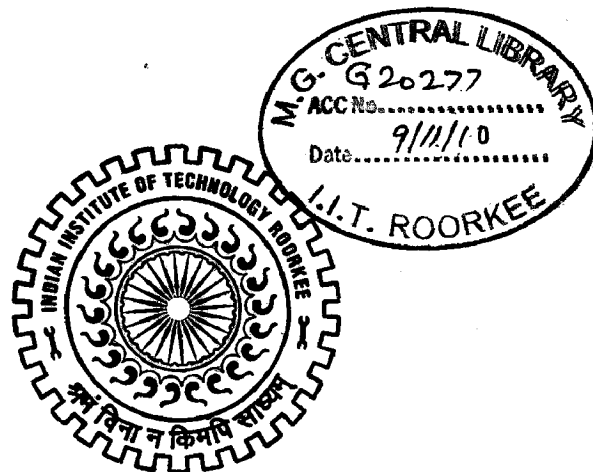
in

ELECTRICAL ENGINEERING

(With Specialization in Electric Drives & Power Electronics)

By

TIRAKALA UPENDRA



DEPARTMENT OF ELECTRICAL ENGINEERING
INDIAN INSTITUTE OF TECHNOLOGY ROORKEE
ROORKEE-247 667 (INDIA)

JUNE, 2010



INDIAN INSTITUTE OF TECHNOLOGY ROORKEE

Candidate's Declaration

I hereby declare that the work which is being presented in the dissertation thesis entitled "**Analysis and Control of Induction Generator**" in partial fulfillment of the requirements for the award of the degree of **Master of Technology in Electrical Engineering** with specialization in **Electric Drives and Power Electronics**, submitted in the **Department of Electrical Engineering, Indian Institute of Technology, Roorkee, India-247667**. This is an authentic record of my own work carried out in the period of last two semesters from July 2009 to June 2010, under the supervision of **Dr. S.P.Singh**, Professor, and **Dr.S.Ghatak Choudhuri**, Assitant Professor Department of Electrical Engineering, Indian Institute of Technology, Roorkee, India-247667.

The matter embodied in this dissertation thesis has not been submitted by me for the award of any other degree or diploma.

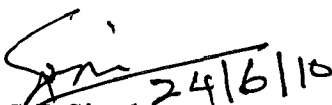
Date:

T. Upendra

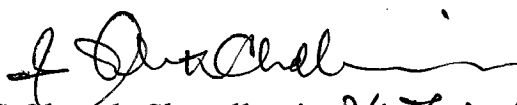
Place:

(TIRAKALA UPENDRA)

This is to certify that the above statement made by the candidate is correct to the best of my knowledge.


Dr.S.P.Singh. 24/6/10

Proffesor,
Department of Electrical Engineering.
Indian Institute of Technology.
Roorkee – 247 667.
INDIA.


Dr.S.Ghatak Choudhuri. 24.06.2010

Assisnt Professor,
DepartmentofElectrical Engineering.
Indian Institute of Technology.
Roorkee – 247 667.
INDIA.

ACKNOWLEDGEMENT

I wish to place on record my deep sense of gratitude and indebtedness to my guides Dr. S.P.Singh, Professor, and Dr.S.Ghathak Choudhuri, Assistant Professor, Department of Electrical Engineering, Indian Institute of Technology, Roorkee, for their wholeheartedness and high dedication with which they were involved in this work. I am grateful for the hours they spent in discussing and explaining even the minute details of the work in spite of their hectic schedule of work. They listened patiently and authoritatively as they guided me and gave their valuable suggestions.

I am grateful to all my teachers of Electric Drives and Power Electronics group for their suggestions and constant encouragements. I am also grateful to the research scholars and the technical assistants of the group for their valuable suggestions and constant encouragement.

I am grateful to my parents for their inspirational impetus and moral support during the course of this work. I owe many things to them.

Finally, I would like to express my deepest gratitude to the almighty and thank him from the bottom of my heart.

ABSTRACT

In this report the main concentration is made on the feasibility of the Induction Generators, so that the wind energy can harness in a very efficient manner. Induction generators are increasingly being used in nonconventional energy systems such as wind, micro/mini hydro, etc. The advantages of using an induction generator instead of a synchronous generator are well known. Some of them are reduced unit cost and size, ruggedness, brushless (in squirrel cage construction), absence of separate dc source, ease of maintenance, self-protection against severe overloads and short circuits, etc. In isolated systems, squirrel cage induction generators with capacitor excitation, known as self-excited induction generators (SEIGs), are very popular. For the process of self excitation, fixed capacitor banks or thyristor switched capacitors (TSC's) are commonly used in practice. A model of Fixed Capacitor-Thyristor Controlled Reactor (FC-TCR) is used for the purpose of self excitation and for variable reactive power and this FC-TCR is controlled by a closed loop fuzzy logic controller by controlling the delay firing angle(α) of the FC-TCR as the load (both R and RL loads ($\cos\phi=0.8$)) varies from no-load to rated load. To increase the controllable range of speed the WRIG (Wound Rotor Induction Generator) are flexible, which get excitation from the grid side, the rotor of WRIG is connected to the grid via the convertor setup. Due to the advances in power electronics it is advantaged to use the doubly fed induction generator (DFIG) system with variable speed connected to the electrical grid through an AC-AC converter, improving the efficiency of the power conversion. The converter topologies are modeled in the simulink environment and integrated the rotor power to the grid by controlling the converters (both grid side and rotor side converter in case of AC/DC/AC converter topology). The Pulse width Modulation (PWM) techniques and Space Vector Pulse Width Modulation (SVPWM) techniques are used for controlling the converters. The Back to Back AC/DC/AC (IGBT) converter setup is modeled and the same is controlled by using PWM and SVPWM techniques. The Matrix Converter is developed in SIMULINK environment and the same is controlled by using closed loop SVPWM technique. The main aim of developing these converter topologies and control circuits is to analyze the DFIG in both sub and super synchronous modes of operation and to ensure the power flow is bidirectional in case of these converter topologies.

CONTENTS

	Page.No
Candidate's Declaration	i
Acknowledgement	ii
Abstract	iii
Contents	iv
List of Figures	vii
Nomenclature	xiii
Abbreviations	xvi
Chapter – 1: Introduction and Literature Review	1
1.1 Introduction	1
1.2 Literature Review	3
1.3 Authors Contribution	6
Chapter – 2: Induction Generators	8
2.1 Classification of Induction Generators based on power generating schemes	8
A) Constant Speed-Constant frequency (CSCF) scheme	8
B) Variable Speed-Constant frequency (VSCF) scheme	9
C) Variable Speed-Variable frequency (VSVF) scheme	11
Chapter – 3: Analysis and design of SEIG model, FC-TCR and Fuzzy logic controller	12
3.1 TCR-Thyristor Controlled Reactor	13
3.2 Concept of FC-TCR	17
3.3 SIMULINK MODEL OF SEIG WITH FC-TCR and FLC	19
3.4 Results and explanation	22
3.5 Conclusion	24

Chapter – 4: Introduction to Wound Rotor Induction Generator	25
4.1 Doubly-fed induction generator	25
4.2 VSCF – DFIG	27
4.3 Description of the DFIG with AC/DC/AC converter system	29
4.4 Operating Principle of DFIG	30
4.5 Doubly-Fed induction generator Equations	32
Chapter – 5: Implementation of Converter Topologies for DFIG and SVM	34
5.1 Static Kramer Drive and SCR Converter Methods	34
5.2 Back-to-Back PWM Converters	35
5.3 MATRIX Converter	36
5.3.1 Description of Matrix Converter	37
5.3.2 Modulation Methods for MC	39
5.3.3 Topology	39
5.3.4. Performance of Matrix Converter	42
5.3.5 Implementation of the Matrix Converter	44
5.4 Space Vector Modulation	48
5.4.1 Distribution of Space Vectors	48
5.4.2 Voltage and Current Space Vectors	49
5.4.3 VSI Output Voltage SVM	50
5.4.4 VSR Input Current SVM	54
5.4.5 MC Output-Voltage and Input-Current SVM	56
5.5 SIMULATION MODELS AND RESULTS	59
5.5.1 The SIMULINK model for the DFIG using AC/DC/AC Back to back converter using SVM	59
5.5.2 Simulation RESULTS for Super synchronous mode DFIG using AC/DC/AC Back to back converter	61
5.5.3 Simulation RESULTS for Sub synchronous mode DFIG using AC/DC/AC Back to back converter	66

List of Figures

<u>Fig No</u>	<u>Caption</u>	<u>Page</u>
2.1	SEIG with Grid connected mode	8
2.2	Induction Generator with Ac-Dc-Ac link	9
2.3	DFIG with Ac-Dc-Ac Link	10
2.4	DFIG with MATRIX converter	11
2.5	SEIG in isolated mode	11
3.1	Basic TCR circuit	14
3.2	Waveforms of currents and voltages for different alpha in TCR	14
3.3	Amplitude variation of fundamental TCR current with delay angle	16
3.4	Simulation block of TCR	17
3.5	Basic FC-TCR	18
3.6	Simulation block of FC-TCR	19
3.7	Simulink Model of SEIG using FC-TCR	19
3.8	Simulink Model for FUZZY Controller	20
3.9	FUZZY Logic Controller relation with input parameter and outputs	20
3.10	Fuzzy membership function plots for the output (alpha for variable R-load)	21
3.11	Fuzzy membership function plots for the output (alpha for variable RL-load)	21
3.12	Line Voltages and Currents for both R load (0.6 to 1sec) and RL load (1 to 1.5 sec), using FCTCR with FUZZY controller	22
3.13	RMS voltage (V) variation with respect to simulation time (sec) using FCTCR with FUZZY controller	22
3.14	Wave forms of the SEIG for both R- loading (Time=0.6 to 1sec) and RL- loadings (Time=1 to 1.5 sec) using FC-TCR with FUZZY Controller	23

3.15	Comparison of RMS voltages variation between fixed capacitor and FC- TCR.	24
4.1	Doubly fed induction machine	26
4.2	Shows the schematic diagram of a DFIG-based wind turbine. The stator of the DFIG is directly connected to the grid, while the rotor is connected to a controllable AC/DC/AC converter setup	27
4.3	Doubly fed induction generator with ac/dc/ac converter topology	29
4.4	Power flow diagram of DFIG	30
4.5	Power flow diagrams (a) sub synchronous speed (b) super synchronous speed	32
5.1	DFIG with static Kramer drive	34
5.2	DFIG with back to back converter	35
5.3	DFIG with MATRIX converter	36
5.4	DFIG with Matrix converter circuit	36
5.5	Schematic circuit of a three-phase to three-phase matrix converter	37
5.6 (a)	Basic power circuit of matrix converter	40
5.6 (b)	General form of switching pattern	40
5.7 (a)	Output voltage waveforms generated by a VSI and a matrix converter	43
5.7 (b)	Matrix converter input current and harmonic spectrum Switching frequency 2kHz	44
5.8	Matrix converter input line-to-neutral voltage, instantaneous input Current and its average value, Switching frequency 2 kHz.	44
5.9	Illegal switching of Matrix Converter	46
5.10	Emulation of VSR-VSI conversion	48
5.11	VSI hexagon	49

5.12	VSI SVM vector addition	50
5.13	(a) Output line voltage 60°-segments (b) Synthesis of VSI output line voltages	54
5.14	VSR hexagon	56
5.15	The SIMULINK model for the DFIG using AC/DC/AC Back to back converters for the rotor circuit for the integration to the grid, which operates in both the sub and super synchronous modes	60
5.16	3 ph stator ph-n voltages and currents for the super synchronous mode of operation for DFIG using AC/DC/AC converter topology	61
5.17	The expanded wave form of fig 5.16	61
5.18	The single phase stator and rotor line voltages after integrating rotor with the grid	62
5.19	The comparison of the line voltages of GSC and output of coupling T/F	63
5.20	The expanded wave form of stator voltage (Ph-n) and ph-current	63
5.21	The expanded wave form of rotor line voltage and current the grid end.	64
5.22	The simulated wave forms of Speed, Tm and Te with respect to time for super synchronous mode of operation	65
5.23	The 3 ph Stator voltages (Ph-n) and current wave forms for the sub synchronous mode of operation	66
5.24	The 3 Ph rotor line voltages at the grid side end of the converter	67
5.25	The 3 Ph rotor ph currents at the grid side end of the converter	67
5.26	The expanded wave forms of rotor line voltage (magnitude decreased for visibility) and current at the grid side converter	68

5.27	Expanded wave forms of single phase stator voltage (L-n) and line current, magnitude adjusted for visibility.	68
5.28	single ph L-L rotor voltage wave forms at the grid side end of the converter for the sub synchronous mode of operation of DFIG using AC/DC/AC converter topology for rotor circuit	69
5.29	The simulated wave forms of the speed, T_m and T_e with respect to time for sub synchronous mode of operation.	70
5.30	The 3 Ph stator voltages (ph-n) and ph currents for both sub and super synchronous mode of operation of DFIG using AC/DC/AC converter topology for the rotor circuit.	71
5.31	3 ph rotor line voltages at the grid side converter end for DFIG operating both in sub and super synchronous modes	72
5.32	Single ph L-L rotor voltage wave forms at the grid side end of the converter for both the sub and super synchronous modes of operation of DFIG using AC/DC/AC converter topology for rotor circuit.	73
5.33	The wave forms of real and reactive power of the DFIG for both sub and super synchronous modes of operation.	74
5.34	The simulated wave forms of the speed, T_m and T_e with respect to time for both sub and super synchronous modes of operation of DFIG	75
5.35	The SIMULINK model for the DFIG using MATRIX converter in the rotor circuit for the integration to the grid, which operates in both the sub and super synchronous modes	77
5.36	3 ph stator L-n voltages and ph currents for the super synchronous mode of operation for DFIG using MATRIX converter topology	78
5.37	3 ph rotor L-n voltages for the super synchronous mode of operation for DFIG using MATRIX converter topology	79

5.38	single ph L-L rotor voltage wave forms at the grid side end of the converter for the super synchronous mode of operation of DFIG using MATRIX converter topology for rotor circuit	79
5.39	The single ph rotor voltage (Ph-n) and line current wave forms for the super synchronous mode of operation of DFIG using MATRIX converter topology	80
5.40	3 ph stator ph-n voltages and ph currents for the sub synchronous mode of operation for DFIG using MATRIX converter topology.	81
5.41	The 3 Ph rotor line voltages at the grid side end of the converter	82
5.42	Single ph L-L rotor voltage wave forms at the grid side end of the 83converter for the sub synchronous mode of operation of DFIG using MATRIX converter topology for rotor circuit.	82
5.43	The wave forms of rotor line voltage and line current at the grid side of the MATRIX converter.	83
5.44	The simulated wave forms of the speed, T_m and T_e with respect to time for sub synchronous mode of operation	84
5.45	The 3 Ph stator voltages (ph-n) and ph currents for both sub and super synchronous mode of operation of DFIG using MATRIX converter topology for the rotor circuit	85
5.46	3 ph rotor line voltages at the grid side converter end for DFIG operating both in sub and super synchronous modes.	86
5.47	Single ph L-L rotor voltage wave forms at the grid side end of the converter for both the sub and super synchronous modes of operation of DFIG using MATRIX converter topology for rotor circuit.	86
5.48	The comparison of the rotor line voltages before and after T/F for both sub and super synchronous modes of operation	87

- 5.49 The expanded wave form of stator voltage (Ph-n) and ph- 88
current for both the sub and super synchronous modes of
operation
- 5.50 The wave forms of real and reactive power of the DFIG (using 88
MATRIX converter topology) for both sub and super
synchronous modes of operation.
- 5.51 The simulated wave forms of the speed, T_m and T_e with 89
respect to time for both sub and super synchronous modes of
operation of DFIG.

NOMENCLATURE

The symbols used in the text have been defined at appropriate places, however, for easy reference the important nomenclatures are given below:

X_C	Capacitive Reactance
Q_c	Reactive power
X_T	Net Reactance
X_L	Inductive Reactance
α	Delay Firing Angle
R	Resistance
L	Inductance
ω	Angular speed of the arbitrary reference frame
φ	Phase angle between Voltage and Current
i_{LF}	Fundamental Reactor current
P_m	Mechanical power
T_m	Mechanical Torque
ω_r	Angular speed of the Rotor
ω_s	Synchronous Speed
P_s	Stator electric Power
T_{em}	Electro Magnetic Torque
P_r	Rotor Power
s	Slip
C_{rotor}	Rotor side Converter
C_{grid}	Grid side Converter
P_{cu}	Copper loss

V_{ds}	Direct axis stator voltage
V_{qs}	Quadrature axis stator voltage
i_{ds}	Direct axis stator Current
i_{qs}	Quadrature axis stator Current
λ_{qs}	Quadrature axis stator flux linkage
λ_{ds}	Direct axis stator flux linkage
V_{dr}	Direct axis
V_{qr}	Quadrature axis
i_{dr}	Direct axis
i_{qr}	Quadrature axis
λ_{dr}	Direct axis rotor flux linkage
λ_{qr}	Quadrature axis rotor flux linkage
L_{ls}	Stator leakage Inductance
L_s	Stator Self Inductance
L_r	Rotor Self Inductance
L_{lr}	Rotor leakage inductance
L_m	Mutual Inductance
p	Time derivative operator
i_{mr}^*	Excitation current
i_m	Magnetizing current
ω_b	Base speed
T^*	Reference torque
τ_r	Rotor time constant
V_o	Output line voltage
V_{in}	Input line voltage

v_{oL} Output line-voltage space vector
 m_v Modulation index
 V_{dc} DC link Voltage

Abbreviations

AC	Alternating Current
CSCF	Constant-Speed Constant-Frequency
CSI	Current Source Inverter
DC	Direct Current
DFIG	Doubly Fed Induction Generator
DOIG	Doubly output Induction Generator
FLC	Fuzzy Logic Controller
FC-TCR	Fixed Capacitor-Thyristor Controlled Reactor
GSC	Grid side converter
IGBT	Insulated Gate Bipolar Transistor
MC	Matrix converter
PWM	Pulse Width Modulation
PI	Proportional Integral
RSC	Rotor Side Converter
SVM	Space Vector Modulation
SVPWM	Space Vector Pulse Width Modulation
SEIG	Self-Excited Induction Generator
SVC	Static VAR Compensator
SCR	Silicon - Controlled Rectifier
TCR	Thyristor Controlled Reactor
TSC	Thyristor switched capacitor
VAR	Volt Ampere Reactive
VSCF	Variable-Speed Constant-Frequency
VSVF	Variable-Speed Variable-Frequency
VSC	Voltage Source converter
VSI	Voltage Source Inverter
VSR	Voltage source rectifier
WRIM	Wound Rotor Induction Machine
WRIG	Wound Rotor Induction Generator

1.1 INTRODUCTION

Most of the present demand in the world is met by fossil and nuclear power plants. A small part is met by renewable energy technologies, such as the wind, solar, biomass, geothermal and the ocean. Among the renewable power sources, wind and solar have experienced a remarkably rapid growth in the past 10 years [45]. Both are pollution free sources of abundant power. Additionally, they generate power near the load centers; hence eliminate the need of running high voltage transmission lines through rural and urban landscapes. The increasing rate of the depletion of conventional energy sources has given rise to an increased emphasis on renewable energy sources such as wind, mini/micro-hydro, etc. Generation of electrical energy mainly so far has been from thermal, nuclear, and hydro plants. They have continuously degraded the environmental conditions. An increasing rate of the depletion of conventional energy sources and the degradation of environmental conditions has given rise to an increased emphasis on renewable energy sources, particularly after the increases in fuel prices during the 1970s. An induction machine connected to an ac source of appropriate voltage and frequency can operate either as a motor or as a generator. Regeneration is possible, if the rotor of the induction machine is made to rotate above synchronous speed decided by the supply frequency and the pole number of the machine. The terminal voltage applied to the machine maintains the excitation by supplying lagging magnetizing current, which in turn results in rotating magnetic field for both the motoring, and generating mode of operation. Use of an induction machine as a generator is becoming more and more popular for the renewable sources. Reactive power consumption and poor voltage regulation under varying speed are the major drawbacks of the induction generators, but the development of static power converters has facilitated the control of the output voltage of induction generators. The advantages of using an induction generator instead of a synchronous generator are well known. Some of them are reduced unit cost and size, ruggedness, brushless (in squirrel cage construction),

absence of separate dc source, ease of maintenance, self-protection against severe overloads and short circuits, etc. In isolated systems, squirrel cage induction generators with capacitor excitation, known as self-excited induction generators (SEIGs), are very popular. Further coming to SEIG's, the concept of variable reactive power is always questioning point. So an attempt is made to develop a variable VAR generator FC-TCR in the MATLAB/SIMULINK environment to supply a continuous VAR for different loading condition. It is obvious that grid-integrated Wind Energy Conversion System (WECS) should generate at constant electrical frequency, determined by the grid. Conventionally grid-connected cage rotor induction machines are used as wind generators at medium power level. When connected to the constant frequency network, the induction generator runs at near synchronous speed drawing the magnetizing current from the mains, thereby resulting in constant speed constant frequency (CSCF) operation. However the power capture due to fluctuating wind speed can be substantially improved if there is flexibility in varying the shaft speed, to maximize power capture with fluctuating wind velocities. Therefore, WECS is a classic example of a variable speed constant frequency (VSCF) system.

The concept of the Doubly Fed Induction Generator (DFIG) is an interesting option with a growing market. The DFIG consists of a WRIG with the stator windings directly connected to the constant-frequency three-phase grid and with the rotor windings mounted to a bidirectional back-to-back IGBT voltage source converter. The term 'doubly fed' refers to the fact that the voltage on the stator is applied from the grid and the voltage on the rotor is induced by the power converter. This system allows a variable-speed operation over a large, but restricted, range. The converter compensates the difference between the mechanical and electrical frequency by injecting a rotor current with a variable frequency. Both during normal operation and faults the behavior of the generator is thus governed by the power converter and its controllers. The power converter consists of two converters, the rotor-side converter and grid-side converter, which are controlled independently of each other. Design of converter topologies for the rotor circuit is the present prevailing major task for an Electrical engineer. Depending on the operating condition of the drive, power is fed into or out of the rotor: in an over synchronous situation, it flows from the rotor via the converter to the grid, whereas it flows in the opposite direction in a

sub synchronous situation. In both cases – sub synchronous and over synchronous – the stator feeds energy into the grid. The converter topologies are modeled in the simulink environment and integrated the rotor power to the grid by controlling the converters (both grid side and rotor side converter in case of AC/DC/AC converter topology). The Pulse width Modulation (PWM) techniques and Space Vector Pulse Width Modulation (SVPWM) techniques are used for controlling the converter.

1.2 Literature review

The concept of self-excitation of induction machine emerged for the first time in 1935, when Basset and Potter [6] reported that the induction machine can be operated as an induction generator in isolated mode by using external capacitor. However, in most of the cases it suffered from the frequency drop and poor voltage regulation. Series capacitors were used to improve the voltage regulation.

Wagner [7] in 1939 gave an approximate method of analysis of self-excited induction generator by separating the real and reactive parts of the circuit. The terminal voltage was determined by equating reactive VAR to zero, and slip by equating real power to zero.

The three-phase induction machine with a squirrel cage rotor or a wound rotor could work as a three-phase induction generator either connected to the utility ac power distribution line or operated in the self-excitation power generation mode with an additional stator terminal excitation capacitor bank was discussed by Lahcene Quazene and George[1], McPherson N.H.Malik and S.E.Haque[2], A.K.Aljabri and A.I.Alolah [3], L.Shridhar, B.P.Singh and C.S.Jha [4], S.P.Singh, M.P.Jain and Bhim Singh,[5].

Barkle and Ferguson [8] has presented the approximate model of both grid-connected and SIEG for studying the general aspects like power factor and short circuit behavior. They found that the induction generator does not contribute to the interrupting duty of the breaker and makes only the sustained contribution to the momentary rating of the device connected to the generator.

T. Ahmed, K. Nishida, and M. Nakaoka proposed have proposed a single phase static VAR (SVC) compensator composed of the thyristor controlled reactor (TCR), thyristor switched capacitor (TSC) and the fixed excitation capacitor (FC) to regulate smoothly the generated output voltage of the standalone single phase induction generator with a variable inductive load. A PI (Proportional Integral) controller is employed to adjust the equivalent capacitance of the single phase SVC [9].

Bhim Singh and Co., [10] [11] [12] [13] have developed a mathematical model and a control strategy for a voltage regulator using a static synchronous compensator (STATCOM). And load controller for DFIG. They have presented huge contribution in this area.

Terminal Voltage Control Scheme based on Static VAR Compensator for Three-Phase Self-Excited Induction Generator was described by Tarek Ahmed, Mutsuo Nakaoka and Osamu Noro [14].

The doubly fed induction generator (DFIG) can supply power at constant voltage and constant frequency while the rotor speed varies. This makes it suitable for variable speed wind energy applications. Additionally, when a bidirectional AC-AC converter is used in the rotor circuit, the speed range can be extended above synchronous speed and power can be generated both from the stator and the rotor. An advantage of this type of DFIG drive is that the rotor converter need only be rated for a fraction of the total output power, the fraction depending on the allowable sub- and super-synchronous speed range. A good introduction to the operational characteristics of the DFIG connected to the grid can be found [16, 17] in which Scherbius schemes using either cycloconverter or six pulses naturally commutated DC-link converters are used.

In [19] Joeng and Park present a working scheme for a DFIG, supplying an isolated load. This system is unable to operate super-synchronously and the harmonic currents drawn by the diode rectifier are undesirable.

R. S. Pena, G. M. Asher, and J. C. Clare, [20] described that the power converters connected to the rotor are for restricted speed range operation, they are rated to only a fraction of the machine nominal power, and vector control is proposed for the controlling the Stator side converter.

Control and operation of grid-connected voltage source converter under grid disturbances in variable- speed wind turbines are discussed by G. Saccomando and J. Svensson, [21]

Mitsutoshi Yamamoto and Osamu Motoyoshi [22] developed a power control system for a doubly-fed wound rotor induction generator. This power control system has applied a control method using a rotating reference frame fixed on the gap flux of the generator and can control active and reactive power independently and stably. The characteristics of the control system have been proved by experiment. Moreover, harmonic currents fed to the rotor windings are transmitted to the stator winding changing its frequency.

M.B.Mohamed, M.Jemli, M-Gossa, K. Jemli [23], described the dq model of the wound rotor induction machine in rotor reference frame and implemented in simulink for fast simulations. In order to control the power flowing between the stator of (DFIG) and the grid, a control law was synthesized using PI controllers. Simulation results have demonstrated.

A grid connected wind power generation scheme using a doubly fed induction generator with a direct AC-AC matrix converter is proposed K.Ghedamsi, D.Aouzellag, E.M.Berkouk [24]. The analysis of stator flux vector control algorithm and a space vector modulated matrix converter to control rotor current was discussed. The matrix converter-based rotor current control scheme is highlighted.

The real development of matrix converter starts with the early work of Venturini and Alesina [25], [26] in 1980. They presented the power circuit of the converter as a matrix of bidirectional switches and they introduced the name 'matrix converter'. Another major contribution of these authors is the development of rigorous

mathematical analysis to describe the low frequency behavior of the converter. In their modulation method, also known as direct transfer function approach, the output voltages are obtained by the multiplication of matrix with the input voltages.

The method of using a space vector concept for deriving the switching instants for pulse width-modulated voltage source inverters is described and compared with the commonly used established sinusoidal concept was done by H. W. vander Broeck, H. C. Skudelny and G. V. Stanke [27].

GUO Yougui, ZHU Jianlin and DENG Cheng [28] discussed the modulation modes of SVM for matrix converter and also two novel modulation modes are described for matrix converter for the first time.

1.3 Author's Contribution:

In this Dissertation, a FUZZY Logic controller based FC-TCR (in delta connection) is modeled to sustain the process of self excitation and terminal voltage regulation of SEIG for the variable R-load and RL-load ($\cos\phi=0.8$), which can vary from no load to full load. The FUZZY controller is designed to control the delay firing angle ' α ' of FC-TCR circuit by taking inputs as 'error in terminal voltage' and 'line currents'. The simulated performance waveforms of SEIG is analyzed with the proposed FUZZY controller based FC-TCR and the voltage regulation of SEIG with this FUZZY controller based FC-TCR is compared with voltage variation of SEIG with the fixed capacitor bank of the same value of capacitance used in FC-TCR. This comparison is done for both variable R-load and RL-load. The simulated results of the SEIG with the proposed model are found satisfactory.

Further, the Converter topologies for the DFIG are discussed and the same are modeled in simulink. The AC/DC/AC back to back IGBT converter topology is controlled by PWM and SVPWM techniques. And the MATRIX converter topology is also modeled and controlled by using SVM technique. The stator of the WRIM is connected to the grid and the rotor is integrated with the grid via these converter setups and a coupling Transformer. The machine operated in both sub and super synchronous modes to ensure that the power flow via converter setup is bi-

directional. The wave forms for all the voltages and currents and the machine performance characteristics, and the power flow indications are plotted in the SIMULINK and are presented in this work.

2.1. CLASSIFICATION OF INDUCTION GENERATORS:

On the basis of rotor construction, induction generators are two types (i.e., the wound rotor induction generator and squirrel cage induction generator). Depending upon the prime movers used (constant speed or variable speed) and their locations (near to the power network or at isolated places), generating schemes can be broadly classified as under [17]:

- A) constant-speed constant-frequency (CSCF)
- B) variable-speed constant-frequency (VSCF)
- C) variable-speed variable-frequency (VSVF).

A. Constant-Speed Constant Frequency:

In this scheme, the prime mover speed is held constant by continuously adjusting the blade pitch and/or generator characteristics. An induction generator can operate on an infinite bus bar at a slip of 1% to 5% above the synchronous speed. Induction generators are simpler than synchronous generators. They are easier to operate, control, and maintain, do not have any synchronization problems, and are economical. The following figure: 2.1 represents SCIG operating as Self Exited Induction Generator (SEIG) with Grid connected mode.

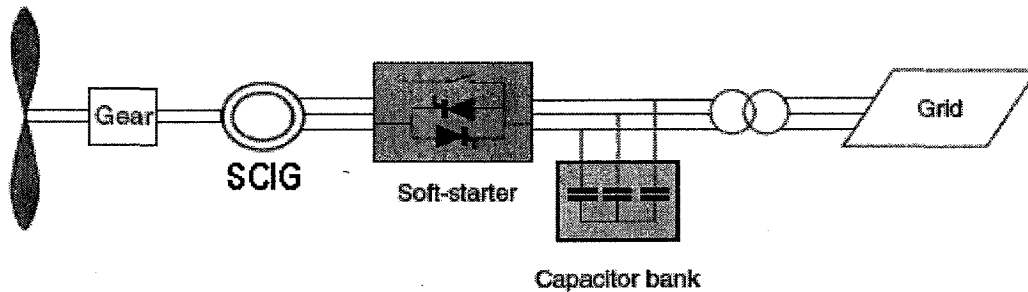


Figure 2.1: SEIG with Grid connected mode

B. Variable-Speed Constant Frequency:

The variable-speed operation of wind electric system yields higher output for both low and high wind speeds [18]. This results in higher annual energy yields per rated installed capacity. Both horizontal and vertical axis wind turbines exhibit this gain under variable-speed operation. Popular schemes to obtain constant frequency output from variable speed are as shown.

B.1. AC-DC-AC Link:

With the advent of high-powered thyristors, the ac output of the three-phase alternator is rectified by using a bridge rectifier and then converted back to ac using line-commutated inverters. Since the frequency is automatically fixed by the power line, they are also known as synchronous inverters.

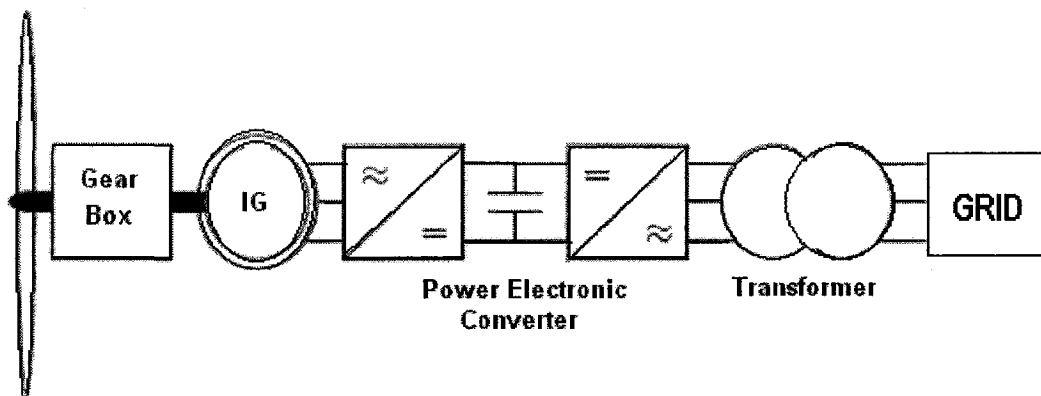


Figure: 2.2 Induction Generator with Ac-Dc-Ac link

B.2. Double Output Induction Generator (DOIG):

The DOIG consists of a three-phase wound rotor induction machine that is mechanically coupled to either a wind or hydro turbine, whose stator terminals are connected to a constant voltage constant frequency utility grid [48]. The variable frequency output is fed into the ac supply by an ac-dc-ac link converter consisting of either a full-wave diode bridge rectifier and thyristor inverter combination or current source inverter (CSI)-thyristor converter link. One of the outstanding advantages of DOIG in wind energy conversion systems is that it is the only scheme in which the generated power is more than the rating of the machine. However, due to operational disadvantages, the DOIG scheme could not be used extensively. The maintenance requirements are high, the power factor is low, and reliability is poor under dusty and abnormal conditions because of the sliding mechanical contacts in the rotor. This scheme is not suitable for isolated power generations because it needs grid supply to maintain excitation.

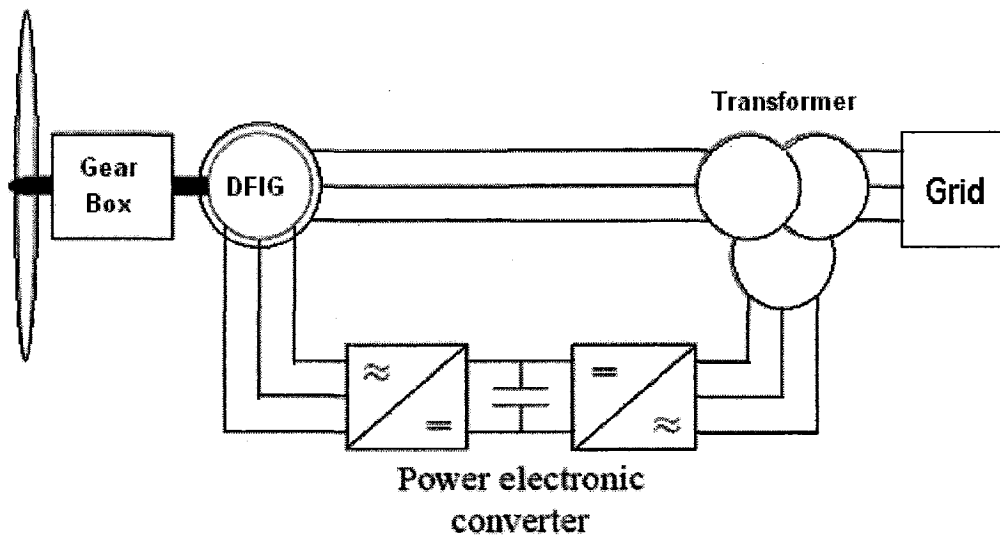


Figure: 2.3 DFIG with Ac-Dc-Ac Link

B.2.1. DFIG with MATRIX CONVERTER:

The matrix converter is capable of converting the variable AC from the generator into constant AC to the grid in one stage, Fig 2.4 Two distinct advantages arise from this topology, the converter requires no bulky energy storage or DC-link and control is performed on just one converter.

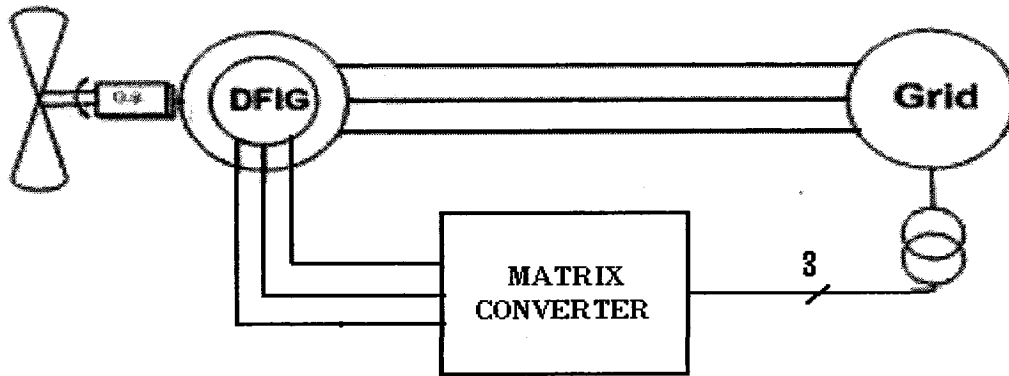


Fig 2.4 DFIG with MATRIX converter

C. Variable-Speed Variable Frequency:

With variable prime mover speed, the performance of synchronous generators can be affected. For variable speed corresponding to the changing derived speed, SEIG can be conveniently used for resistive heating loads, which are essentially frequency insensitive. [17].

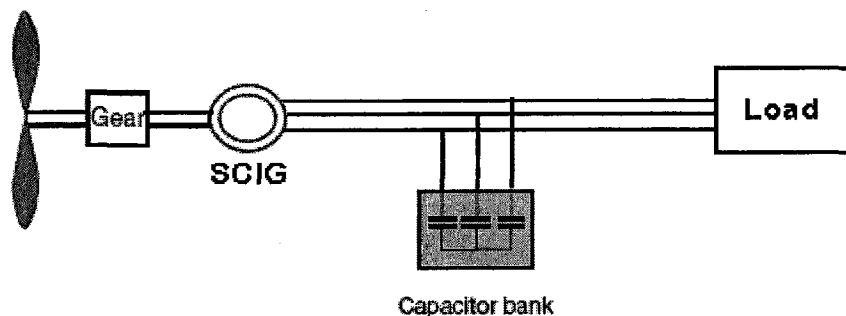


Fig 2.5 SEIG in isolated mode

CHAPTER -3

Analysis and design of SEIG model,

FC-TCR and Fuzzy logic controller

A 3HP, 440V, 4 poles, 50Hz, 1500 rpm star connected Squirrel Cage Induction Machine in isolated mode was chosen in MATLAB. To run it as a Generator and for the smooth controlling of reactive power to sustain the process of self excitation a Fixed Capacitor – Thyristor Controlled Reactor (FC-TCR) is designed in SIMULINK environment, which is used in delta connection instead of a fixed capacitor bank. The value of capacitance needed per phase would vary as the load on the machine varies. i.e., as load on the machine increases, the reactive power requirement (capacitance requirement) is also increases to maintain the constant voltage at the terminals. So connecting a fixed capacitor bank is always not a valid option. So in the present work a controller (in FUZZY) is designed in such a way that the delay firing angle (α) of the anti parallel connected thyristors of the TCR (Thyristor Controlled Reactor) is controlled such that the inductive reactance of the TCR is controlled, in turn the net reactance (capacitive, since the C and L was chosen to make the net reactance in capacitive zone) of the parallel combination of the Fixed Capacitor and Reactor is controlled, as the load varies from no load to full load. The only limitation in FC-TCR is that we need to compensate the inductive reactance with the capacitive reactance, so the capacitor size will be little larger than usual fixed capacitor. But this will provide a constant terminal voltage (of 440V) always by controllable variable reactive power. In this case change in current ranges and terminal voltage error are fed as an inputs to Fuzzy logic Controller (Mamdani), and the controller will give the output alpha (α) called the delay firing angle which is fed to firing circuit of the FC-TCR. The rules in the Fuzzy logic Controller is framed based on the variation of the net reactance of FC-TCR with the delay firing angle alpha(α) for different steps of Resistive loads and RL loads ($\cos\phi=0.8$) ranging from no load to full load. So whatever may be the loading within this, the controller will give the delay firing angle (α) and this is fed to the anti parallel thyristor valves with proper phase shifts (180° phase shift to the negative cycle conducting thyristor valve). Thus the reactive power feeding to the SEIG is controlled and the terminal

voltage is maintained constant (440V), since reactive power $Q_c = V^2 \omega c$, and the net reactance $X_T(\alpha) = \left[\frac{X_L(\alpha) X_C}{X_L(\alpha) + X_C} \right]$, where the inductive reactance $X_L(\alpha) = \omega L \left[\frac{\pi}{\pi - 2\alpha - \sin 2\alpha} \right]$, (α) is the delay firing angle of the anti-parallel thyristors, and X_C is the reactance of Fixed capacitor.

Fuzzy logic based closed loop controller is modeled to vary the reactance of FC-TCR to regulate the terminal voltage. The overall system consists of SEIG, delta connected FC-TCR's, Fuzzy logic controller, firing circuit, prime mover and variable loads (of R and RL ($\cos\phi=0.8$) loads). This combined system is modeled in MATLAB/simulink environment to confirm its effectiveness and robustness. The FUZZY logic controller is designed to control the delay firing angle ' α ' of FC-TCR circuit by taking inputs as 'error in terminal voltage' and 'line currents'. The simulated performance waveforms of SEIG is analyzed with the proposed FUZZY logic controller based FC-TCR and the voltage regulation of SEIG with this FUZZY logic controller based FC-TCR is compared with voltage variation of SEIG with the fixed capacitor bank of the same value of capacitance used in FC-TCR. This comparison is done for both variable R-load and RL-load ($\cos\phi=0.8$). The simulated results of the SEIG with the proposed model are found to be satisfactory. The RMS voltages variation for both SEIG with fixed capacitor and SEIG with FC-TCR is observed. The RMS voltage is not maintained at desired voltage level (440 V) for SEIG with fixed capacitors, where as for SEIG with FC-TCR simulation with FUZZY logic controller the RMS voltage is maintained at 440 Volts for both the variable R load and RL load ($\cos\phi=0.8$).

3.1 TCR-Thyristor Controlled Reactor:

A basic single phase TCR (Thyristor Controlled Reactor) [46] [47] comprises an anti parallel thyristor valves, T1 and T2, in series with a linear air core reactor, as shown in Fig: (3.1). The anti Parallel -connected thyristor pair acts as a bidirectional switch, with thyristor valve T1 conducting in positive half cycle of the current and T2 in the negative half cycle, so the current in the reactor can be controlled from, maximum (when the thyristor valve is closed) to zero (thyristor valve is open) by the method of firing delay control, that is the closure of the thyristor valve is delayed

with respect to the peak of the applied voltage in each half cycle, and thus the duration of the current conduction intervals is controlled as shown in Fig: (3.2)

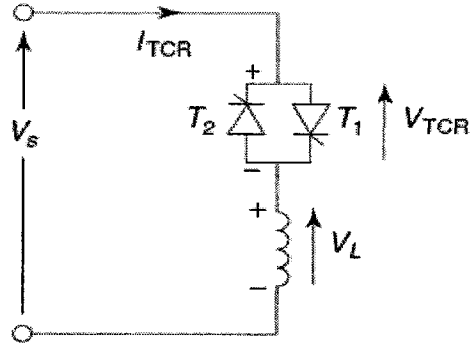
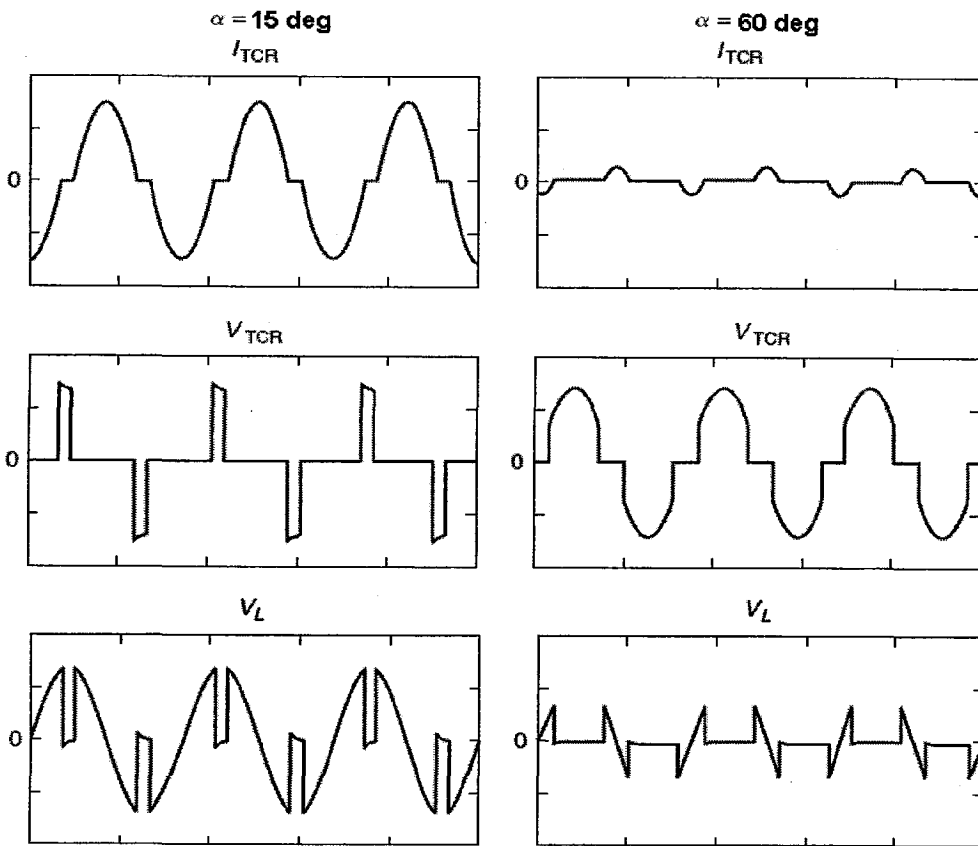


Fig (3.1): Basic TCR circuit [46]



Current and voltages for different α in a TCR

Fig (3.2): Waveforms of currents and voltages for different alpha in TCR [47]

When the gating of the valve is delayed by an angle ' α ' ($0^\circ \leq \alpha \leq 90^\circ$) with respect to the crest as the voltage, the current in the reactor can be expressed with $v(t) = V \cos \omega t$ as follows:

$$i_L(t) = \frac{1}{L} \int_{\alpha}^{\omega t} v(t) dt = \frac{V}{\omega L} (\sin \omega t - \sin \alpha) \quad (3.1)$$

Since the thyristor valve, by definition, opens as the current reaches zero, the above equation is valid ($\alpha \leq \omega t \leq \pi - \alpha$.) For the subsequent positive half cycle intervals the same expression obviously remains valid. For subsequent negative half cycle intervals, the sign term will become opposite.

The amplitude of a fundamental reactor current $i_{LF}(\alpha)$ can be derived by Fourier analysis as given below

$$i_{LF}(\alpha) = a_1 \cos \omega t + b_1 \sin \omega t \quad (3.2)$$

$i_L(t)$ is symmetric and periodic, so a_1 term will become zero (since half wave symmetry)

$$a_1 = \frac{2}{T} \int_0^T f(t) \cos \omega t d\omega t = 0 \quad (3.3)$$

And b_1 is given by,

$$b_1 = \frac{2}{T} \int_0^T f(t) \sin \omega t d\omega t \quad (3.4)$$

$$\begin{aligned} &= \frac{2}{\pi} \int_0^{\pi} \frac{v}{\omega L} (\sin \omega t - \sin \alpha) \sin \omega t dt \\ &= \frac{2v}{\pi \omega L} \left[\int_{\alpha}^{\pi-\alpha} \sin^2 \omega t d\omega t - \int_{\alpha}^{\pi-\alpha} \sin \omega t \sin \alpha d\omega t \right] \\ &= \frac{2v}{\pi \omega L} \left[\int_{\alpha}^{\pi-\alpha} \frac{1 - \cos 2\omega t}{2} d\omega t - \sin \alpha \int_{\alpha}^{\pi-\alpha} \sin \omega t d\omega t \right] \\ &= \frac{2v}{\pi \omega L} \left[\frac{1}{2} \left((\pi - 2\alpha) - \frac{\sin 2\pi - 2\alpha}{2} + \frac{\sin 2\alpha}{2} \right) + \sin \alpha [\cos(\pi - \alpha) - \cos \alpha] \right] \\ &= \frac{2v}{\pi \omega L} \left[\frac{1}{2} - \alpha + \frac{\sin 2\alpha}{4} + \frac{\sin 2\alpha}{4} + \sin \alpha [-2 \cos \alpha] \right] \\ &= \frac{2v}{\pi \omega L} \left[\frac{\pi}{2} - \alpha + \frac{\sin 2\alpha}{2} - 2 \sin \alpha \cos \alpha \right] \end{aligned}$$

It is clear from the above fig (3.3) that the TCR can control the fundamental current continuously from zero (valve open) to maximum (valve closed) as if it was variable reactive impedance. Thus, an effective $X_L(\alpha)$, for the TCR can be defined. This impedance, as a function of angle α , can be written directly from equation (3.6), i.e

$$X_L(\alpha) = \omega L \left[\frac{\pi}{\pi - 2\alpha - \sin 2\alpha} \right] \quad (3.7)$$

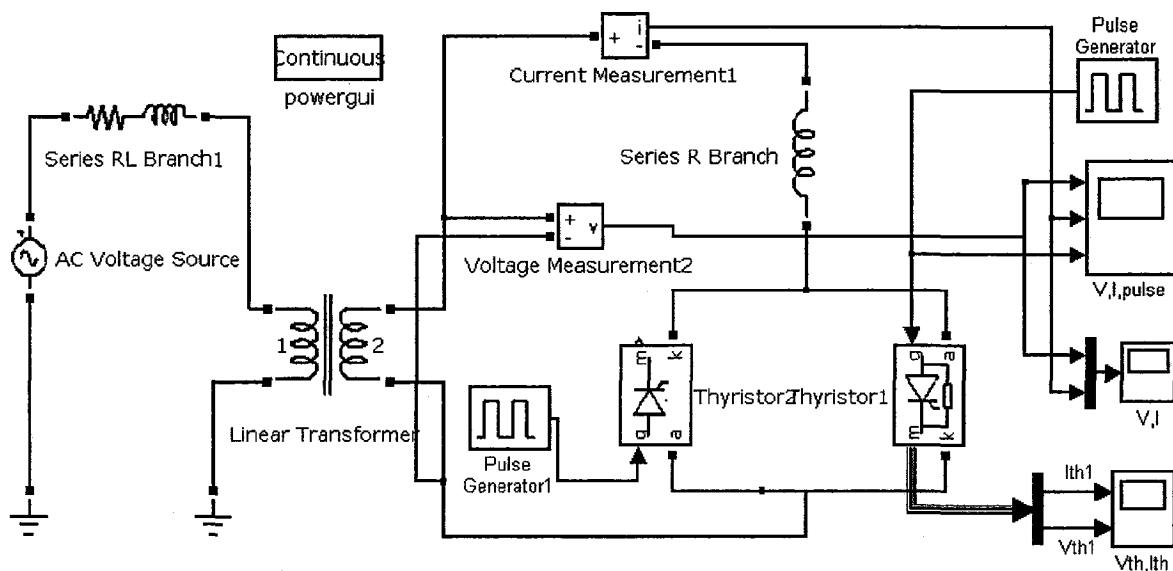


Fig (3.4) Simulation block of TCR [50]

3.2 Concept of FC-TCR:

Instead of using a fixed capacitor for the process of self excitation, use of FC-TCR [46] [47] will allow us to have a control on the reactive power supply to the Induction generator, as to keep the desired voltage level at the load terminals. The figure (3.5) below shows the basic diagram of a FC-TCR. The variation of inductive reactance depends on the delay firing angle ' α ', as explained in the TCR section. So for a fixed capacitance, the parallel combination of L and C, the inductive reactance $X_L(\alpha)$ can be varied and in turn to vary the net capacitive reactance $X_T(\alpha)$ of the parallel combination (L and C should take in such a way that the net reactance

should be always in capacitive zone for supply of reactive power) can be controlled by varying the delay firing angle ' α '. The following equations disclose the variation of $X_L(\alpha)$ in turn $X_T(\alpha)$ with respect to variation of ' α ' ($0^\circ \leq \alpha \leq 90^\circ$) from the inductor current zero crossing points.

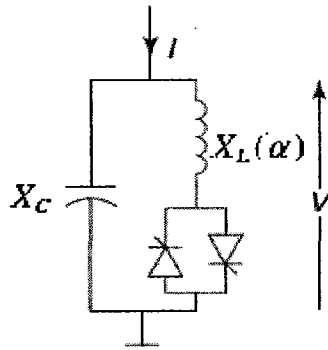


Fig (3.5) Basic FC-TCR [47]

$$X_L(\alpha) = \omega L \left[\frac{\pi}{\pi - 2\alpha - \sin 2\alpha} \right]$$

$$X_T(\alpha) = X_L(\alpha) // X_C$$

$$X_T(\alpha) = \left[\frac{X_T(\alpha) \cdot X_C}{X_T(\alpha) + X_C} \right]$$

L and C should take in such a way that the net reactance should be always in capacitive zone for supply of reactive power. Therefore the reactive power supplied by FC-TCR is given by,

$$Q_c = \frac{V^2}{X_T(\alpha)}$$

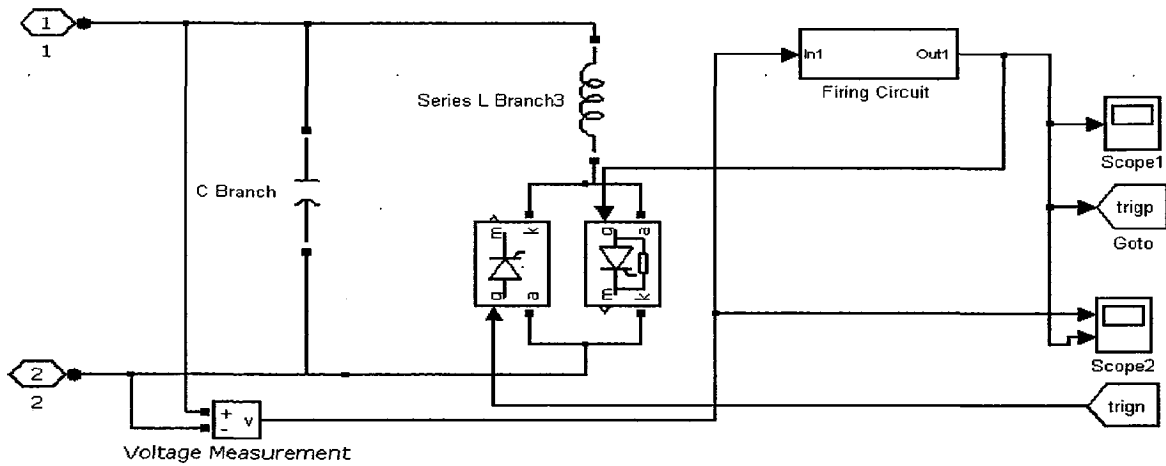


Fig (3.6) Simulation block of FC-TCR [50]

3.3 SIMULINK MODEL OF SEIG WITH FC-TCR and FLC:

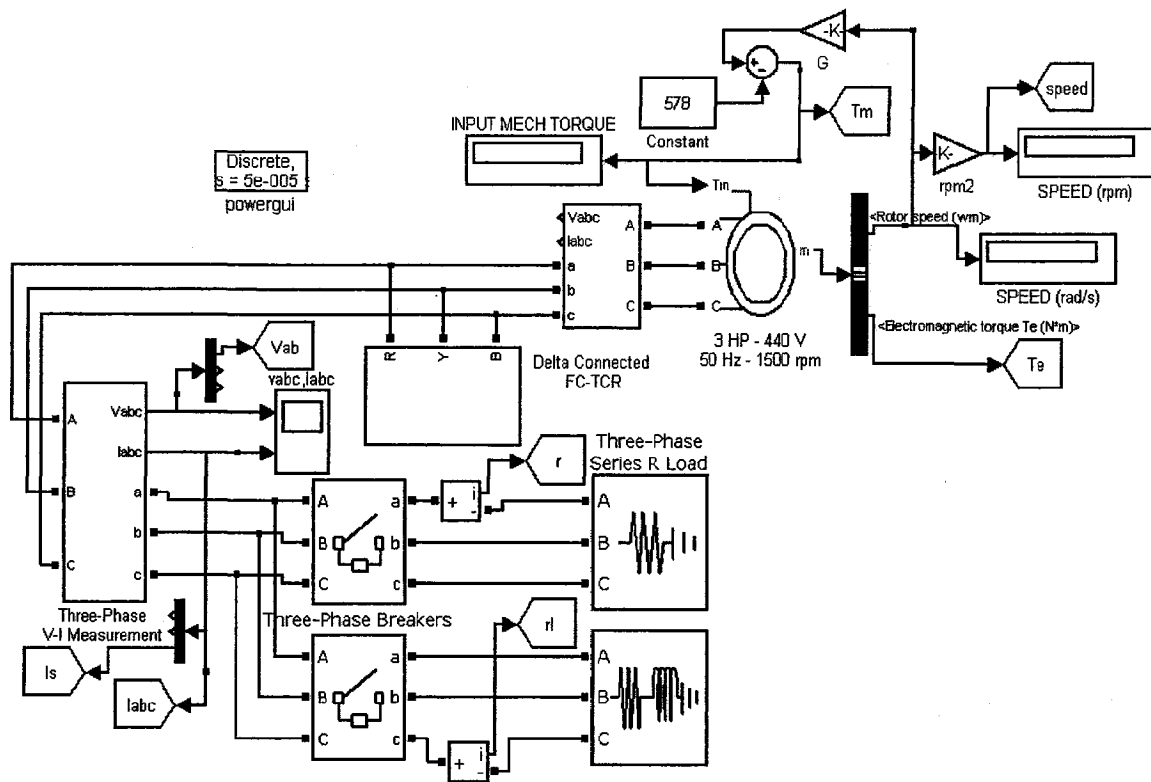


Fig 3.7: Simulink Model of SEIG using FC-TCR

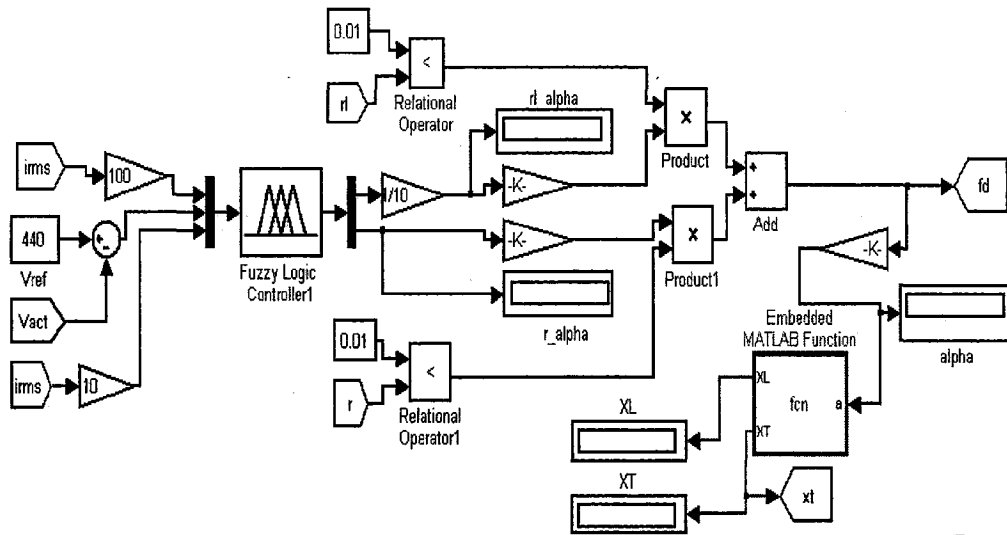


Fig 3.8: Simulink Model for FUZZY Controller

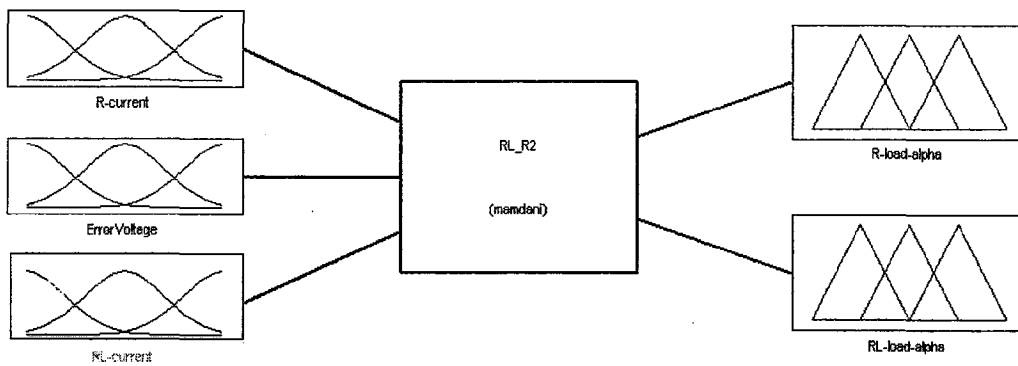
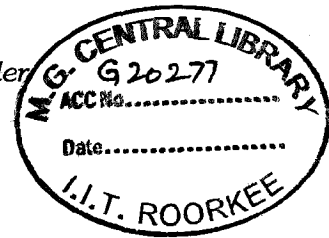


Fig 3.9: FUZZY Logic Controller relation with input parameter and outputs

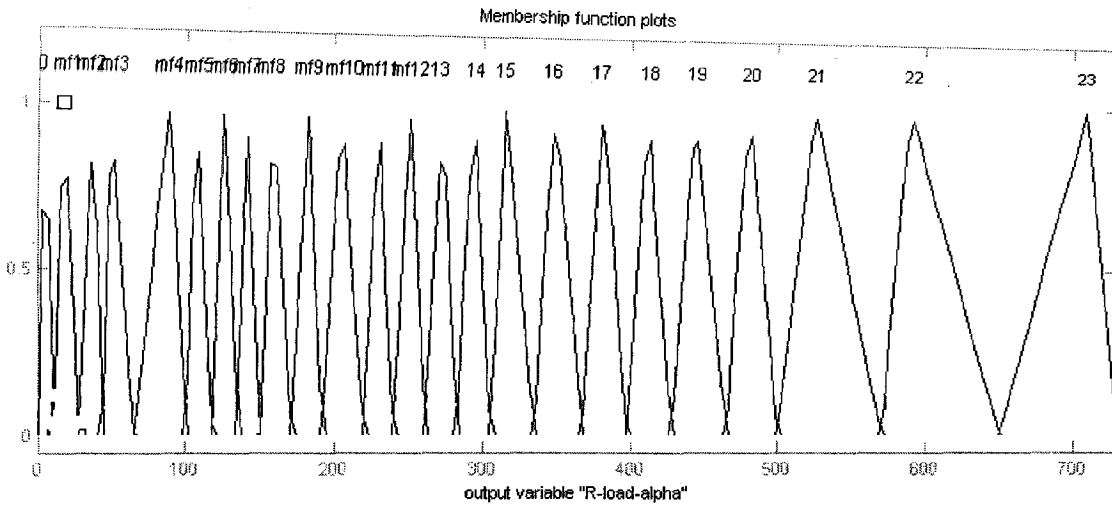


Fig 3.10: Fuzzy membership function plots for the output (α for variable R-load)

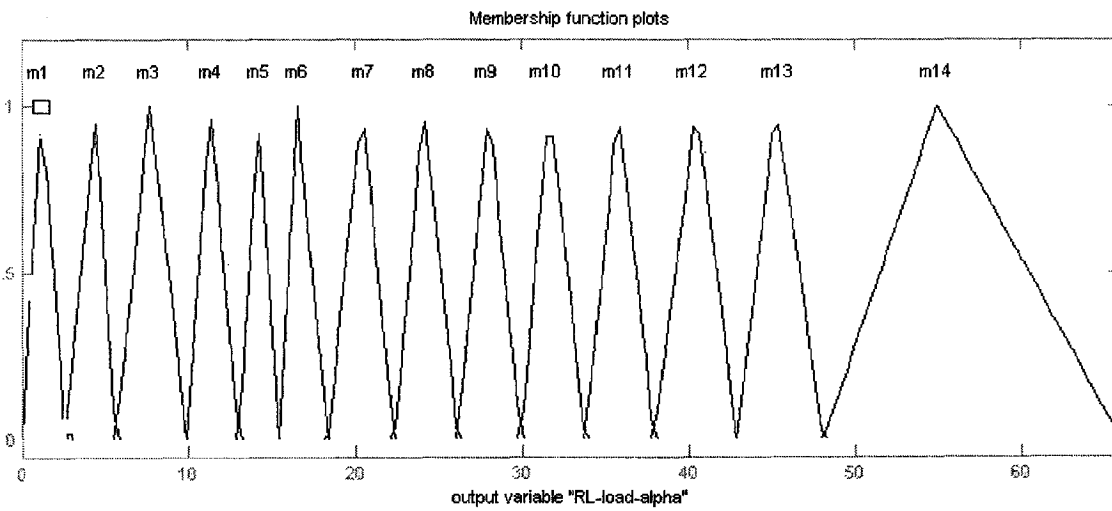


Fig 3.11: Fuzzy membership function plots for the output (α for variable RL-load)

Introduction to Wound Rotor Induction Generator:

Squirrel cage induction machine is used in several wind energy conversion systems. This machine has proven its efficiency due to qualities such as robustness, low cost and simplicity when it is directly connected to the grid. However, the wind turbine must be designed to keep the machine's speed constant near the synchronous speed. This constraint reduces the possibility to increase the electrical energy produced for high wind speeds. A converter can be used between the stator of the machine and the grid but it has to handle full power and must be correctly cooled. To overcome these disadvantages, a solution consists in using a doubly-fed induction generator (DFIG) where the rotor is wounded and fed by slip rings. It is then less robust and more expensive than the squirrel cage one. However, it allows putting a converter between the rotor and the grid which is designed only for a part of the full power of the machine (about 30 %) [29], [30]. By controlling correctly this converter, variable-speed operation is allowed and electrical power can be produced from the stator to the grid and also from the rotor to the grid. The control law can be used in order to extract maximum power of the wind turbine for different wind speeds.

4.1 Doubly-fed induction generator:

The concept of the DFIG is an interesting option with a growing market. The converters for the rotor circuit can be a bidirectional back-to-back IGBT voltage source converter or matrix converter. The term 'doubly fed' refers to the fact that the voltage on the stator is applied from the grid and the voltage on the rotor is induced by the power converter. This system allows a variable-speed operation over a large, but restricted, range. The converter compensates the difference between the mechanical and electrical frequency by injecting a rotor current with a variable frequency. Both during normal operation and faults the behavior of the generator is thus governed by the power converter and its controllers. The power converter in case of bidirectional back-to-back IGBT consists of two converters, the rotor-side converter and grid-side converter, which are controlled independently of each other.

The main idea is that the rotor-side converter controls the active and reactive power by controlling the rotor current components, while the line-side converter controls the DC-link voltage and ensures a converter operation at unity power factor (i.e. zero reactive power).

Depending on the operating condition of the drive, power is fed into or out of the rotor: in an over synchronous situation, it flows from the rotor via the converter to the grid, whereas it flows in the opposite direction in a sub synchronous situation. In both cases – sub synchronous and over synchronous – the stator feeds energy into the grid.

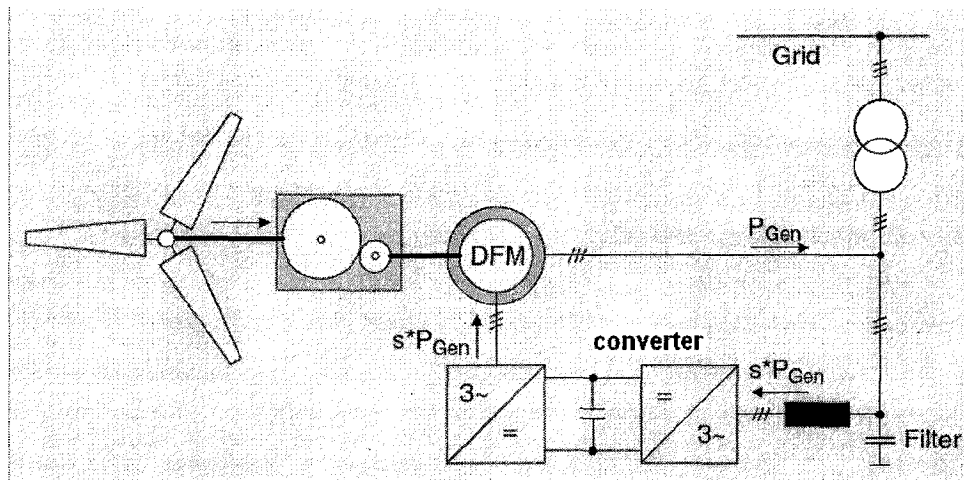
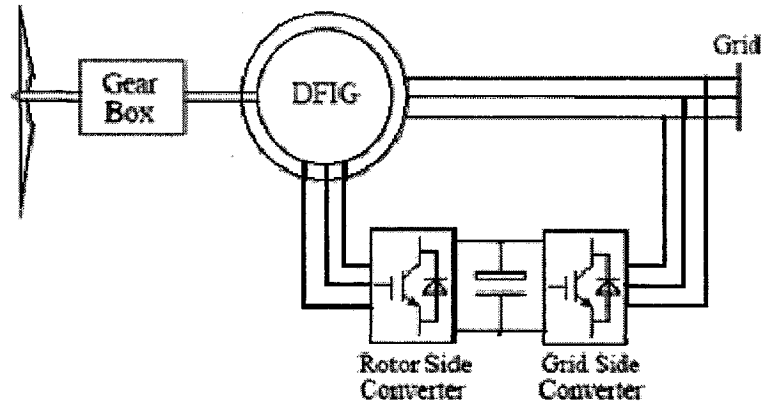


Fig 4.1 : Doubly fed induction machine

4.2 VSCF – DFIG:



Schematic diagram of VSCF-DFIG wind energy generation system

Fig. 4.2 shows the schematic diagram of a DFIG-based wind turbine. The stator of the DFIG is directly connected to the grid, while the rotor is connected to a controllable AC/DC/AC converter setup.

Advantages of WRIG (DFIG):

- Improved system efficiency and power factor control can be implemented at lower cost, the converter has to provide only excitation energy
- Only the electric power injected by the rotor needs to be handled by the convert implying a less cost AC-AC converter
- Half of the world's leading wind turbine manufacturers use the doubly fed induction generator systems. This is due to the fact that the power electronic converter only has to handle a fraction (20% – 30%) of the total power, i.e., the slip power. This means that if the speed is in the range $\pm 30\%$ around the synchronous speed, the converter has a rating of 30% of the rated turbine power, reducing the losses in the power electronic converter, compared to a system where the converter has to handle the total power.
- Due to the advances in power electronics it is advantaged to use the doubly fed induction generator system with variable speed connected to the electrical grid through an AC-AC converter, improving the efficiency of the power conversion.

- If the slip is positive, the rotor receives electric energy from the grid, but the stator keeps on delivering electric energy to the grid, this is sub-synchronous generating mode, which is a special feature of WRIGs.

This DFIG offers the following advantages over other schemes of Wind Energy Conversion System.

- (1) The ability to output more than its rated power without becoming overheated.
- (2) The transfer of maximum power over a wide speed range in both sub-synchronous and super-synchronous modes.
- (3) Reduced inverter cost, because inverter rating is typically 25% of total system power, while the speed range of the ASG is 33% around the synchronous speed.
- (4) Reduced cost of the inverter filters and EMI filters, because filters are rated for 0.25 p.u. of total system power, and inverter harmonics represent a smaller fraction of total system harmonics.
- (5) Improved system efficiency; approximately 2-3% efficiency improvement can be obtained.
- (6) Power-factor control can be implemented at lower cost, because the DFIG system (four-quadrant converter and induction machine) basically operates similar to a synchronous generator, the converter has to provide only excitation energy. In addition compared to silicon - controlled rectifier (SCR) based Kramer drives the DFIG with a four -quadrant converter in the rotor circuit enables decoupled control of active and reactive power of the generator.

Disadvantages of DFIG:

- (1) Increased control complexity due to increased number of switches in converter.
- (2) Stator winding is directly connected to the grid may result in grid disturbances.
- (3) Need for periodic slip ring maintenance.

4.3 Description of the DFIG with AC/DC/AC converter system:

Wind turbines use a doubly-fed induction generator (DFIG) consisting of a wound rotor induction generator and an AC/DC/AC IGBT-based PWM converter. The stator winding is connected directly to the 50 Hz grid while the rotor is fed at variable frequency through the AC/DC/AC converter. The DFIG technology allows extracting maximum energy from the wind for low wind speeds by optimizing the turbine speed, while minimizing mechanical stresses on the turbine during gusts of wind. The optimum turbine speed producing maximum mechanical energy for a given wind speed is proportional to the wind speed. Another advantage of the DFIG technology is the ability for power electronic converters to generate or absorb reactive power, thus eliminating the need for installing capacitor banks as in the case of squirrel-cage induction generator.

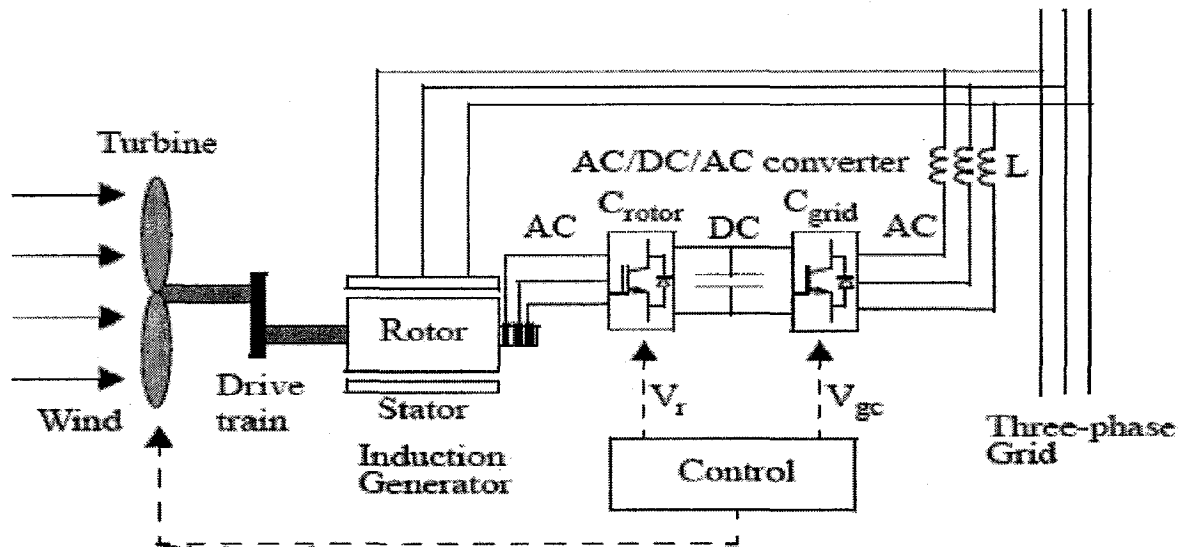


Fig 4.3: Doubly fed induction generator with ac/dc/ac converter topology

Where V_r is the rotor voltage and V_{gc} is grid side voltage. The AC/DC/AC converter is basically a PWM converter which uses sinusoidal PWM technique to reduce the harmonics present in the wind turbine driven DFIG system. Here C_{rotor} is rotor side converter and C_{grid} is grid side converter. To control the speed of wind turbine gear boxes or electronic control can be used.

4.4 Operating Principle of DFIG:

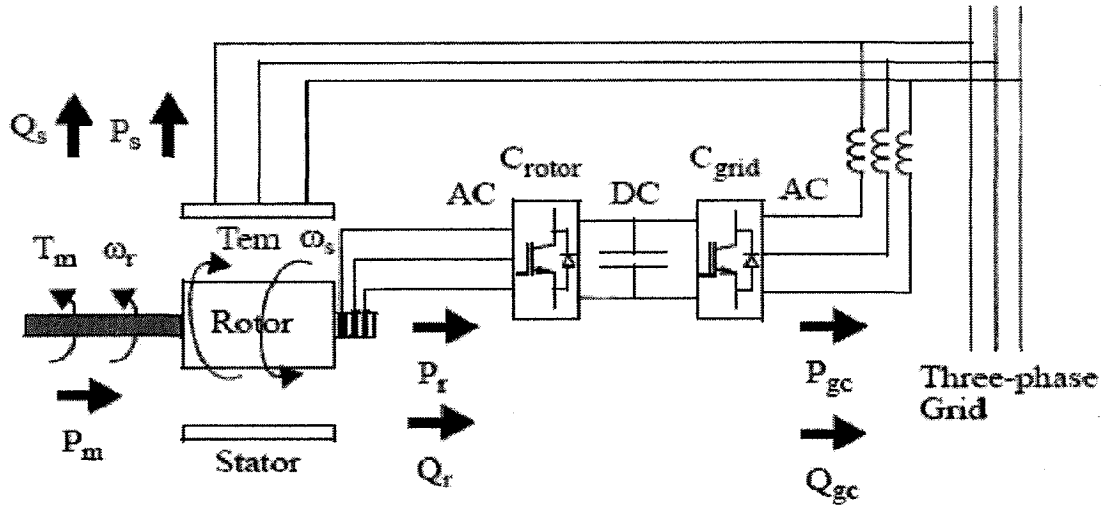


Fig 4.4 Power flow diagram of DFIG

The stator is directly connected to the AC mains, while the wound rotor is fed from the Power Electronics Converter via slip rings to allow DFIG to operate at a variety of speeds in response to changing wind speed. Indeed, the basic concept is to interpose a frequency converter between the variable frequency induction generator and fixed frequency grid. The DC capacitor linking stator- and rotor-side converters allows the storage of power from induction generator for further generation. To achieve full control of grid current, the DC-link voltage must be boosted to a level higher than the amplitude of grid line-to-line voltage. The slip power can flow in both directions, i.e. from the rotor to the supply and from supply to the rotor and hence the speed of the machine can be controlled from either rotor- or stator-side converter in both super and sub-synchronous speed ranges.

The mechanical power and the stator electric power output are computed as follows:

$$P_m = T_m * \omega_r$$

$$P_s = T_{em} * \omega_s$$

For a loss less generator the mechanical equation is:

$$J(d\omega_r/dt) = T_m - T_{em}$$

In steady-state at fixed speed for a loss less generator:

$$T_m = T_{em} \text{ and } P_m = P_s + P_r$$

And it follows that:

$$P_r = P_m - P_s = T_m * \omega_r - T_{em} * \omega_s = -s P_s$$

Where

$$S = (\omega_s - \omega_r)/\omega_r \text{ is defined as the slip of the generator.}$$

Generally the absolute value of slip is much lower than 1 and, consequently, P_r is only a fraction of P_s . Since T_m is negative for power generation and since ω_s is positive and constant for a constant frequency grid voltage, the sign of P_r is a function of the slip sign. P_r is positive for negative slip (speed greater than synchronous speed) and it is negative for positive slip (speed lower than synchronous speed). For super synchronous speed operation, P_r is transmitted to DC bus capacitor and tends to raise the DC voltage. For sub-synchronous speed operation, P_r is taken out of DC bus capacitor and tends to decrease the DC voltage. C_{grid} is used to generate or absorb the power P_{gc} in order to keep the DC voltage constant. In steady-state for a lossless AC/DC/AC converter P_{gc} is equal to P_r and the speed of the wind turbine is determined by the power P_r absorbed or generated by C_{rotor} . The phase-sequence of the AC voltage generated by C_{rotor} is positive for sub-synchronous speed and negative for super synchronous speed. The frequency of this voltage is equal to the product of the grid frequency and the absolute value of the slip. C_{rotor} And C_{grid} have the capability for generating or absorbing reactive power and could be used to control the reactive power or the voltage at the grid terminals.

Fig.4.5 shows the power flow diagram in the rotor circuit for **(a)** speeds below the synchronous speed, and **(b)** speeds above the rated rotor speed. Note that, in sub region I at super synchronous speeds, the power flow diagram that will be used in the analysis depends on the operating strategy chosen.

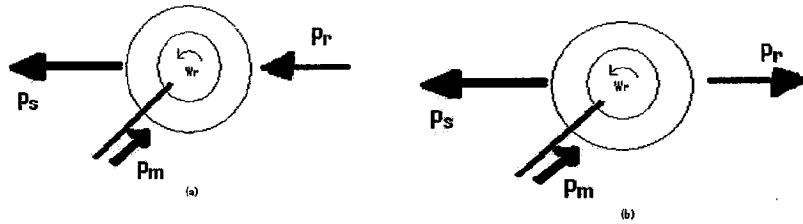


Fig 4.5: power flow diagrams (a) sub synchronous speed (b) super synchronous speed

4.5 Doubly-Fed induction generator Equations:

The DFIG can be described, using an arbitrary reference frame, by the following equations

1. Voltage equations:

Stator Voltage Equations:

$$V_{ds} = r_s i_{ds} - \omega \lambda_{qs} + p \lambda_{ds}$$

$$V_{qs} = r_s i_{qs} + \omega \lambda_{ds} + p \lambda_{qs}$$

Rotor Voltage Equations:

$$V_{dr} = r_r i_{dr} - (\omega - \omega_r) \lambda_{qr} + p \lambda_{dr}$$

$$V_{qr} = r_r i_{qr} - (\omega - \omega_r) \lambda_{dr} + p \lambda_{qr}$$

2. Power Equation

$$P_s = 3/2 (V_{ds} i_{ds} + V_{qs} i_{qs})$$

3. Torque Equation:

$$T_g = -3P/4 (\lambda_{ds} i_{qs} - \lambda_{qs} i_{ds})$$

4. Flux Linkage Equations:

Stator Flux Equations:

$$\lambda_{ds} = L_s i_{ds} + M i_{qr}$$

$$\lambda_{qs} = L_s i_{qs} + M i_{dr}$$

Rotor Flux Equations:

$$\lambda_{qr} = L_r i_{qr} + M i_{ds}$$

$$\lambda_{dr} = L_r i_{dr} + M i_{qs}$$

Where $L_s = L_{ls} + L_m$ and $L_r = L_{lr} + L_m$ are self-inductance of the stator and the rotor windings, respectively, and $M = L_m$ is the mutual inductance between a stator and a rotor winding. The operator p is the time derivative operator, ω and ω_r are the angular speeds of the arbitrary reference frame and rotor respectively.

Implementation of Converter Topologies for DFIG and SVM

In this chapter the possible converter topology for DFIG is presented. The use of power electronic converters allows for variable speed operation of the wind turbine, and enhanced power extraction. In variable speed operation, a control method designed to extract maximum power from the turbine and provide constant grid voltage and frequency is required.

5.1 STATIC KRAMER DRIVE AND SCR CONVERTER METHODS:

It consists of a diode rectifier on the rotor side and a line commutated inverter connected to the supply-side Fig. 5.1

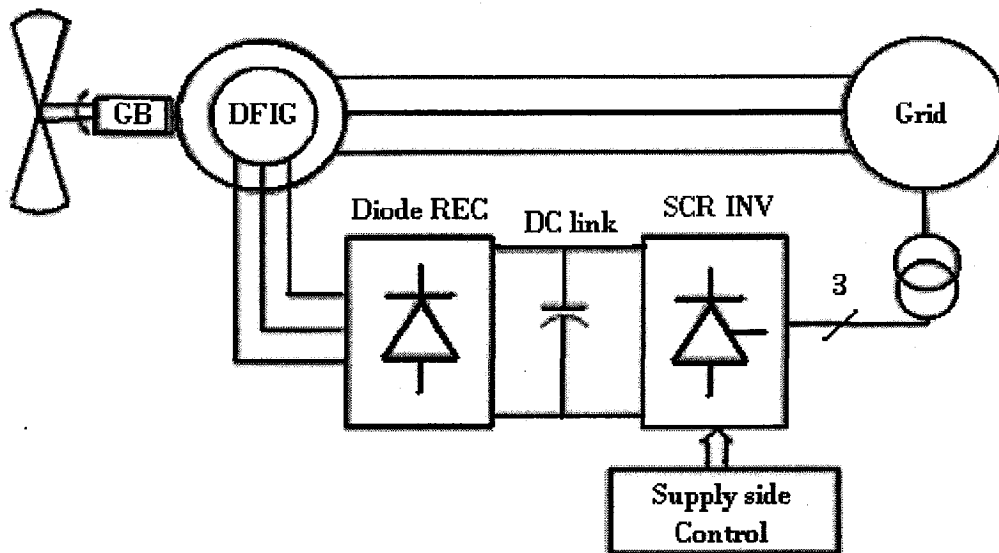


Fig 5.1 DFIG with static Kramer drive

This converter is only able to provide power from both stator and rotor circuits, under super-synchronous operation. To solve this problem, other methods replace the diode rectifier with another thyristor rectifier (SCR). The inclusion of a second SCR allows the generator reactive power demand to be satisfied by the rotor-side converter system.

5.2 BACK-TO-BACK PWM CONVERTERS:

The back-to-back converter is a bidirectional power converter consisting of two Conventional pulse-width modulated (PWM) VSC converters. The topology is shown in Fig 5.2. The DC link voltage is boosted to a level higher than the amplitude of the grid line-to-line voltage in order to achieve full control of the grid current [41].

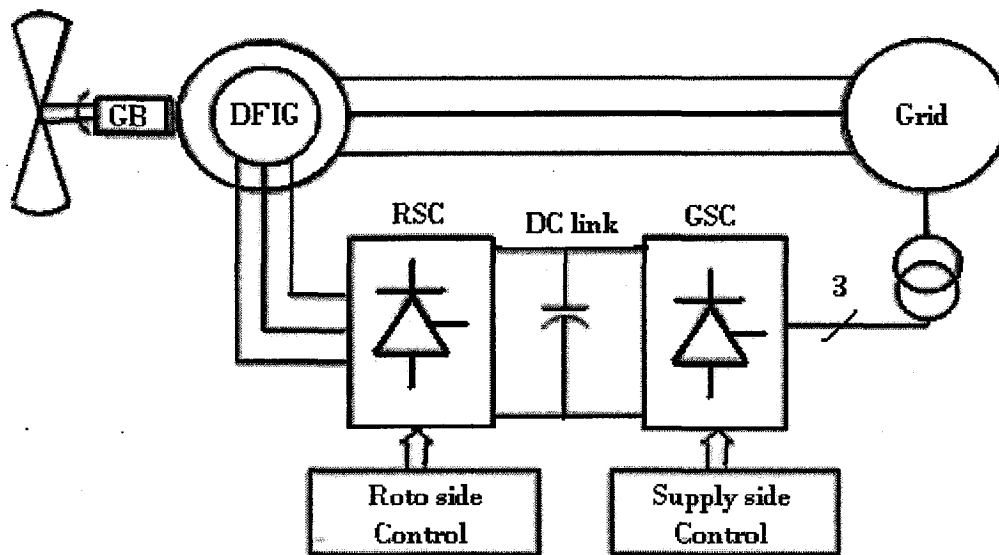


Fig 5.2 DFIG with back to back converter

The presence of the boost inductance reduces the demands on the input harmonic filter and offers some protection for the converter against abnormal conditions on the grid. The capacitor between the inverter and rectifier makes it possible to decouple the control of the two inverters, allowing the compensation of asymmetry on both the generator side and the grid side, without affecting the other side of the converter. The power flow at the grid-side converter is controlled to keep the DC link voltage constant, and the control of the generator-side converter is set to suit the magnetization demand and the desired rotor speed. The presence of the DC link capacitor in a back-to back converter reduces the overall lifetime and efficiency

of the system compared with a converter without a DC link capacitor. In this scheme switching losses are high.

5.3 MATRIX CONVERTER:

The matrix converter is capable of converting the variable AC from the generator into constant AC to the grid in one stage, Fig 5.3 Two distinct advantages arise from this topology, the converter requires no bulky energy storage or DC-link and control is performed on just one converter.

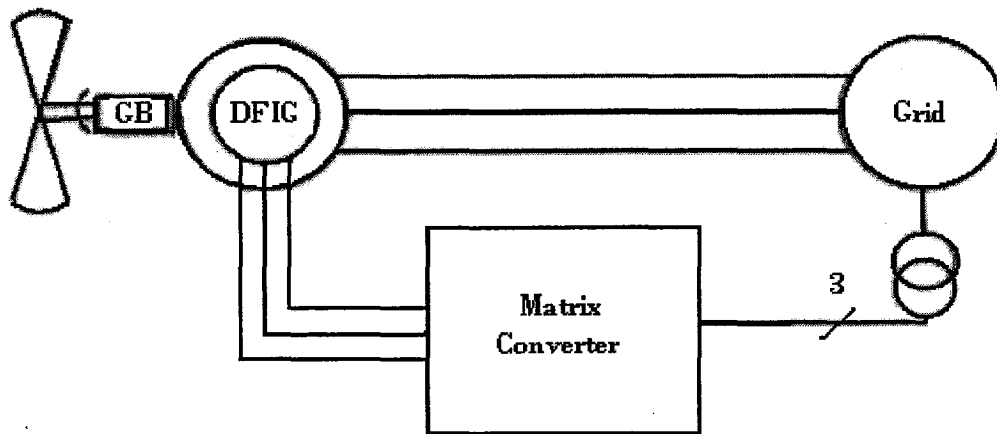


Fig 5.3 DFIG with MATRIX converter

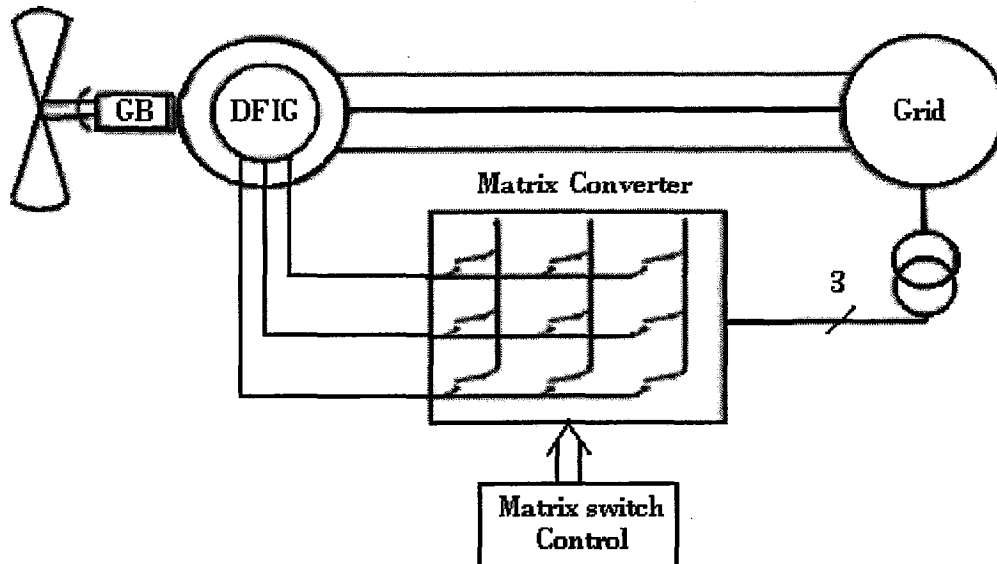


Fig 5.4 DFIG with Matrix converter circuit

The matrix converter consists of nine bidirectional switches (18 total), arranged in a manner such that any input phase may be connected to any output phase at any time. Each individual switch is capable of rectification and inversion. The matrix converter is controlled using double space vector PWM, employing the use of input current and output voltage SVM. One of the major drawbacks of a matrix converter is that 18 total switches are required, causing an increase in converter semiconductor cost.

5.3.1 Description of Matrix Converter:

A cycloconverter is a direct AC/AC converter. The matrix converter is nothing but a three-phase to three-phase forced commutated cycloconverter. It has a voltage source of fixed magnitude and frequency as input and which outputs a voltage which is having variable magnitude and variable frequency. It can have ‘m’ number of inputs and ‘n’ number of outputs. Each output line is connected to one of the m inputs and connection to the appropriate input will give rise to desired output voltage. In general, there is m x n number of switches any of the m switches connected to one output line is switched on

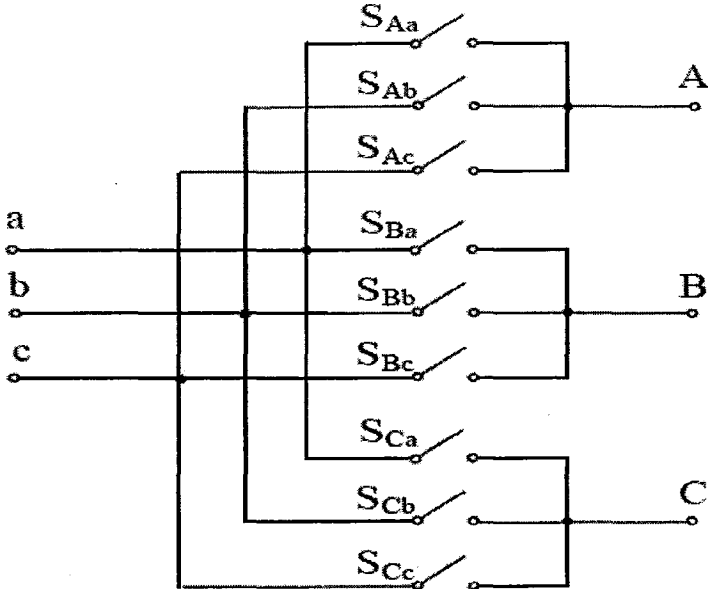


Fig. 5.5: Schematic circuit of a three-phase to three-phase matrix converter [31].

-to connect it to one of the input terminals. Most commonly used configuration is the 3x3 matrix converter. A 3 ph to 3 ph matrix converter is schematically represented in fig 5.5

Matrix converter which was proposed first proposed in 1976 attempts to control the speed of three phase machines and can render operation in all four quadrants with low harmonic contents in the input current and with high power factor. [31]

Matrix converter has many advantages over other converters. These advantages can be enumerated as follows:

Advantages: [31]

- 1) Simple and compact power circuit due to absence of large energy storage elements.
- 2) Generation of output voltage with arbitrary amplitude and frequency.
- 3) Sinusoidal input and output currents.
- 4) Operation at unity input power factor.
- 5) Bidirectional power flow.
- 6) 4-quadrant operation.
- 7) High reliability.
- 8) Harmonic reduction

Limitations: [31]

- 1) Lack of bidirectional switches.
- 2) Lower voltage transfer ratio.
- 3) Sensitive to power disturbances as they will transmit directly to output side of the converter.
- 4) No freewheeling paths, it is difficult to reliably commutate current from one switch to another.
- 5) Input power factor cannot be lower than output power factor.

5.3.2 Modulation Methods for MC:

There are many techniques proposed at different times for the control of these switches to have a fast dynamic response of the machines along with low harmonic pollution and high power factor. The most popular modulation techniques are:

- 1) Venturini method
- 2) Space vector modulation

In this work space vector modulation method is used. This modulation technique has been discussed in section 5.4.

5.3.3 Topology:

Matrix converter, in general, is a single stage converter with a matrix of $m \times n$ bidirectional power switches, designed to connect m -phase voltage sources to n -phase load. The matrix converter of 3×3 switches, shown in Fig 5.6 (a) connects a three phase source to three phase load.

In the basic topology of the Matrix Converter shown in Fig 5.6 (a), V_{si} , $i=\{A,B,C\}$, are the source voltages, i_{si} , $i=\{A, B,C\}$, are the source currents, V_{jn} , $j=\{a, b, c\}$, are the load voltages with respect to neutral n , and i_j , $j=\{a, b, c\}$, are the load currents. Additionally, other auxiliary variables have been defined to be used as a basis of the modulation and control strategies: V_i , $i=\{A, B,C\}$, are the matrix converter input voltages i_i , $i=\{A, B,C\}$, are the converter input currents.[31]

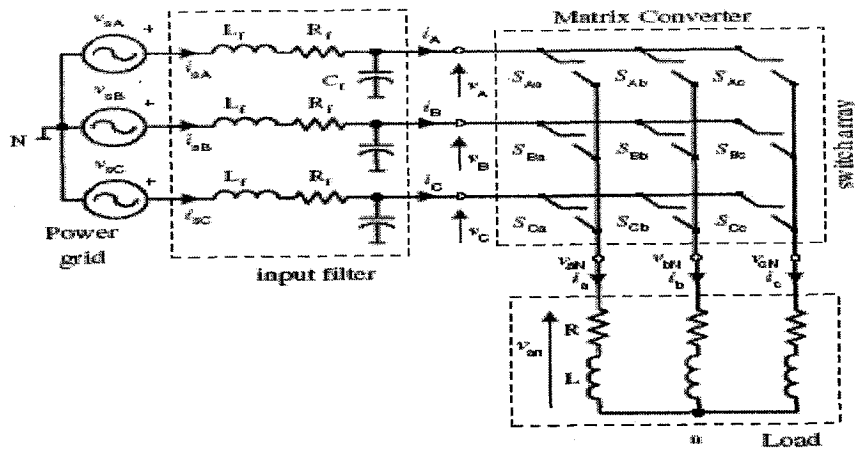


Fig 5.6 (a): Basic power circuit of matrix converter [31]

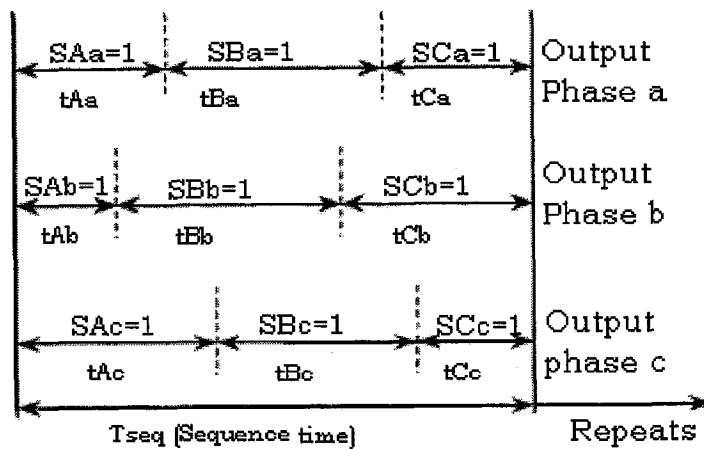


Fig 5.6 (b): General form of switching pattern [31].

Each switch S_{ij} , $i = \{A, B, C\}$, $j = \{a, b, c\}$, can connect or disconnect phase i of the supply to phase j of the load and, with a proper combination of the conduction states of these switches, arbitrary output voltages V_{jN} can be synthesized. Each switch is characterized by a switching function, defined as follows:

$$\begin{aligned}
 S_{ij}(t) &= 0 \text{ if switch } S_{ij} \text{ is open} \\
 S_{ij}(t) &= 1 \text{ if switch } S_{ij} \text{ is closed}
 \end{aligned}
 \tag{5.1}$$

Two basic switching state rules must be followed:

- 1) Two different input lines should not be connected to same output line. This results in short circuit of the supply.
- 2) None of the output lines should be disconnected. This results in open circuit of the load which may cause overvoltage as the load is inductive load.[31]

These conditions can be stated in more compact form as follows:

$$\sum_{i=A,B,C} S_{ij}(t) = 1; j = \{a, b, c\} \quad (5.2)$$

Applying Kirchhoff's voltage law to the switch array, it can be easily found that

$$\begin{bmatrix} V_{aN}(t) \\ V_{bN}(t) \\ V_{cN}(t) \end{bmatrix} = \begin{bmatrix} S_{Aa}(t) & S_{Ba}(t) & S_{Ca}(t) \\ S_{Ab}(t) & S_{Bb}(t) & S_{Cb}(t) \\ S_{Ac}(t) & S_{Bc}(t) & S_{Cc}(t) \end{bmatrix} \begin{bmatrix} V_{AN}(t) \\ V_{BN}(t) \\ V_{CN}(t) \end{bmatrix} \quad (5.3a)$$

$$V_o(t) = S(t) \cdot V_{in}(t) \quad (5.3b)$$

It is worth noting that equation (5.3) is only valid if (5.2) holds. Otherwise, these equations are inconsistent with physical element distribution of Fig 5.7. Applying Kirchhoff's current law to the switch array, it is found that:

$$\begin{bmatrix} i_A(t) \\ i_B(t) \\ i_C(t) \end{bmatrix} = \begin{bmatrix} S_{Aa}(t) & S_{Ab}(t) & S_{Ac}(t) \\ S_{Ba}(t) & S_{Bb}(t) & S_{Bc}(t) \\ S_{Ca}(t) & S_{Cb}(t) & S_{Cc}(t) \end{bmatrix} \begin{bmatrix} i_a(t) \\ i_b(t) \\ i_c(t) \end{bmatrix} \quad (5.4a)$$

$$I_{in}(t) = S^T(t) \cdot I_o(t) \quad (5.4b)$$

Where $S^T(t)$ is the transpose of matrix $S(t)$.

Equation (5.3) and (5.4) are the basis of all modulation methods which consists in selecting appropriate combinations of open and closed switches to generate the desired output voltages. It is important to note that the output voltages V_{jn} , $j=\{a, b, c\}$, are synthesized using the three input voltages V_i , $i=\{A, B, C\}$ and that the input currents i_i , $i=\{A, B, C\}$ are the results from the connection of output lines to the supply. Output currents i_j , $j=\{a, b, c\}$ which are sinusoidal if the load has a low pass frequency response.

5.3.4. Performance of Matrix Converter:

This section gives a short account of the performance of the matrix converter along with its qualitative analysis.

Output Voltage Magnitude and Frequency:

The instantaneous output voltage of any phase of a matrix converter is nothing but the input phase to which the output phase is connected through the switch of the matrix converter. A sampling period which is very low compared to the time periods of both the output and input is considered in which the average of the output voltage obtained from the three input phases is equal to the target value. Hence it is obvious that the profile of the output voltage has to fit within the profile of the input voltage. This fact sets a limit on the maximum value of the output voltage that can be obtained using a matrix converter. This value is $\sqrt{3}/2$ times the input voltage without going to the region of over modulation.

The frequency of the output is limited by the sampling frequency. For all practical purposes, the output frequency should never be more than a tenth of the sampling frequency.

Fig 5.7 (a) shows the output voltage of a matrix converter side by side a voltage source inverter. The matrix converter has its output node voltage equal to any of the input voltages depending on which one among the switches is connected. So it depends on time varying value of the supply voltage. This causes a reduction in the harmonics.

Whereas the output of the VSI is one of the bus voltages of the dc link which is fixed in time, matrix converter will have output voltage equal to any of the m input lines and these voltages is time varying in magnitude. [31]

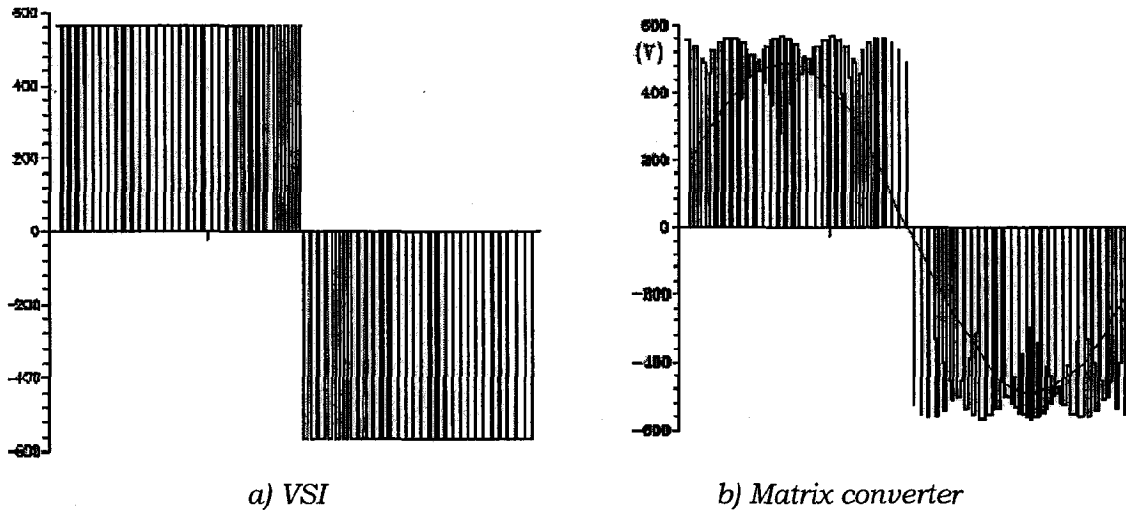


Fig 5.7(a); Output voltage waveforms generated by a VSI and a matrix converter

Input Current:

The input current of the matrix converter is the result of connection of the output phase with the input lines. Depending on which output phase is connected to the input line the instantaneous input currents are obtained. It is a piecewise sampling of the output current which composes the input current. Since the load is acting as a low pass filter, the output current is almost sinusoidal, but the input current which is composed of different output currents at different instants is rich in harmonics. Particularly the harmonics of the frequency of sampling frequency will have magnitude almost equal to the fundamental. Hence an input filter is essential to filter out these components. But in VSI, even lower order harmonics have significant magnitude. So, it needs heavier filters. Because matrix converter needs these filters, it is not an all-silicon converter to the strictest sense of the expression.

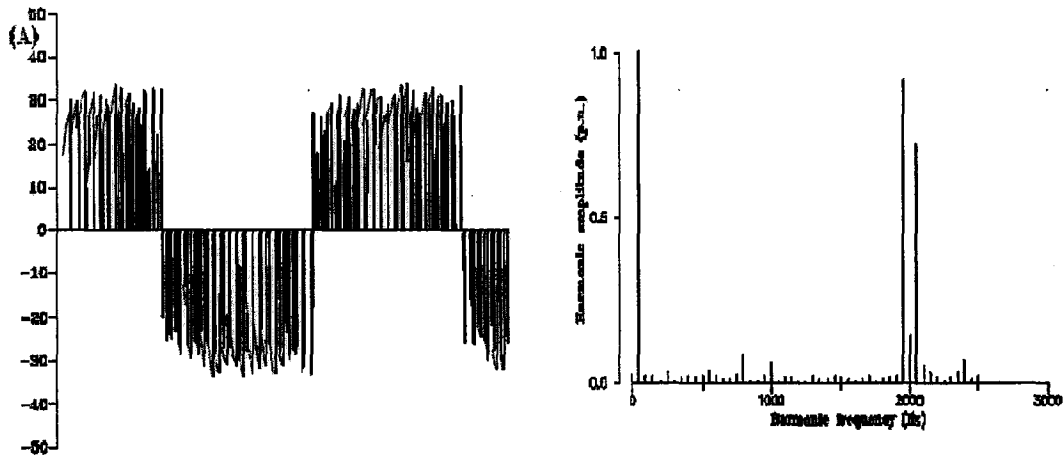


Fig.5.7 (b): Matrix converter input current and harmonic spectrum. Switching Frequency 2 kHz.

The input power factor control:

The input power factor control capability is another attractive feature of matrix converters, which holds for most of the control algorithms.

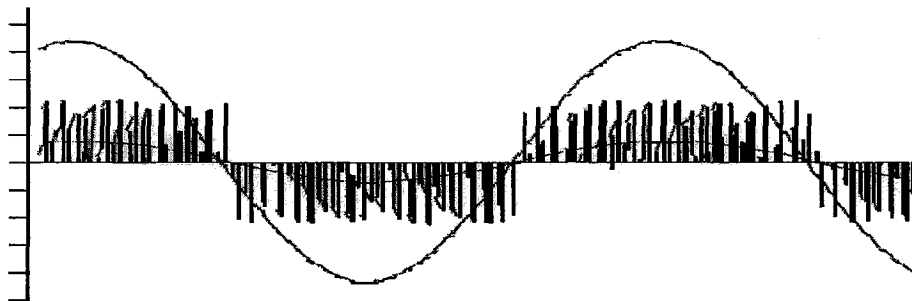


Fig.5.8: Matrix converter input line-to-neutral voltage, instantaneous input Current and its average value, Switching frequency 2 kHz.

5.3.5 Implementation of the Matrix Converter:

From the theory of the matrix converter, one might have an impression that it is having a wide acceptance in its use. But, a number of practical problems associated with this topology have led to limited acceptance of matrix converter. The unavailability of bidirectional switches and commutation of these switches in a systematic manner are the challenges posed by topology of matrix converter.

Bidirectional Switch Realization:

A matrix converter being an ac converter needs to conduct current in both directions as well as block voltages in both directions when necessary. Unfortunately, there is no single device available today which can serve the above needs. So, these properties of the switches are obtained by combining more than one device. This results in more complexity and higher losses associated with the switches both during switching and when the devices are ON. The switches are classified into four categories depending upon the direction of conduction and their capability to block voltage. It shows:

- a) Switches with bidirectional operations featured by 4 basic operations.
- b) Switches without direction operations featured by 2 basic operations.

Two different states of gate G; 1: charged 0: uncharged. Indexed v: forward r: reverse) leads in the case of topology with two transistor/gates to four different states of a bidirectional switch.

- I. Forward blocking reverse blocking-that is interruption.
- II. Forward conducting reverse blocking-that is ideal diode.
- III. Forward blocking reverse conducting -that is ideal reverse diode.
- IV. Forward conducting reverse conducting-that is bidirectional close.

Current Commutation:

Current commutation in matrix converter is more complicated than that in voltage source inverters. This is due to the absence of any freewheeling path in matrix converters. The two rules which should be followed to turn on the switches (mentioned in article 5.3) make the process more difficult since there is no switch that can turn off and on instantaneously. Matrix converter requires an instantaneous switching off of the outgoing device and instantaneous switching on the incoming device. If there is a delay between switching on and switching off, then rule 2 is violated. Again an overlap period between the incoming and outgoing switch

will cause short circuit of the supply. These two violations are shown in fig 5.9. The row 1 has open circuit of the load with all S_{11} , S_{21} and S_{31} off, causing phase 1 of the load to be open circuited. The row 2 has two switches on: S_{22} and S_{32} causing phase 2 and 3 of the input to be shorted.

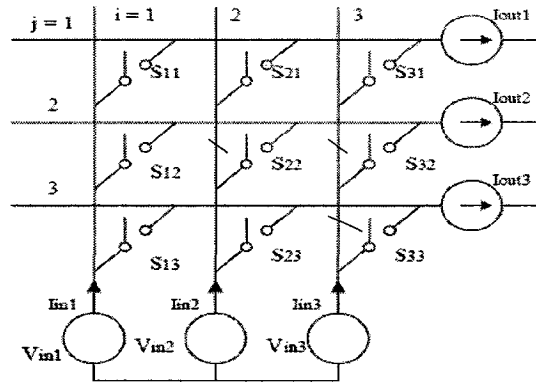


Fig 5.9: Illegal switching of Matrix Converter

There are several techniques that can be used for current commutation:

- 1) Dead-time current commutation
- 2) Overlap time current commutation
- 3) Semi soft current commutation

In this work, dead time current commutation has been used.

Dead-Time Current Commutation:

In this method the outgoing device is turned off first and then only the incoming device is turned on. Apparently, there is a momentary open circuit of the load terminal at this time. Now, the load current is carried by the snubber circuit connected across the switches. This causes increased complexity in the design of the snubber circuit and additional losses. Moreover the sizes of the clamping devices increase making the converter more bulky.

Semiconductor losses:

Due to the unavailability of suitable bidirectional devices, the switches are fabricated using two or more devices. This leads to more switching loss and conduction loss. Moreover, the switching losses are proportional to the switching frequency. In case of the combination of the diode bridge and the IGBT, we see in any path there are three devices in series. The loss in any device is the product of the on-state voltage and current. So the losses in this case are more. [31]

Modulation techniques:

Modulation is used to generate the gate signals to the switches of a converter at opportune moments to get the desired output voltage from a fixed supply having fixed magnitude and frequency. There are different modulation techniques: venturini method, space vector modulation

Conclusion:

The matrix converter is a simple device in topology without much complexity. Some problems associated with it are the lack of bidirectional switches. So, these switches are made of multiple devices increasing the conduction losses. The absence of freewheeling path also complicates the design of the snubber circuits and additional clamping circuits are needed to protect the converter and the load during faults.

5.4 Space Vector Modulation:

Introduction:

In this section the space vector modulation (SVM) method of control of matrix converter has been discussed. First, the voltage space vector modulation in a voltage source inverter (VSI) is considered, and then the space vector modulation on the voltage source rectifier (VSR) is considered. The dc link of the VSI is supplied by the VSR. The input current of the VSR should be sinusoidal. So SVM is applied to the input current of the VSR.

The concept of this VSI-VSR combination is extended to matrix converter as the dc link in the VSR-VSI combination can be taken as a short circuit between the two. Figure 5.10 illustrates a VSR-VSI combination.

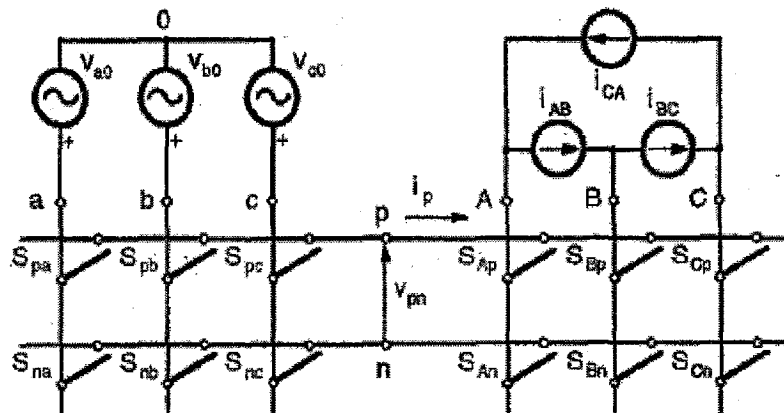


Fig 5.10: Emulation of VSR-VSI conversion [32]

5.4.1 Distribution of Space Vectors:

In a matrix converter, there are nine switches each having two states (ON and OFF). So there can be $2^9 = 512$ switching combinations. But the equation (5.2) specifies the two rules which should be followed for a matrix converter. This limits the number of valid switching combinations to 27. These 27 combinations are classified into 3 groups according to the nature of the vectors they generate:

- *Group I:* Each of the output lines are connected to different input lines, resulting in a vector of constant magnitude rotating in space at a constant speed and capable of rotating in both the directions.

- *Group II:* Here two output lines are connected to one input line and the other output line is connected to a different input line. These results in a vector having a fixed direction in space and occupying one of the 6 positions regularly spaced on the sextant. The maximum magnitude of these vectors is $2/\sqrt{3}$ times V_{env} . Where V_{env} is the instantaneous value of the output of the VSR.

- *Group III:* All output lines are connected to a common input line. Output space vectors have zero amplitude (i.e., located at the origin).

Group I vectors are not used as they have changing directions. The desired vector with a particular magnitude and direction is obtained using group II and III vectors. The voltage hexagon is shown in fig 5.11.

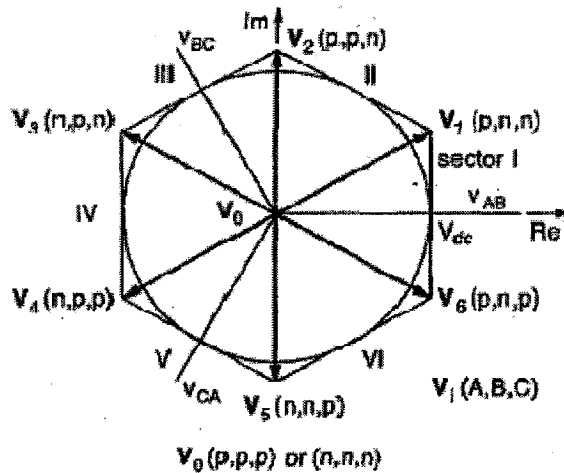


Fig 5.11: VSI hexagon [12]

5.4.2 Voltage and Current Space Vectors:

The output voltage of the VSI is controlled using SVM so that it contains minimum harmonics. Similarly, the input current from the supply should be rid of harmonics and so the input current of the VSR is controlled by SVM. In this article first the transformation matrix for the VSI is derived and then the same is

derived for VSR. Next, the two matrices are combined in order to implement SVM in matrix converter.

5.4.3 VSI Output Voltage SVM:

Consider the VSI part of the circuit in Fig. 5.10 as a standalone VSI supplied by a dc voltage source, $v_{pn} = V_{dc}$. The VSI switches can assume only six allowed combinations which yield nonzero output voltages, and two combinations with zero output voltages. Hence, the resulting output line-voltage space vector defined by

$$v_{oL} = \frac{2}{3} \cdot (v_{AB} + v_{BC} \cdot e^{+j120^\circ} + v_{CA} \cdot e^{-j120^\circ}) \quad (5.5)$$

The above equation can assume only seven discrete values, $V_0 - V_6$ in Fig. 5.11, called voltage switching state vectors (SSV's). The space vector of the desired output line voltages is given by

$$\bar{v}_{oL} = \sqrt{3} \cdot V_{om} \cdot e^{j(\omega_o t - \varphi_o + 30^\circ)} \quad (5.6)$$

The above equation can be approximated by two adjacent SSV's, V_α , and V_β , and the zero voltage vector, V_0 , using PWM as shown in Fig. 5.12, where V_{oL} is the sampled value of \bar{v}_{oL} , at an instant within the switching cycle T_s . Using the law of sines, the duty cycles of the SSV's are

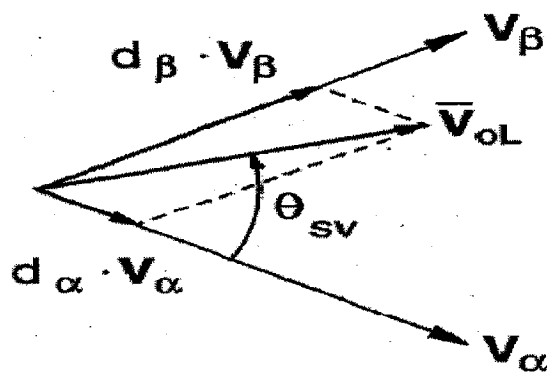


Fig 5.12: VSI SVM vector addition. [32]

$$\begin{aligned}
d_{\alpha} &= T_{\alpha}/T_s = m_v \cdot \sin(60^{\circ} - \theta_{sv}), \\
d_{\beta} &= T_{\beta}/T_s = m_v \cdot \sin(\theta_{sv}), \\
d_{ov} &= T_{ov}/T_s = 1 - d_{\alpha} - d_{\beta}
\end{aligned} \tag{5.7}$$

Where m_v is the VSI modulation index

$$0 \leq m_v = (\sqrt{3} \cdot V_{om})/V_{dc} \leq 1 \tag{5.8}$$

Table 5.1*

3Φ-3Φ MC Switching Combinations[32]

Group	A B C	V _{AB} V _{BC} V _{CA}	i _a i _b i _c	S _{Aa} S _{Ab} S _{Ac}	S _{Ba} S _{Bb} S _{Bc}	S _{Ca} S _{Cb} S _{Cc}
I	a b c	V _{ab} V _{bc} V _{ca}	i _A i _B i _C	1 0 0	0 1 0	0 0 1
	a c b	-V _{ca} -V _{bc} -V _{ab}	i _A i _C i _B	1 0 0	0 0 1	0 1 0
	b a c	-V _{ab} -V _{ca} -V _{bc}	i _B i _A i _C	0 1 0	1 0 0	0 0 1
	b c a	V _{bc} V _{ca} V _{ab}	i _C i _A i _B	0 1 0	0 0 1	1 0 0
	c a b	V _{ca} V _{ab} V _{bc}	i _B i _C i _A	0 0 1	1 0 0	0 1 0
	c b c	-V _{bc} -V _{ab} -V _{ca}	i _C i _B i _A	0 0 1	0 1 0	1 0 0
II-A	a c c	-V _{ca} 0 V _{ca}	i _A 0 -i _A	1 0 0	0 0 1	0 0 1
	b c c	V _{bc} 0 -V _{bc}	0 i _A -i _A	0 1 0	0 0 1	0 0 1
	b a a	-V _{ab} 0 V _{ab}	-i _A i _A 0	0 1 0	1 0 0	1 0 0
	c a a	V _{ca} 0 -V _{ca}	-i _A 0 i _A	0 0 1	1 0 0	1 0 0
	c b b	-V _{bc} 0 V _{bc}	0 -i _A i _A	0 0 1	0 1 0	0 1 0
	a b b	V _{ab} 0 -V _{ab}	i _A -i _A 0	1 0 0	0 1 0	0 1 0
II-B	c a c	V _{ca} -V _{ca} 0	i _B 0 -i _B	0 0 1	1 0 0	0 0 1
	c b c	-V _{bc} V _{bc} 0	0 i _B -i _B	0 0 1	0 1 0	0 0 1
	a b a	V _{ab} -V _{ab} 0	i _B i _B 0	0 0 0	0 1 0	1 0 0
	a c a	-V _{ca} V _{ca} 0	-i _B 0 i _B	1 0 0	0 0 1	1 0 0
	b c b	V _{bc} -V _{bc} 0	0 -i _B i _B	0 1 0	0 0 1	0 1 0
	b a b	-V _{ab} V _{ab} 0	i _B -i _B 0	0 1 0	1 0 0	0 1 0
II-C	c c a	0 V _{ca} -V _{ca}	i _C 0 -i _C	0 0 1	0 0 1	1 0 0
	c c b	0 -V _{bc} V _{bc}	0 i _C -i _C	0 0 1	0 0 1	0 1 0
	a a b	0 V _{ab} -V _{ab}	i _C i _C 0	1 0 0	1 0 0	0 1 0
	a a c	0 -V _{ca} V _{ca}	-i _C 0 i _C	1 0 0	1 0 0	0 0 1
	b b c	0 V _{bc} -V _{bc}	0 -i _C i _C	0 1 0	0 1 0	0 0 1
	b b a	0 -V _{ab} V _{ab}	i _C -i _C 0	0 1 0	0 1 0	1 0 0
III	a a a	0 0 0	0 0 0	1 0 0	1 0 0	1 0 0
	b b b	0 0 0	0 0 0	0 1 0	0 1 0	0 1 0
	c c c	0 0 0	0 0 0	0 0 1	0 0 1	0 0 1

*In table 5.1 abc are inputs and ABC are outputs

The sectors of the VSI hexagon in Fig. 5.11 correspond directly to the six 60°-segments within a period of the desired 3Φ output line voltages shown in Fig.5.13.

The synthesis of the output line voltages for a switching cycle within the first 60°-segment is shown in Fig. 5.13(b), as an example. The local averaged output line voltages are

$$\begin{aligned} \begin{bmatrix} \bar{v}_{AB} \\ \bar{v}_{BC} \\ \bar{v}_{CA} \end{bmatrix} &= \begin{bmatrix} d_\alpha + d_\beta \\ -d_\alpha \\ -d_\beta \end{bmatrix} \cdot V_{dc} \\ &= m_v \cdot \begin{bmatrix} \cos(\theta_{sv} - 30^\circ) \\ -\sin(60^\circ - \theta_{sv}) \\ -\sin(\theta_{sv}) \end{bmatrix} \cdot V_{dc} \end{aligned} \quad (5.9)$$

For the first 60°-segment

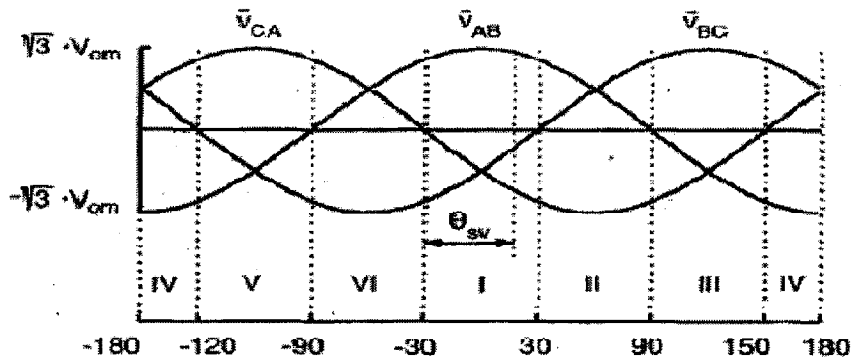
$$\begin{aligned} -30^\circ &\leq \omega_o t - \varphi_o + 30^\circ \leq +30^\circ \\ \theta_{sv} &= (\omega_o t - \varphi_o + 30^\circ) + 30^\circ \end{aligned} \quad (5.10)$$

By substitution of (5.10) in (5.9)

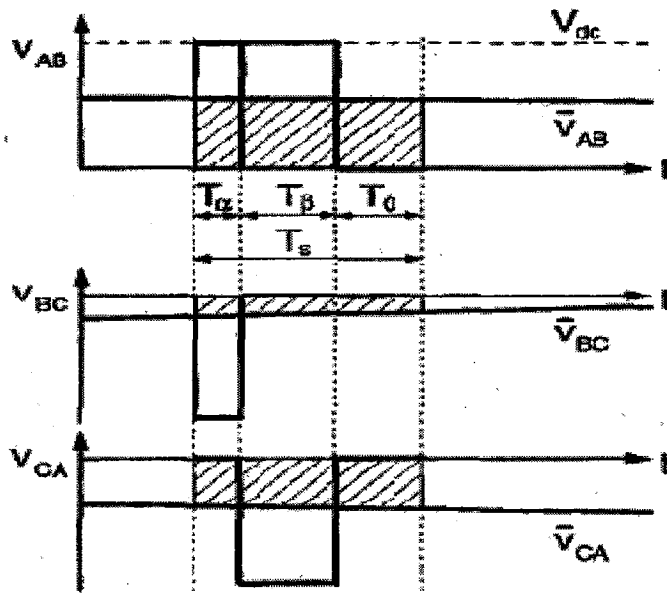
$$\begin{aligned} \begin{bmatrix} \bar{v}_{AB} \\ \bar{v}_{BC} \\ \bar{v}_{CA} \end{bmatrix} &= m_v \cdot \begin{bmatrix} \cos(\omega_o t - \varphi_o + 30^\circ) \\ \cos(\omega_o t - \varphi_o + 30^\circ - 120^\circ) \\ \cos(\omega_o t - \varphi_o + 30^\circ + 120^\circ) \end{bmatrix} \cdot V_{dc} \\ &= \bar{T}_{VSI} \cdot V_{dc} \end{aligned} \quad (5.11)$$

The VSI local-averaged input current is determined as

$$\bar{i}_p = T_{VSI}^T \cdot i_{oL} = \frac{\sqrt{3}}{2} \cdot I_{om} \cdot m_v \cdot \cos(\varphi_L) = const \quad (5.12)$$



(a)



(b)

Fig 5.13: (a) Output line voltage 60°-segments. [32]

(b) Synthesis of VSI output line voltages. [32]

5.4.4 VSR Input Current SVM:

Consider the VSR part of the circuit in Fig. 5.10 as a standalone VSR loaded by a dc current generator, $i_p = I_{dc}$. The VSR input-current SVM is completely analogous to the VSI output-voltage SVM. The VSI subscripts α , β and s_v , are

replaced with the VSR subscripts μ , ν and sc , respectively. The VSR hexagon is shown in Fig. 5.14. The VSR duty cycles are [33]

$$\begin{aligned}d_{\mu} &= T_{\mu}/T_s = m_c \cdot \sin(60^{\circ} - \theta_{sc}) \\d_{\nu} &= T_{\nu}/T_s = m_c \cdot \sin(\theta_{sc}) \\d_{oc} &= T_{oc}/T_s = 1 - d_{\mu} - d_{\nu}\end{aligned}\tag{5.13}$$

Where m_c , is the VSR modulation index

$$0 \leq m_c = (I_{tm})/I_{dc} \leq 1\tag{5.14}$$

Examples of the local-averaged input phase currents, for a switching cycle within the first sector of the VSR hexagon, are

$$\begin{aligned}\begin{bmatrix} \bar{i}_a \\ \bar{i}_b \\ \bar{i}_c \end{bmatrix} &= \begin{bmatrix} d_{\mu} + d_{\nu} \\ -d_{\mu} \\ -d_{\nu} \end{bmatrix} \cdot I_{dc} \\ &= m_c \cdot \begin{bmatrix} \cos(\theta_{sc} - 30^{\circ}) \\ -\sin(60^{\circ} - \theta_{sc}) \\ -\sin(\theta_{sc}) \end{bmatrix} \cdot I_{dc}\end{aligned}\tag{5.15}$$

By substitution of

$$\begin{aligned}\theta_{sc} &= (\omega_i t - \varphi_i) + 30^{\circ} \\ -30^{\circ} &\leq \omega_o t - \varphi_o + 30^{\circ} \leq +30^{\circ}\end{aligned}\tag{5.16}$$

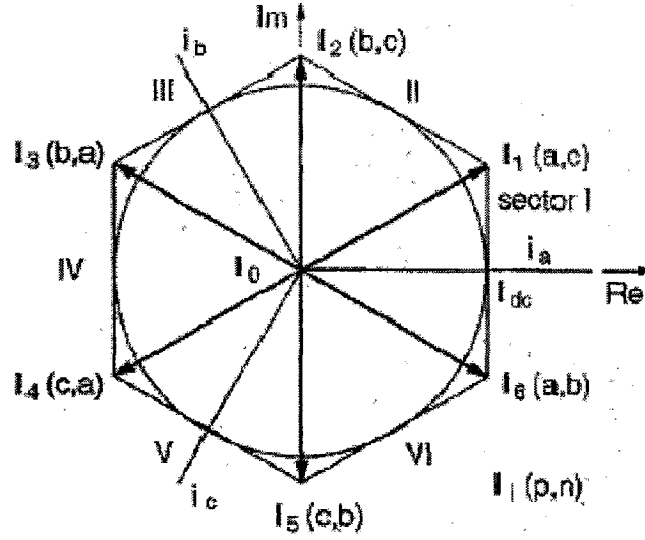


Fig 5.14: VSR hexagon. [33]

For first sector in equation (5.15), LF transfer matrix of the VSR, T_{VSR} , is defined as

$$\begin{bmatrix} \bar{i}_a \\ \bar{i}_b \\ \bar{i}_c \end{bmatrix} = m_c \cdot \begin{bmatrix} \cos(\omega_i t - \varphi_i) \\ \cos(\omega_i t - \varphi_i - 120^\circ) \\ \cos(\omega_i t - \varphi_i + 120^\circ) \end{bmatrix} \cdot I_{dc} = \bar{T}_{VSR} \cdot I_{dc} \quad (5.17)$$

The VSR local averaged output voltage is determined as

$$\begin{aligned} \bar{v}_{pn} &= \bar{T}_{VSR}^T \cdot v_{iph} \\ &= \frac{3}{2} \cdot m_c \cdot V_{im} \cdot \cos(\varphi_i) = const \end{aligned} \quad (5.18)$$

5.4.5 MC Output-Voltage and Input-Current SVM:

As the local-averaged output voltage of the SVM VSR, eq (5.18), and the local-averaged input current of the SVM VSI, eq (5.12), is constant, from the local-averaged point of view the SVM VSR and the SVM VSI can be directly connected. Substituting v_{pn} from eq(5.18) for v_{dc} in eq (5.11) and using T_{VSR} from eq (5.17), the same expression for the LF transfer matrix of the 3Φ-3Φ, MC is obtained as

$$\bar{T}_{PhL} = m \cdot \begin{bmatrix} \cos(\omega_i t - \varphi_i) \\ \cos(\omega_i t - \varphi_i - 120^\circ) \\ \cos(\omega_i t - \varphi_i + 120^\circ) \end{bmatrix}^T \cdot \begin{bmatrix} \cos(\omega_o t - \varphi_o + 30^\circ) \\ \cos(\omega_o t - \varphi_o + 30^\circ - 120^\circ) \\ \cos(\omega_o t - \varphi_o + 30^\circ + 120^\circ) \end{bmatrix} \quad (5.19)$$

with $m = m_c \cdot m_v$. For simplicity, it is convenient to choose $m_c = 1$ and $m = m_v$. This completes the first step of the HF-synthesis procedure. Since both the VSI and the VSR hexagons contain six sectors, there are $6 \times 6 = 36$ combinations or operating modes. If at a particular instant, the first output-voltage 60° -segment and the first input-current 60° -segment are active, then by using (5.10) and (5.16), the LF transfer matrix (5.19) becomes

$$\bar{T}_{PhL} = m \cdot \begin{bmatrix} \cos(\theta_{sv} - 30^\circ) \\ -\sin(60^\circ - \theta_{sv}) \\ -\sin(\theta_{sv}) \end{bmatrix}^T \cdot \begin{bmatrix} \cos(\theta_{sc} - 30^\circ) \\ -\sin(60^\circ - \theta_{sc}) \\ -\sin(\theta_{sc}) \end{bmatrix} \quad (5.20)$$

Substituting (5.9) and (5.15) in (5.20), with $m = m_v \cdot m_c$, the local-averaged output line-voltages are

$$\begin{bmatrix} \bar{v}_{AB} \\ \bar{v}_{BC} \\ \bar{v}_{CA} \end{bmatrix} = \begin{bmatrix} d_\alpha + d_\beta \\ -d_\alpha \\ -d_\beta \end{bmatrix} \cdot \begin{bmatrix} d_\mu + d_v \\ -d_\mu \\ -d_v \end{bmatrix}^T \cdot \begin{bmatrix} v_{ao} \\ v_{bo} \\ v_{co} \end{bmatrix} \quad (5.21)$$

Using

$$v_{ab} = v_{ao} - v_{bo} \quad \text{and} \quad v_{ac} = v_{ao} - v_{co} \quad (5.22)$$

it is finally obtained

$$\begin{bmatrix} \bar{v}_{AB} \\ \bar{v}_{BC} \\ \bar{v}_{CA} \end{bmatrix} = \begin{bmatrix} d_{\alpha\mu} + d_{\beta\mu} \\ -d_{\alpha\mu} \\ -d_{\beta\mu} \end{bmatrix} \cdot v_{ab} + \begin{bmatrix} d_{\alpha v} + d_{\beta v} \\ -d_{\alpha v} \\ -d_{\beta v} \end{bmatrix} \cdot v_{ac} \quad (5.23)$$

Where

$$\begin{aligned} d_{\alpha\mu} &= d_\alpha \cdot d_\mu = m \cdot \sin(60^\circ - \theta_{sv}) \cdot \sin(60^\circ - \theta_{sc}) = T_{\alpha\mu}/T_s \\ d_{\beta\mu} &= d_\beta \cdot d_\mu = m \cdot \sin(\theta_{sv}) \cdot \sin(60^\circ - \theta_{sc}) = T_{\beta\mu}/T_s \\ d_{\alpha v} &= d_\alpha \cdot d_v = m \cdot \sin(60^\circ - \theta_{sv}) \cdot \sin(\theta_{sc}) = T_{\alpha v}/T_s \\ d_{\beta v} &= d_\beta \cdot d_v = m \cdot \sin(\theta_{sv}) \cdot \sin(\theta_{sc}) = T_{\beta v}/T_s \end{aligned} \quad (5.24)$$

As can be seen, the output line voltages are synthesized inside each switching cycle from samples of two input line voltages, v_{ab} and v_{ac} , for the above example. By comparison of (5.23) and (5.24), it can be concluded that simultaneous output-voltage and input-current SVM can be obtained by employing the standard VSI SVM sequentially in two VSI-sub topologies of the 3Φ - 3Φ MC. When the standard VSI SVM is applied in the first VSI-sub topology, where $v_{pn} = v_{ab}$, the duty cycles of the two adjacent voltage SSV's are $d_{\alpha\mu}$ and $d_{\beta\mu}$, as defined in (5.24). The standard VSI SVM in the second VSI-sub topology, with $v_{pn} = v_{ac}$, results in the SSV duty cycles $d_{\alpha\nu}$ and $d_{\beta\nu}$, also defined in (5.24). During the remaining part of the switching cycle [22]

$$d_o = 1 - d_{\alpha\mu} - d_{\beta\mu} - d_{\alpha\nu} - d_{\beta\nu} = T_o/T_s \quad (5.25)$$

The output line voltages are equal to zero, by employing a zero SSV.

A switching sequence within one switching cycle requires decisions on which of the three switching combinations from Group III is used for the zero SSV, and on how the five switching combinations are ordered within the switching cycle. Among the possible combinations, those which require switches to change state only once during a switching cycle should be used. In this paper, the switching sequence $d_{\alpha\mu} \rightarrow d_{\beta\mu} \rightarrow d_{\beta\nu} \rightarrow d_{\alpha\nu} \rightarrow d_o$ is used, and the optimum zero SSV is chosen for each of the 36 operating modes.

Conclusion:

Space vector modulation strategy for matrix converters has been presented in this section. The modulation is done in such a way that the input current has minimum harmonics and has a power factor close to unity.

5.5 SIMULATION MODELS AND RESULTS:

5.5.1 *The SIMULINK model for the DFIG using AC/DC/AC Back to back converter using SVM:*

A 5Hp, 575V, 4poles, 50Hz, 1500 rpm, star connected Wound Rotor Induction Machine (WRIM) is chosen in the MATLAB environment. The stator of the WRIM is connected to the grid. The AC/DC/AC back to back IGBT converters are connected in the rotor circuit to integrate the rotor circuit with the grid. The machine operated in both sub and super synchronous modes to see that the power flow via converter setup is bi-directional. The Grid side converter (GSC) is controlled with the Space Vector Modulation (SVM) Technique for the process of inversion as explained in section 5.4, and for the process of rectification the GSC operates as a bridge rectifier in sub synchronous mode. The Rotor Side Converter (RSC) is controlled by a simple sinusoidal PWM technique for inversion and for rectification it acts as a simple bridge rectifier. The only strategy differs is the operating frequency in both these converters. For to integration of Rotor to grid the Voltage and the Frequency should match the Grid Voltage and frequency, for this reason a coupling transformer (which boost the voltage level to the grid voltage) is connected after the GSC. And also a star connected passive R-C filter is connected to eliminate the harmonics in the Voltage and current wave forms. The wave forms for all the voltages and currents and the machine performance characteristics, and the power flow indications are plotted in the SIMULINK and are presented in this section.

In fig 5.15 the DFIG can run both in sub synchronous mode and super synchronous mode, to make this possible the input mechanical torque is given in two steps with a timer circuit as mechanical input to the DFIG. The grid parameters are taken from MATLAB help file. The value of DC link capacitance is given as 5mF. The values of R and C in the filter circuit are 5 ohm and 5 microfarad respectively. The speed ranges are maintained as 1440rpm in sub synchronous mode and 1560 rpm in super synchronous mode.

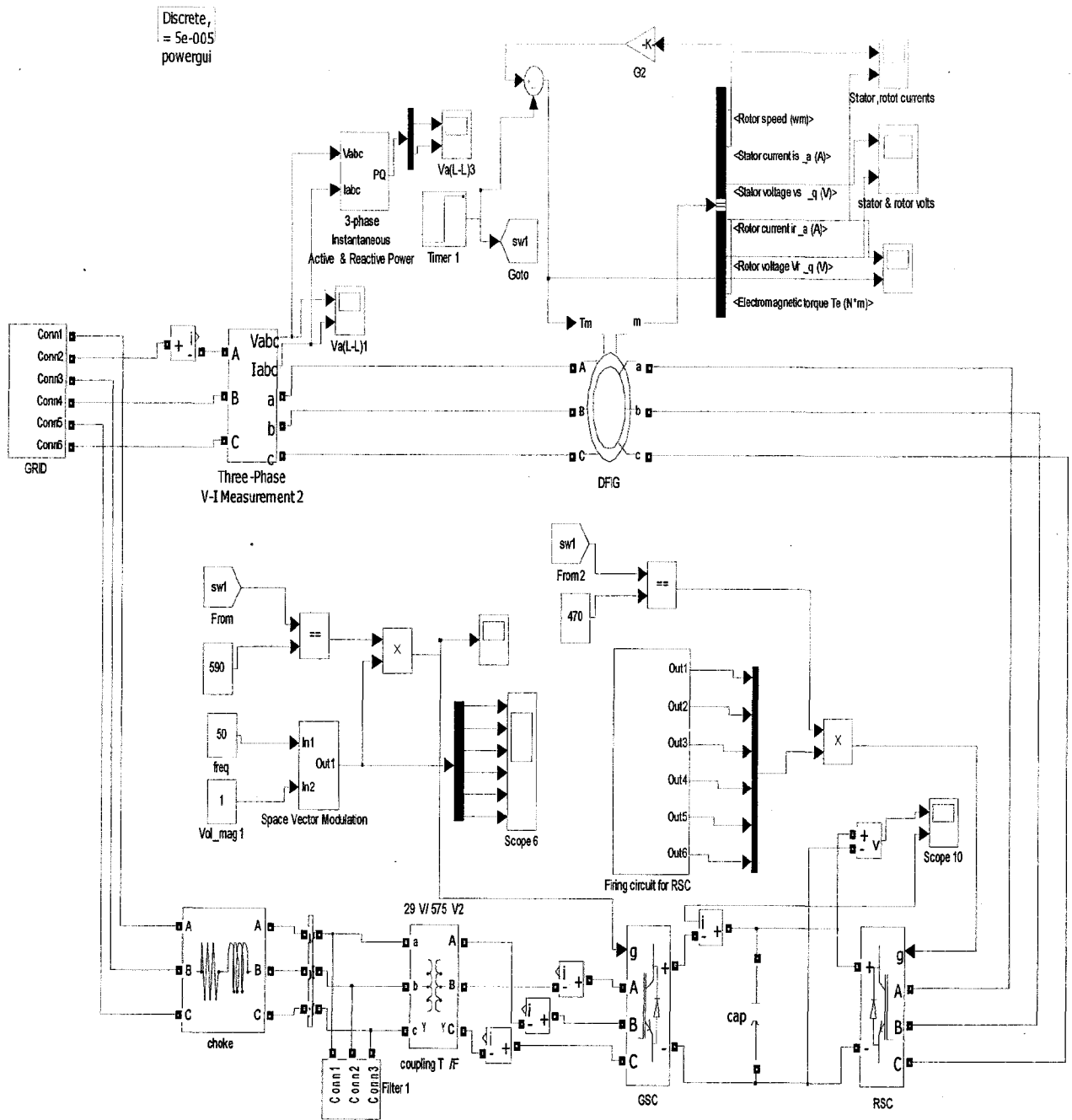


Fig5.15: The SIMULINK model for the DFIG using AC/DC/AC Back to back converters for the rotor circuit for the integration to the grid, which operates in both the sub and super synchronous modes.

5.5.2 Simulation RESULTS for Super synchronous mode DFIG using AC/DC/AC Back to back converter:

Super synchronous mode of operation of DFIG using Back to back AC/DC/AC converter topology in the rotor circuit for the integration of rotor and grid

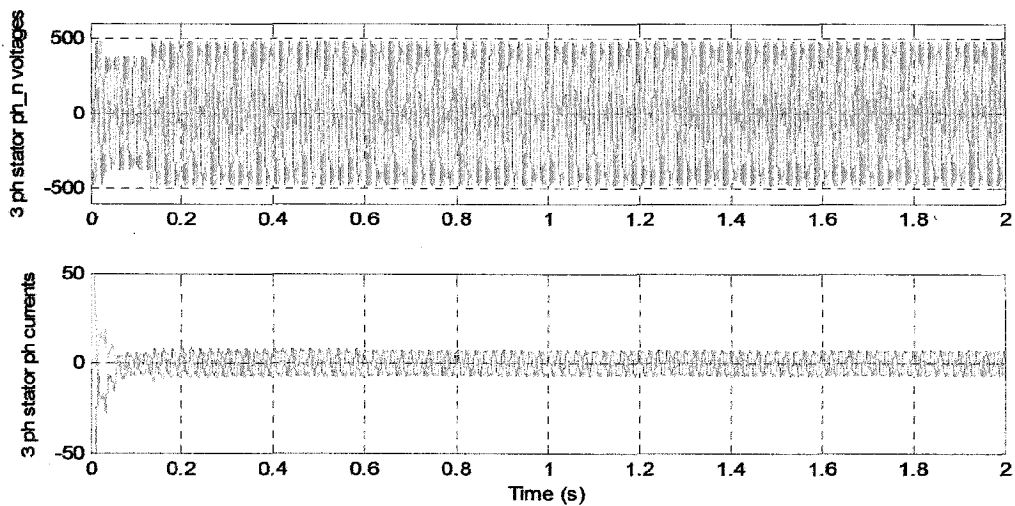


Fig5.16: 3 ph stator ph-n voltages and currents for the super synchronous mode of operation for DFIG using AC/DC/AC converter topology.

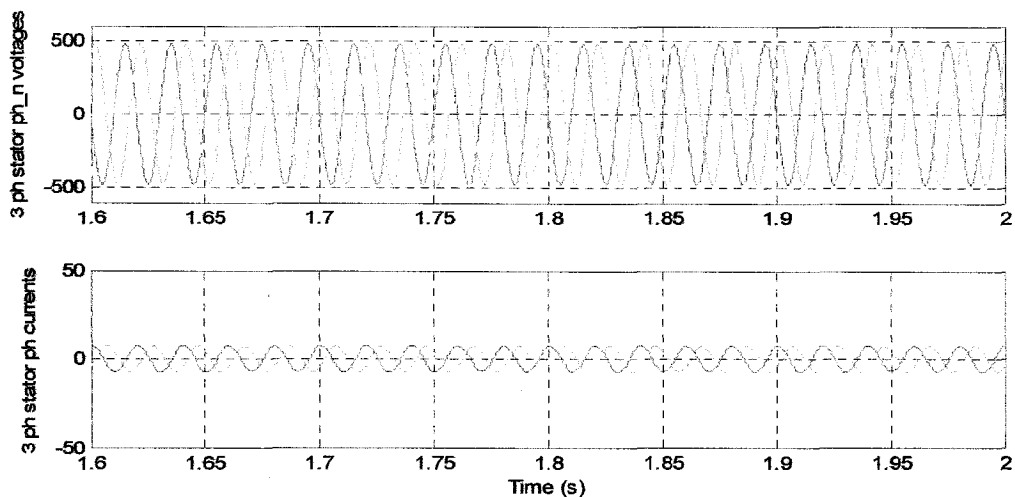


Fig5.17: The expanded wave form of fig 5.16

In figs 5.16 and 5.17 the 3-ph stator line to neutral voltages and line currents are shown, this waveform is for super synchronous mode of operation of DFIG, where the speed of DFIG is above the synchronous speed. We can observe from the waveform that the magnitude is maintained constant throughout the simulation time.

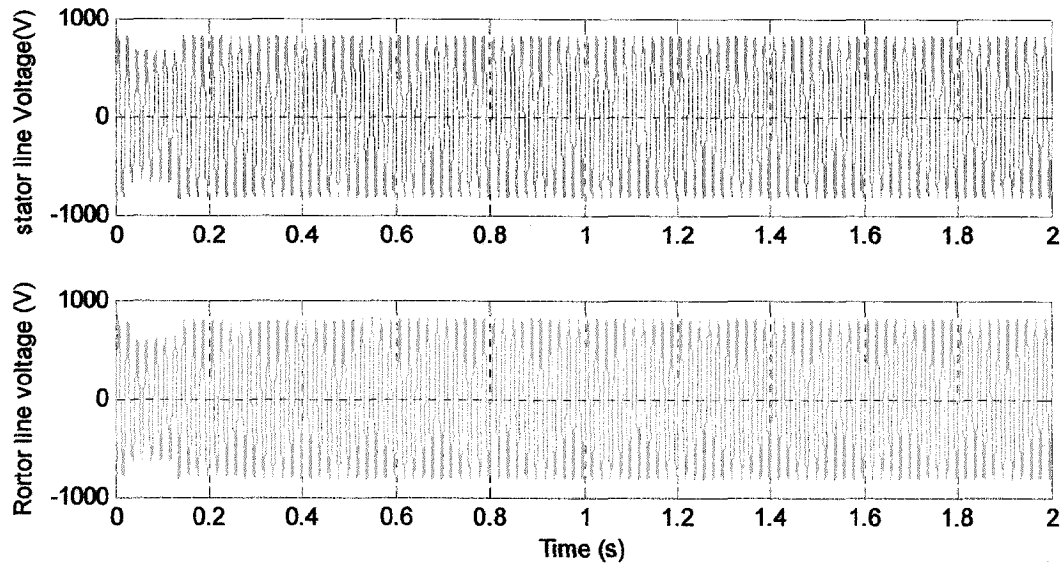


Fig5.18: The single phase stator and rotor line voltages after integrating rotor with the grid.

In fig 5.18 the simulated waveforms of single phase stator and rotor line voltages are shown. The rotor line to line voltage shown in above figure is the voltage taken in between Grid circuit and coupling transformer and the stator voltage is line to line voltage of stator terminals.

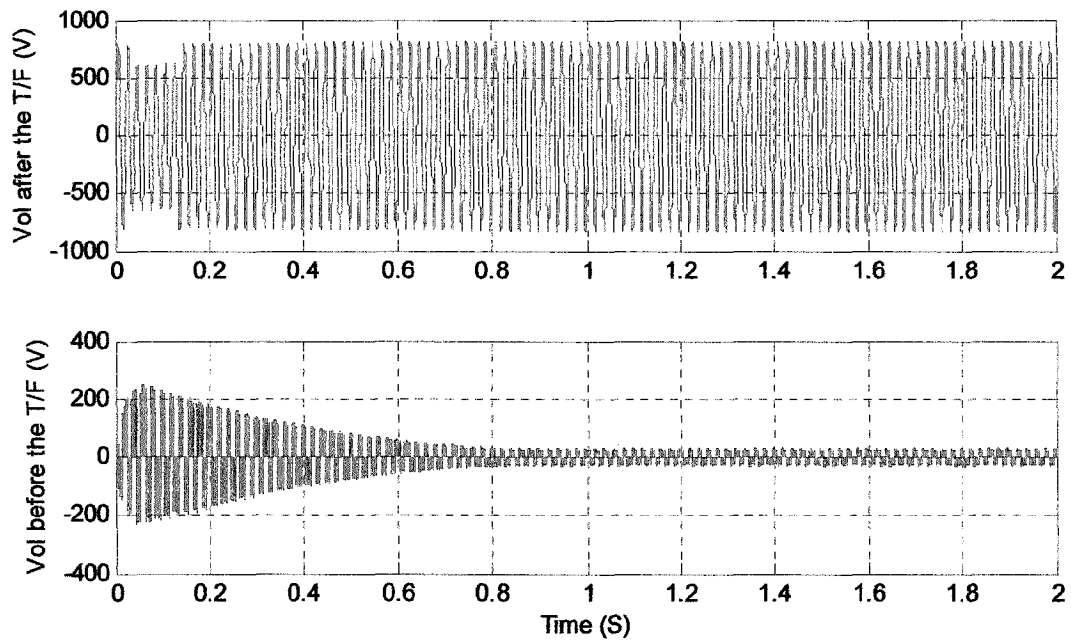


Fig5.19: The comparison of the line voltages of GSC and output of coupling T/F

In fig 5.19 the lower wave form is the line voltage at the GSC and the upper wave form is for line to line voltage taken in between grid circuit and the coupling transformer. In the GSC rotor voltage we can observe the line to line voltage of GSC is becoming constant in magnitude after 0.7 sec of simulation time. This voltage is given to the coupling transformer and thus boosted up to the grid voltage level i.e, 575 V RMS line to line, whereas the frequency of the output voltage of GSC is exactly 50Hz.

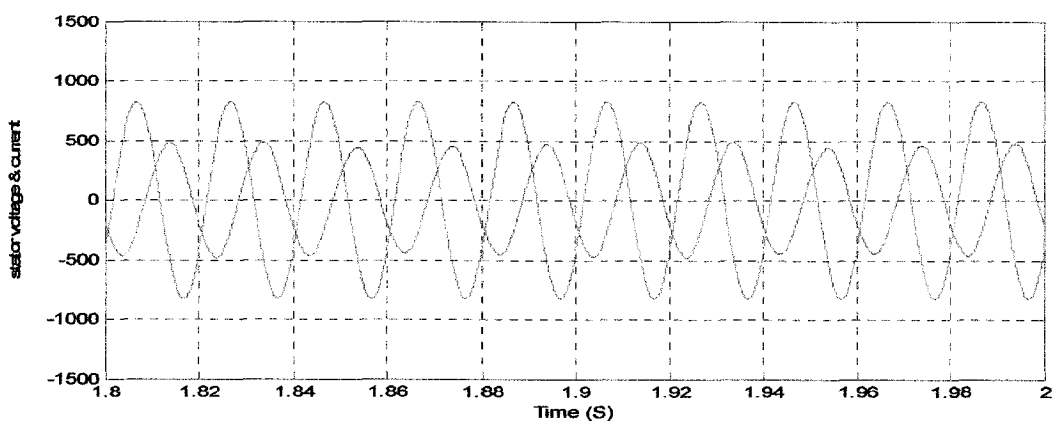


Fig5.20: The expanded wave form of stator voltage (Ph-n) and ph-current (magnitude adjusted for visibility).

In fig5.20 the line to neutral voltage and current waveforms of the stator is shown. These wave forms are adjusted in the magnitude to see the voltage and current on the same scale. The red coloured wave form is current and green coloured wave form is voltage. From the above wave forms it clear that the net power is flowing from the stator to grid, though here the power factor is not unity.

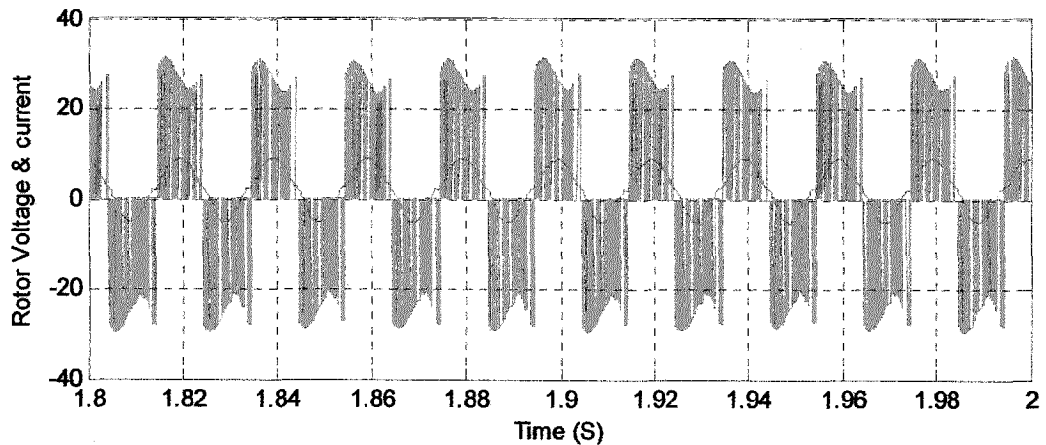


Fig5.21: The expanded wave form of rotor line voltage and current (magnitude increased for visibility) at the grid end.

In fig5.21 the line to line voltage and current waveforms of the rotor at GSC is shown. These wave forms are adjusted in the magnitude to see the voltage and current on the same scale. The green coloured wave form is current and red coloured wave form is voltage. From the voltage and current are in phase and it is clear that power is flowing from the rotor to grid, since it the DFIG is operating in super synchronous mode.

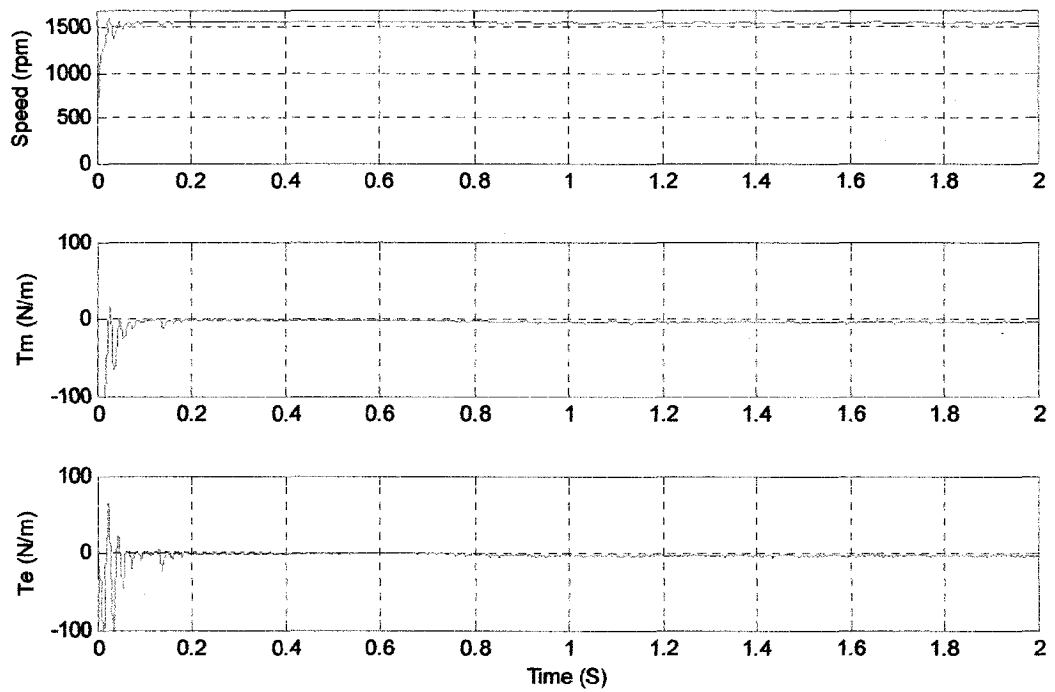


Fig5.22: The simulated wave forms of Speed, Tm and Te with respect to time for super synchronous mode of operation

In fig 5.22 the simulated waveforms of speed, input mechanical torque and electromagnetic torque of the DFIG are shown for super synchronous mode of operation. We can observe that the speed is above 1500 rpm in the top wave form in the above figure. And the waveforms of Tm and Te for super synchronous mode are negative.

5.5.3 Simulation RESULTS for Sub synchronous mode DFIG using AC/DC/AC Back to back converter:

Sub synchronous mode of operation of DFIG using Back to back AC/DC/AC converter topology in the rotor circuit for the integration of rotor and grid

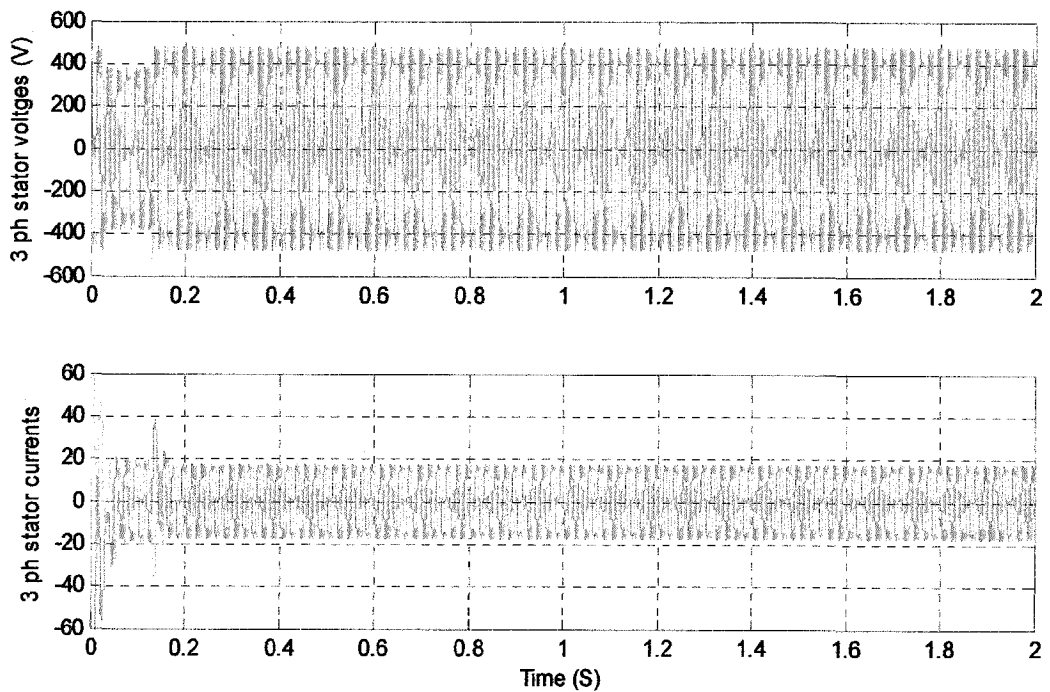


Fig5.23: The 3 ph Stator voltages (Ph-n) and current wave forms for the sub synchronous mode of operation.

In fig 5.23 the 3-ph stator line to neutral voltages and line currents are shown, this waveform is for sub synchronous mode of operation of DFIG, where the speed of DFIG is below the synchronous speed. We can observe from the waveform that the magnitude is maintained constant throughout the simulation time.

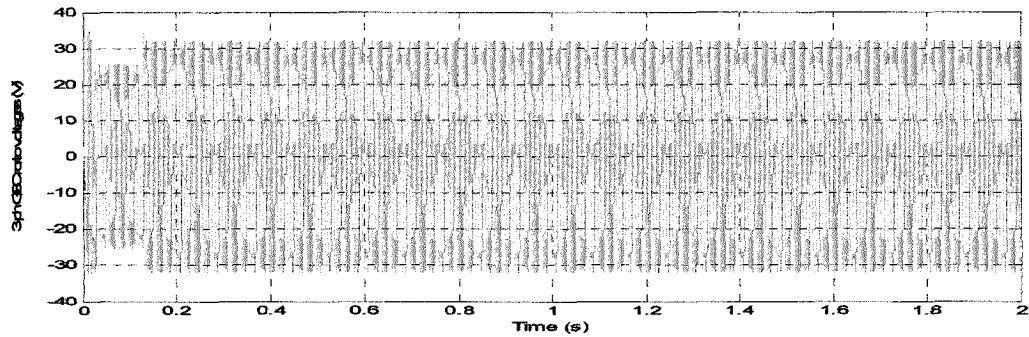


Fig5.24: The 3 Ph rotor line voltages at the grid side end of the converter.

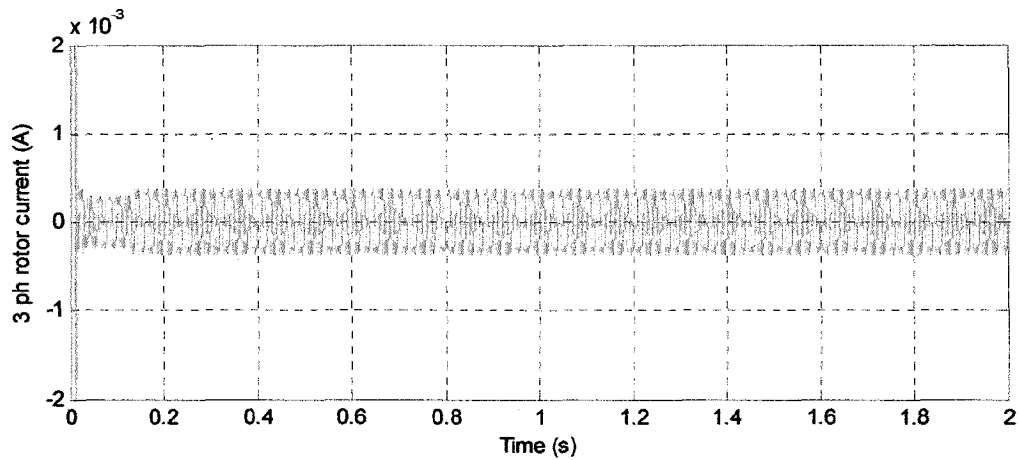


Fig5.25: The 3 Ph rotor ph currents at the grid side end of the converter.

In fig 5.24 and 5.25 the 3-ph rotor line to line voltages and line currents are shown, these waveforms are for sub synchronous mode of operation of DFIG, where the speed of DFIG is below the synchronous speed. We can observe from the waveform that the magnitude is maintained constant throughout the simulation time. These are sinusoidal and acting as the input for GSC to maintain the DC link voltage.

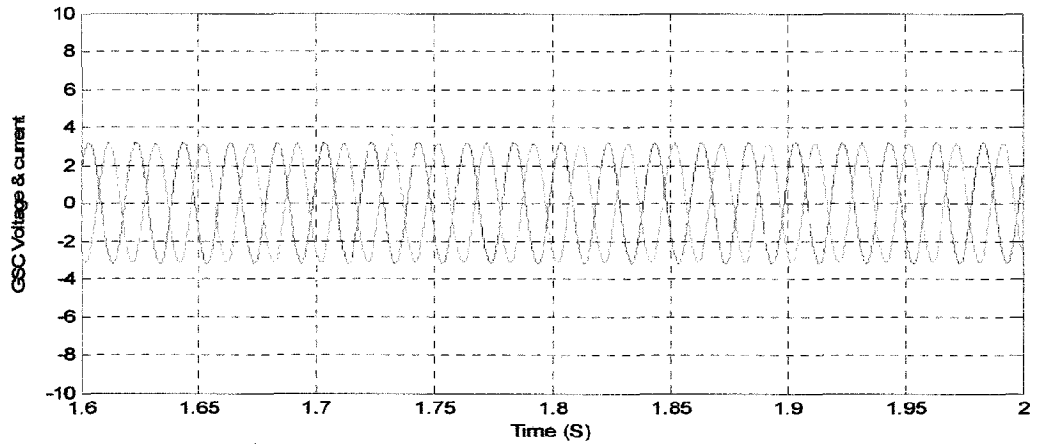


Fig5.26: The expanded wave forms of rotor line voltage (magnitude decreased for visibility) and current at the grid side converter.

From fig5.26 the line to line voltage and current waveforms of the rotor at GSC is shown. These wave forms are adjusted in the magnitude to see the voltage and current on the same scale. The green coloured wave form is current and red coloured wave form is voltage. From the voltage and current are in out of phase and it is clear that power is flowing from the grid to rotor, since it the DFIG is operating in sub synchronous mode.

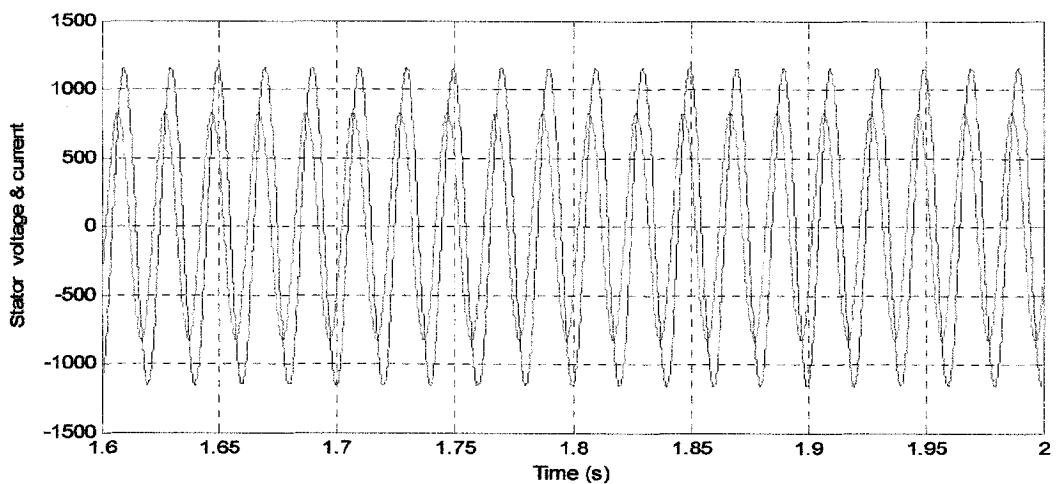


Fig5.27: Expanded wave forms of single phase stator voltage (L-n) and line current, magnitude adjusted for visibility.

From fig5.27 the line to neutral voltage and current waveforms of the stator is shown. These wave forms are adjusted in the magnitude to see the voltage and current on the same scale. The red coloured wave form is current and green coloured wave form is voltage. From the above wave forms it clear that the net power is flowing from the stator to grid, though here the power factor is not unity.

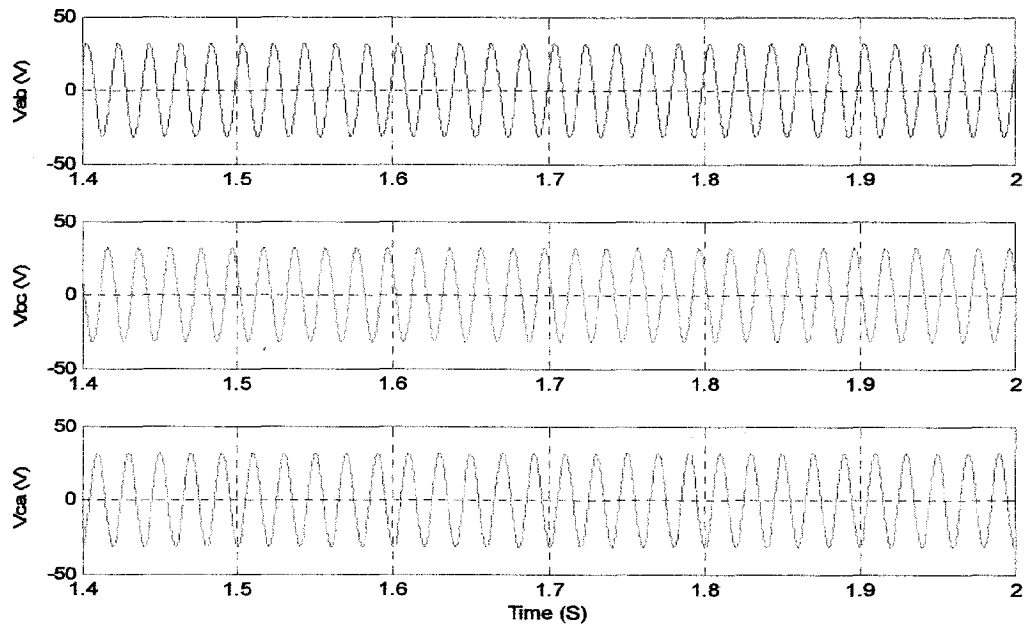


Fig5.28: single ph L-L rotor voltage wave forms at the grid side end of the converter for the sub synchronous mode of operation of DFIG using AC/DC/AC converter topology for rotor circuit.

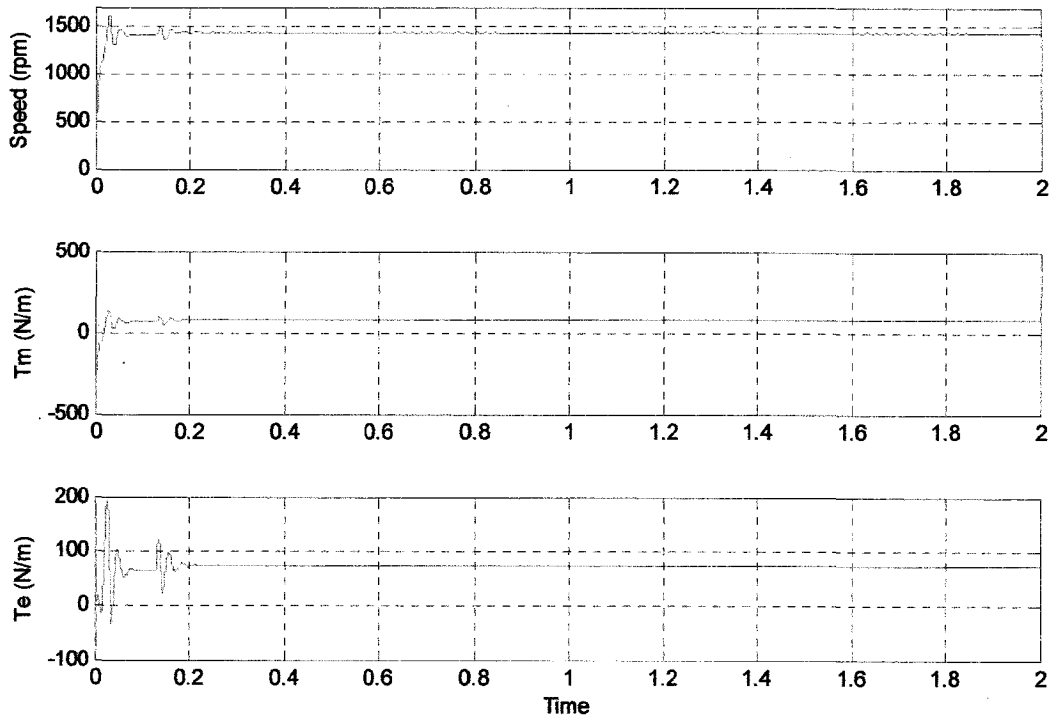


Fig5.29: The simulated wave forms of the speed, T_m and T_e with respect to time for sub synchronous mode of operation.

In fig 5.29 the simulated waveforms of speed, input mechanical torque and electromagnetic torque of the DFIG are shown for sub synchronous mode of operation. We can observe that the speed is below 1500 rpm in the top wave form in the above figure. And the waveforms of T_m and T_e for sub synchronous mode are positive.

5.5.4 Simulation RESULTS for both Sub and Super Synchronous mode DFIG using AC/DC/AC Back to back converter:

Both sub and super synchronous mode of operation of DFIG using Back to back AC/DC/AC converter topology in the rotor circuit for the integration of rotor and grid with vector control implementation

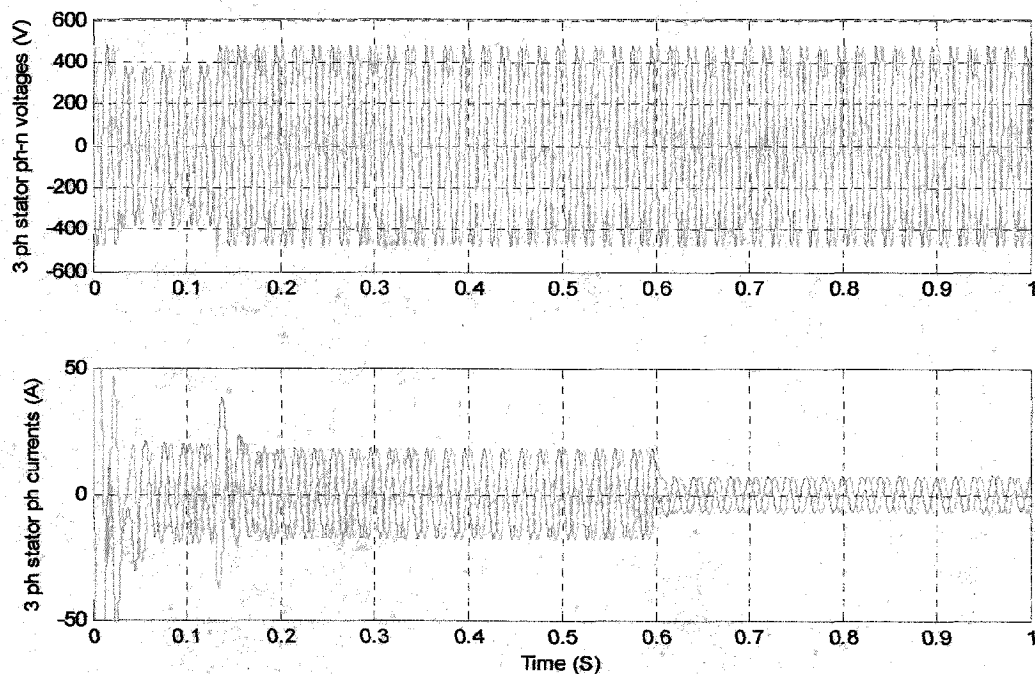


Fig5.30: The 3 Ph stator voltages (ph-n) and ph currents for both sub and super synchronous mode of operation of DFIG using AC/DC/AC converter topology for the rotor circuit.

In fig 5.30 the 3-ph stator line to neutral voltages and line currents are shown, these waveforms are simulated for both sub synchronous mode and super synchronous mode of operations of DFIG. We can observe from the waveform that the magnitude is not maintained constant throughout the simulation time. From time 0 sec to 0.6 sec the DFIG runs in sub synchronous mode and from 0.6 sec to 1 sec it runs in

super synchronous mode. We can observe the magnitude variation the both voltage and currents.

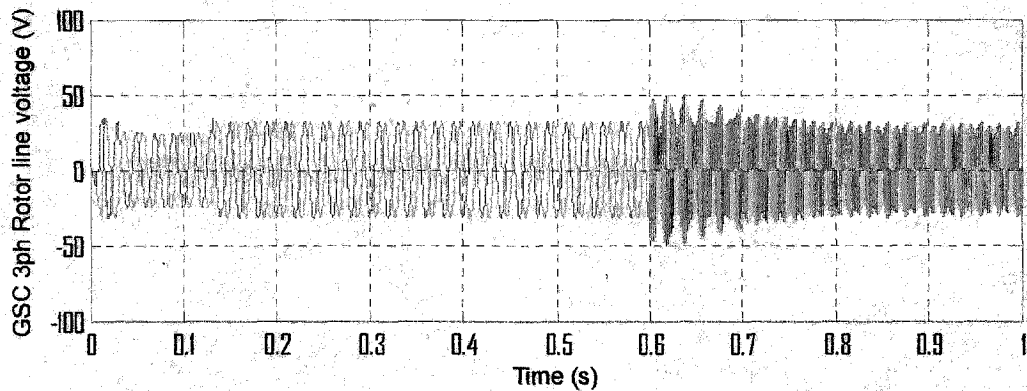


Fig5.31: 3 ph rotor line voltages at the grid side converter end for DFIG operating both in sub and super synchronous modes.

In fig 5.31 the 3-ph rotor line to line voltages at the GSC are shown, these waveforms are simulated for both sub synchronous mode and super synchronous mode of operations of DFIG. We can observe from the waveform that the shape is not maintained same throughout the simulation time. From time 0 sec to 0.6 sec the DFIG runs in sub synchronous mode and from 0.6 sec to 1 sec it runs in super synchronous mode. We can observe the GSC input is sinusoidal in sub synchronous mode and GSC output is square wave in super synchronous mode. But the frequency of both the wave forms is at 50Hz

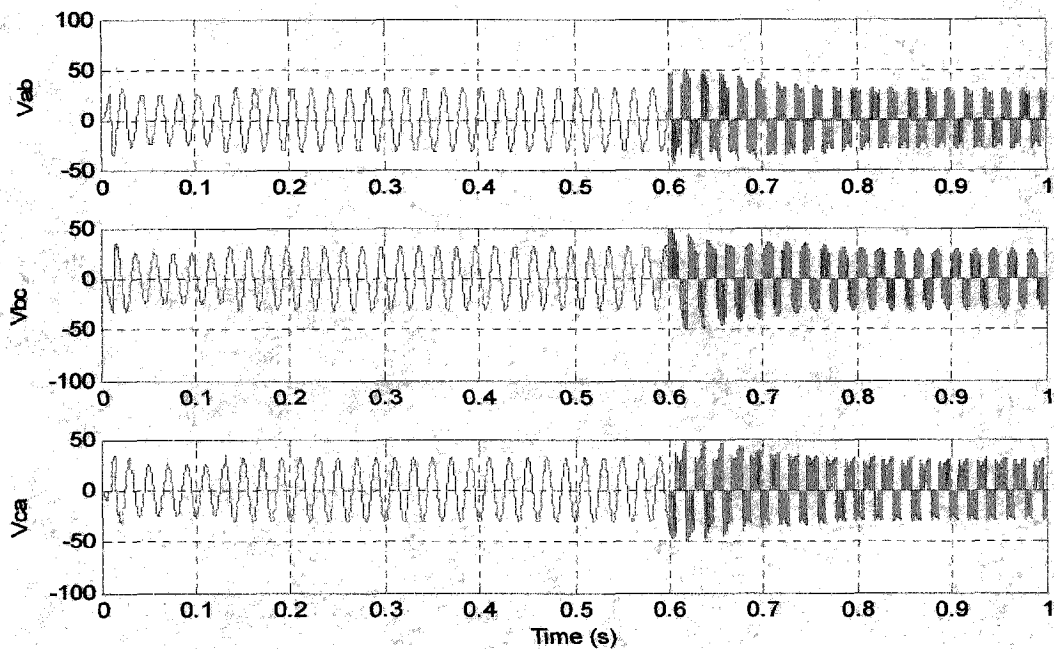


Fig5.32: single ph L-L rotor voltage wave forms at the grid side end of the converter for both the sub and super synchronous modes of operation of DFIG using AC/DC/AC converter topology for rotor circuit.

In fig 5.32 the single-ph rotor line to line voltages at the GSC are shown, these waveforms are simulated for both sub synchronous mode and super synchronous mode of operations of DFIG. We can observe from the waveform that the shape is not maintained same throughout the simulation time. From time 0 sec to 0.6 sec the DFIG runs in sub synchronous mode and from 0.6 sec to 1 sec it runs in super synchronous mode. We can observe the GSC input is sinusoidal in sub synchronous mode and GSC output is square wave in super synchronous mode. But the frequency of both the wave forms is at 50Hz

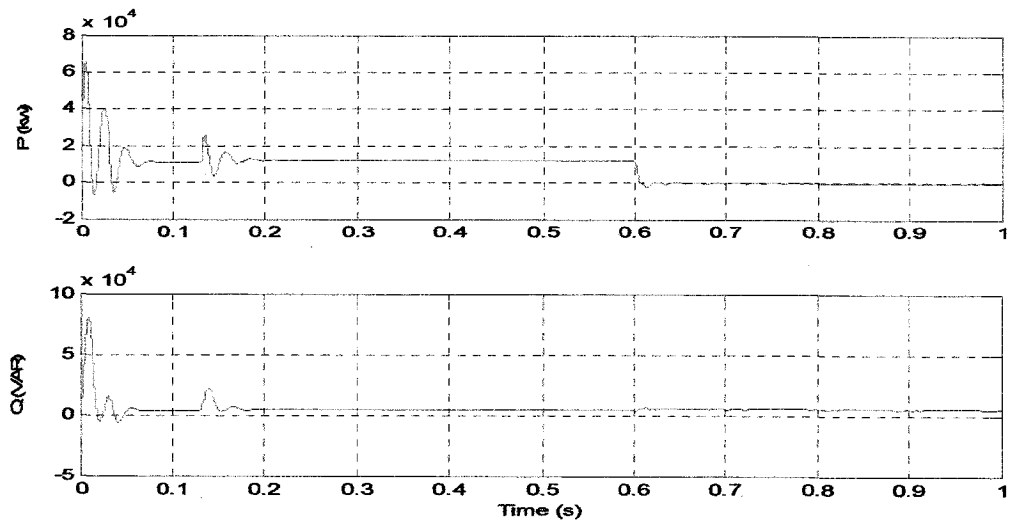


Fig5.33: The wave forms of real and reactive power of the DFIG for both sub and super synchronous modes of operation.

In fig 5.33 the simulated wave forms of real and reactive powers obtained from stator voltages and currents are shown. These waveforms are simulated for both sub synchronous mode and super synchronous mode of operations of DFIG, from time 0 sec to 0.6 sec the DFIG operates in sub synchronous mode and from 0.6 sec to 1 sec it operates in super synchronous mode.

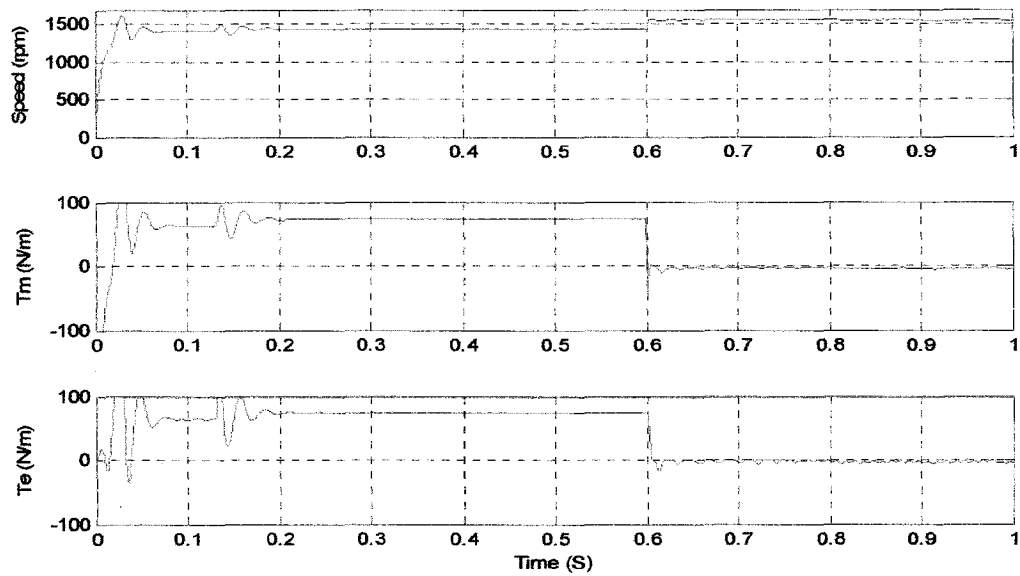


Fig5.34: The simulated wave forms of the speed, T_m and T_e with respect to time for both sub and super synchronous modes of operation of DFIG.

In fig 5.34 the simulated waveforms of speed, input mechanical torque and electromagnetic torque of the DFIG are shown for both sub-synchronous mode and super-synchronous mode of operations of DFIG, from time 0 sec to 0.6 sec the DFIG operates in sub synchronous mode and from 0.6 sec to 1 sec it operates in super synchronous mode. We can clearly observe the change in the magnitudes of the above wave forms after 0.6 sec. And the waveforms of T_m and T_e for sub synchronous mode are positive and for super synchronous mode they are negative.

5.5.5 The SIMULINK model for the DFIG using MATRIX converter:

A 5Hp, 575V, 4poles, 50Hz, 1500 rpm, star connected Wound Rotor Induction Machine (WRIM) is chosen in the MATLAB environment. The stator of the WRIM is connected to the grid. The AC-AC MATRIX converter is connected in the rotor circuit to integrate the rotor circuit with the grid. The machine operated in both sub and super synchronous modes to see that the power flow via converter setup is bi-directional. The VSI-VSR combination setup of MATRIX converter is controlled by the Space Vector Modulation (SVM) technique as explained in section 5.4. For to integration of Rotor to grid the Voltage and the Frequency should match the Grid Voltage and frequency, for this reason a coupling transformer (which boost the voltage level to the grid voltage) is connected and the frequency is maintained constant (50Hz) by the matrix converter. And also a star connected passive R-C filter is connected to eliminate the harmonics in the Voltage and current wave forms. The waveforms for all the voltages and currents, the machine performance characteristics, and the power flow indications waveforms are plotted in the SIMULINK and are presented in this section.

In fig 5.35 the DFIG can run both in sub synchronous mode and super synchronous mode, to make this possible the input mechanical torque is given in two steps with a timer circuit as mechanical input to the DFIG. The grid parameters are taken from MATLAB help file. The values of R and C in the filter circuit are 5 ohm and 5 microfarad respectively. The speed ranges are maintained as 1440rpm in sub synchronous mode and 1560 rpm in super synchronous mode.

The SIMULINK model for the DFIG using MATRIX converter in the rotor circuit for the integration to the grid

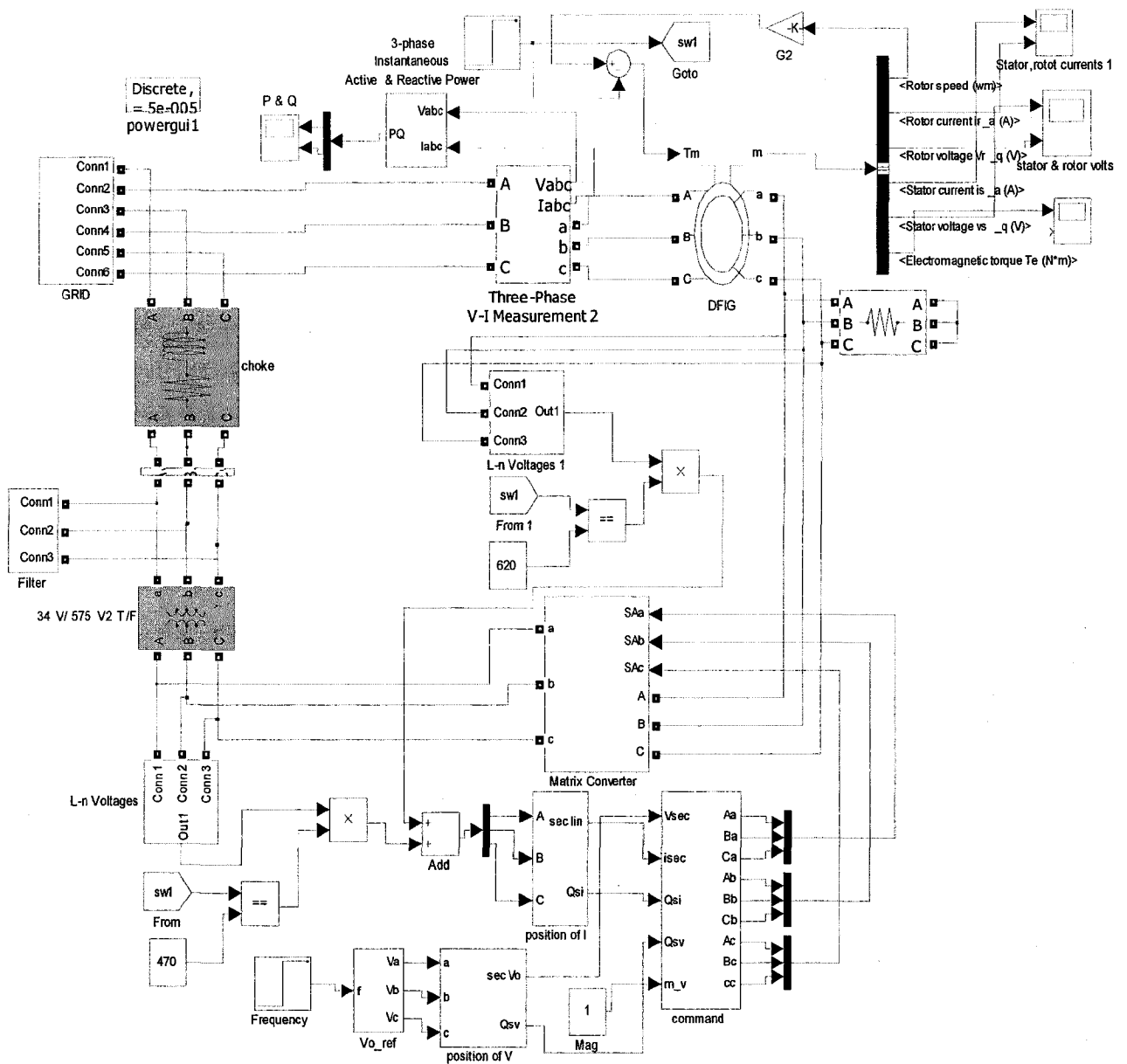


Fig5.35: The SIMULINK model for the DFIG using MATRIX converter in the rotor circuit for the integration to the grid, which operates in both the sub and super synchronous modes.

Super synchronous mode of operation of DFIG using MATRIX converter topology in the rotor circuit for the integration of rotor and grid:

5.5.6 Simulation RESULTS for Super synchronous mode DFIG using MATRIX converter:

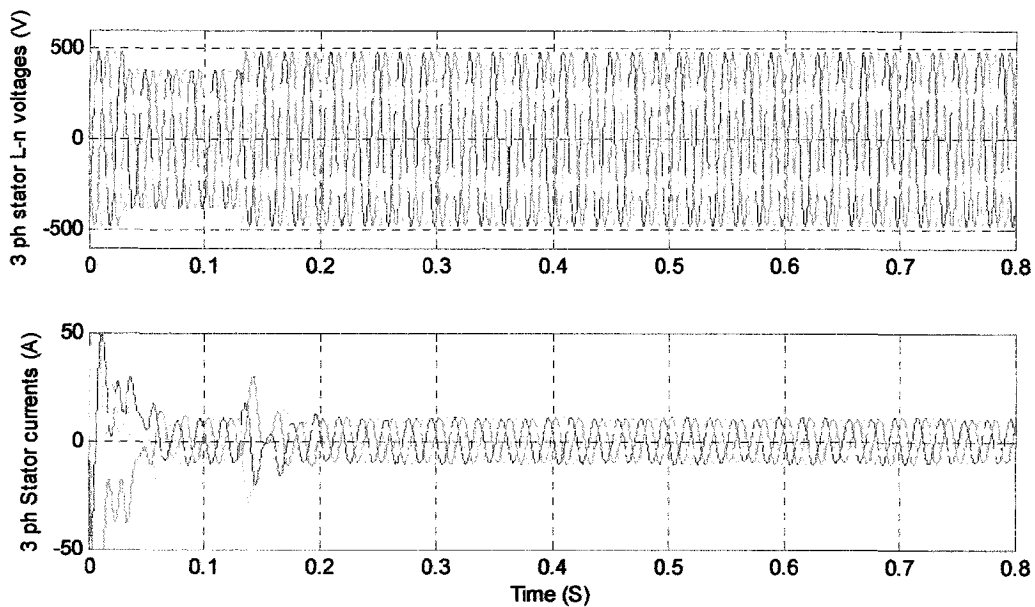


Fig5.36: 3 ph stator L-n voltages and ph currents for the super synchronous mode of operation for DFIG using MATRIX converter topology.

In figs 5.36 the 3-ph stator line to neutral voltages and line currents are shown, these waveforms are for super synchronous mode of operation of DFIG, where the speed of DFIG is above the synchronous speed. We can observe from the waveform that the magnitude is maintained constant throughout the simulation time.

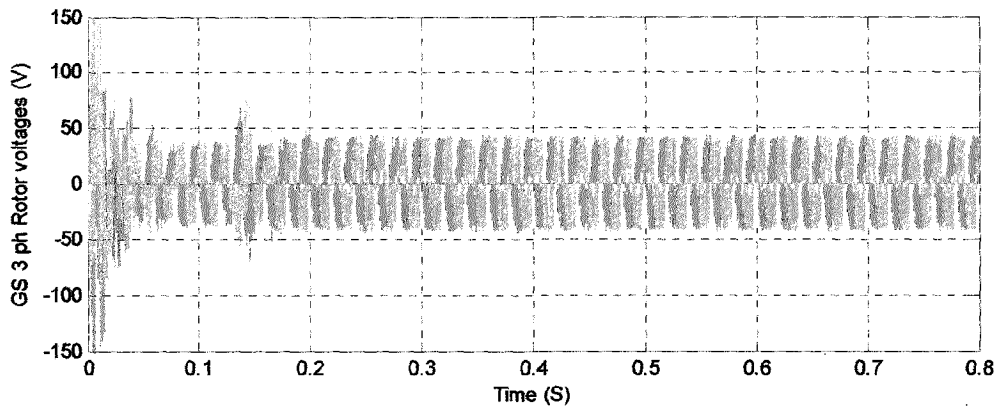


Fig5.37: 3 ph rotor L-n voltages for the super synchronous mode of operation for DFIG using MATRIX converter topology.

In fig 5.37 the simulated wave form of the 3 ph rotor line voltages at the output of MATRIX converter are shown. In the above wave form we can observe the line to line voltage of rotor is becoming constant in magnitude after 0.15 sec of simulation time. This voltage is given to the coupling transformer and thus boosted up to the grid voltage level i.e, 575 V RMS line to line, whereas the frequency of the output voltages of MATRIX converter is exactly 50Hz. This above waveform is simulated in super synchronous mode of operation for DFIG.

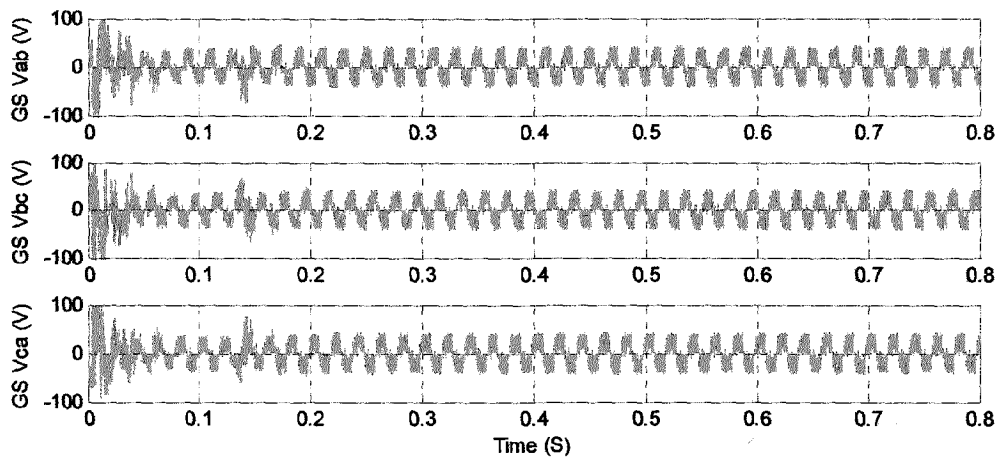


Fig5.38: single ph L-L rotor voltage wave forms at the grid side end of the converter for the super synchronous mode of operation of DFIG using MATRIX converter topology for rotor circuit.

In fig 5.38 the simulated wave form of the single ph rotor line voltages at the output of MATRIX converter are shown. In the above wave forms we can observe the line to line voltage of rotor is becoming constant in magnitude after 0.15 sec of simulation time, the frequency of the output voltages of MATRIX converter is exactly 50Hz. This above waveform is simulated in super synchronous mode of operation for DFIG.

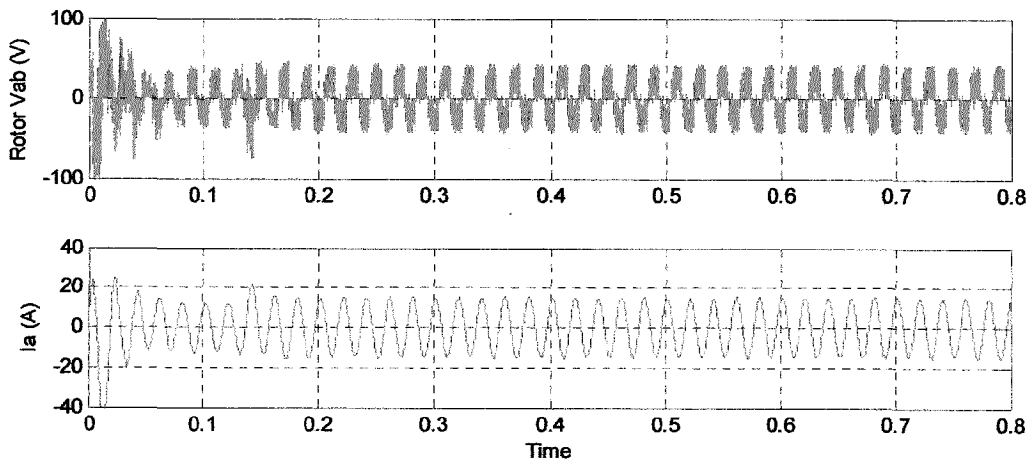


Fig5.39: The single ph rotor voltage (Ph-n) and line current wave forms for the super synchronous mode of operation of DFIG using MATRIX converter topology.

In fig 5.39 the simulated wave form of the single ph rotor line voltage and line current at the output of MATRIX converter are shown. The frequency of the output voltages and current of MATRIX converter is exactly 50Hz. This above waveform is simulated in super synchronous mode of operation for DFIG

5.5.7 Simulation RESULTS for Sub synchronous mode DFIG using MATRIX converter:

Sub synchronous mode of operation of DFIG using MATRIX converter topology in the rotor circuit for the integration of rotor and grid

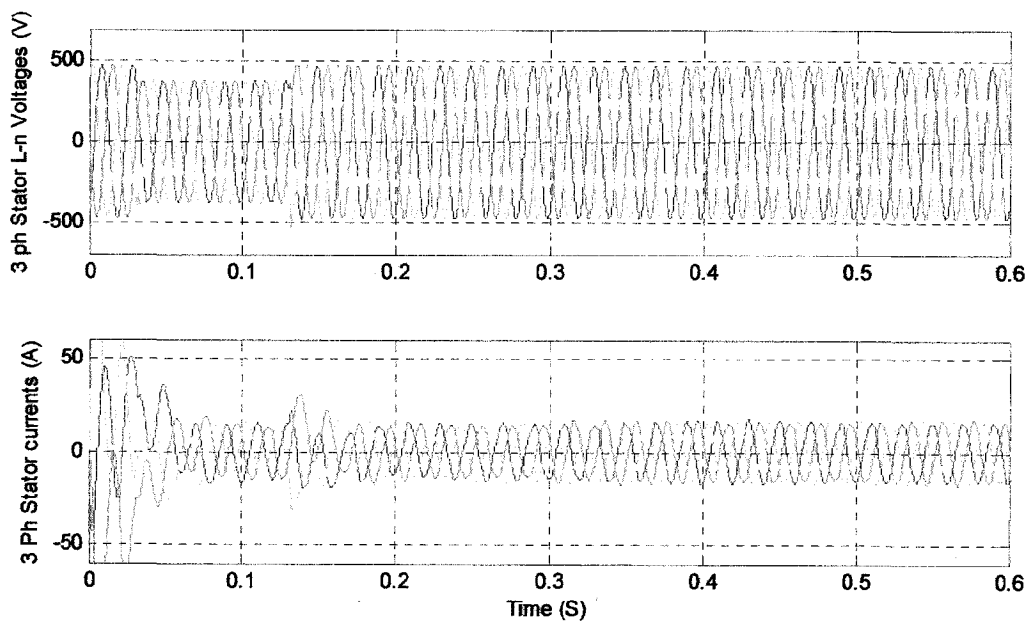


Fig5.40: 3 ph stator ph-n voltages and ph currents for the sub synchronous mode of operation for DFIG using MATRIX converter topology.

In figs 5.40 the 3-ph stator line to neutral voltages and line currents are shown, these waveforms are for sub synchronous mode of operation of DFIG, where the speed of DFIG is below the synchronous speed. We can observe from the waveform that the magnitude is maintained constant throughout the simulation time.

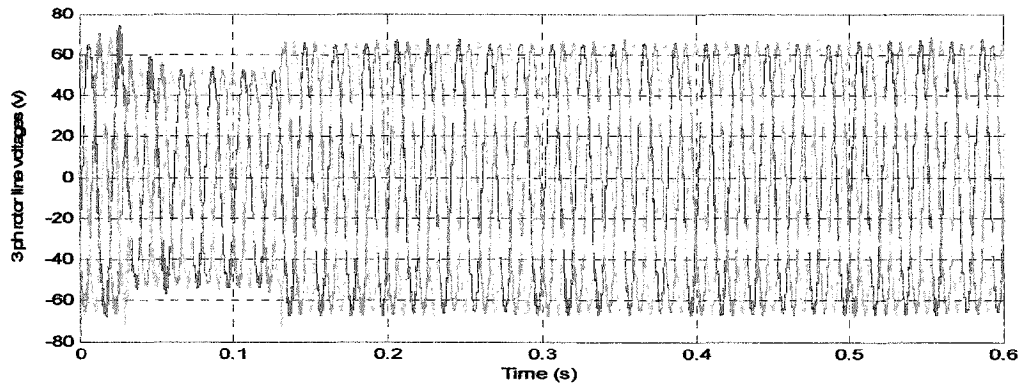


Fig5.41: The 3 Ph rotor line voltages at the grid side end of the converter.

In fig 5.41 the simulated wave form of the 3 ph rotor line voltages at the grid side end of MATRIX converter are shown. In the above wave form we can observe the line to line voltages of rotor are constant throughout the simulation time. This above waveform is simulated in sub synchronous mode of operation for DFIG.

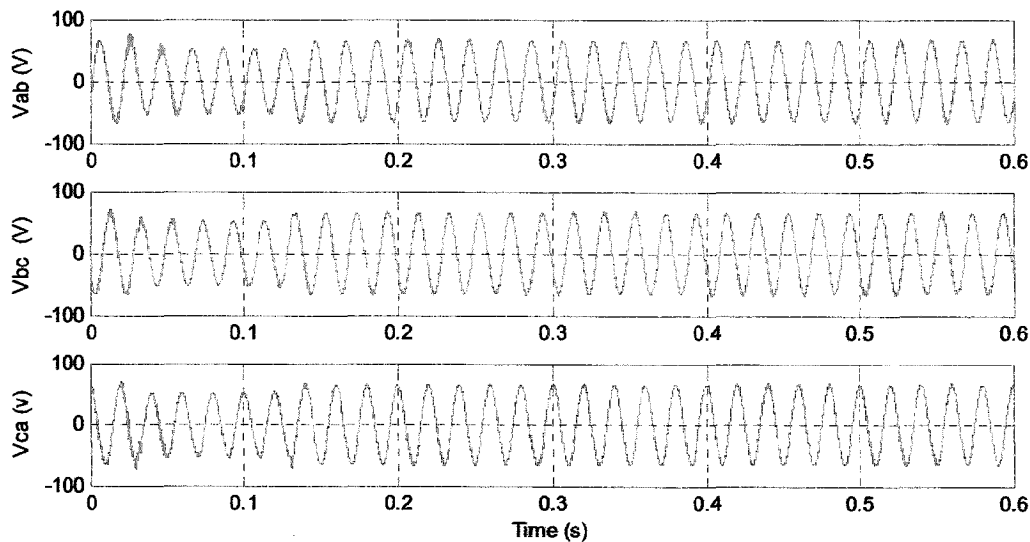


Fig5.42: single ph L-L rotor voltage wave forms at the grid side end of the converter for the sub synchronous mode of operation of DFIG using MATRIX converter topology for rotor circuit.

In fig 5.42 the simulated wave form of the single ph rotor line voltages at the grid side end of MATRIX converter are shown. In the above wave form we can observe the line to line voltage of rotor is constant throughout the simulation time. This above waveform is simulated in sub synchronous mode of operation for DFIG.

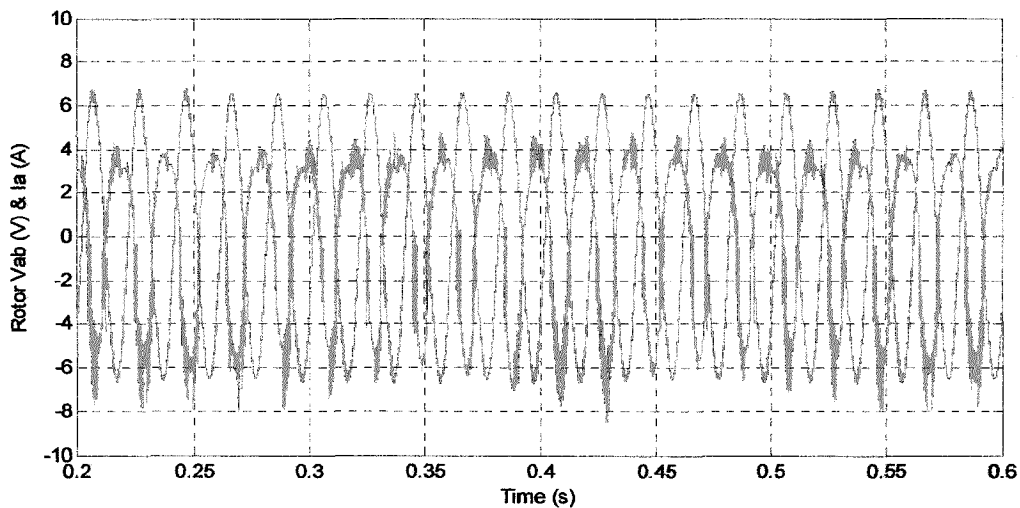


Fig5.43: The wave forms of rotor line voltage and line current at the grid side of the MATRIX converter.

In fig5.43 the line to line voltage and current waveforms of the rotor at GS of MATRIX converter is shown. These wave forms are adjusted in the magnitude to see the voltage and current on the same scale. The green coloured wave form is current and red coloured wave form is voltage. From the voltage and current are in out of phase and it is clear that power is flowing from the grid to rotor, since it the DFIG is operating in sub synchronous mode.

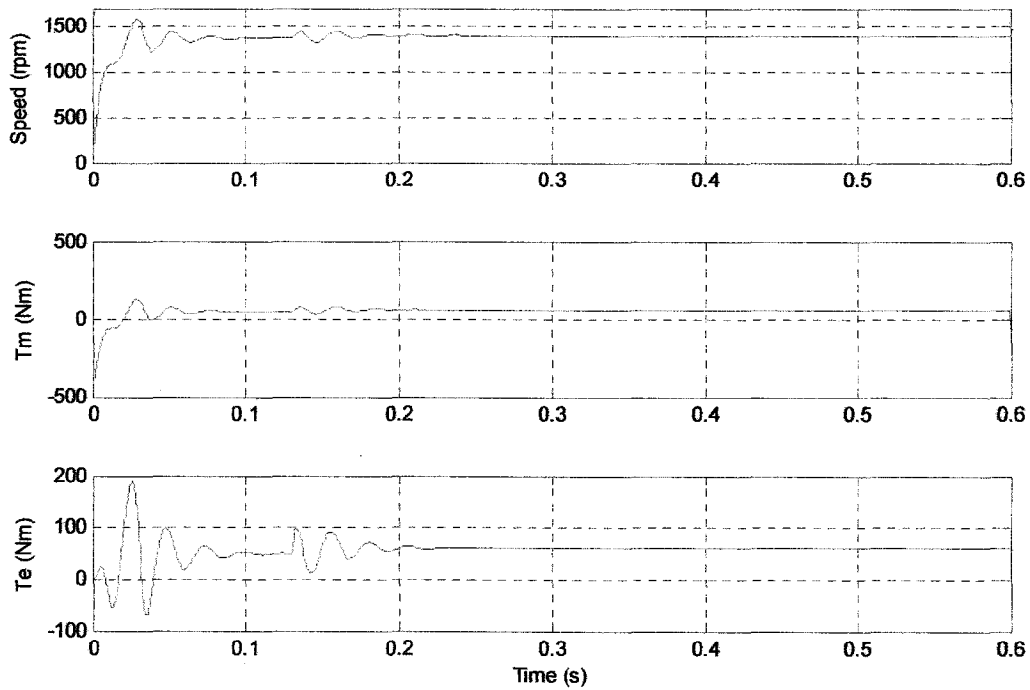


Fig5.44: The simulated wave forms of the speed, T_m and T_e with respect to time for sub synchronous mode of operation

In fig 5.44 the simulated waveforms of speed, input mechanical torque and electromagnetic torque of the DFIG are shown for sub synchronous mode of operation. We can observe that the speed is below 1500 rpm in the top wave form in the above figure. And the waveforms of T_m and T_e for sub synchronous mode are positive.

5.5.8 Simulation RESULTS for both Sub and Super synchronous mode DFIG using MATRIX converter:

Both sub and super synchronous modes of operation of DFIG using MATRIX converter topology in the rotor circuit for the integration of rotor and grid

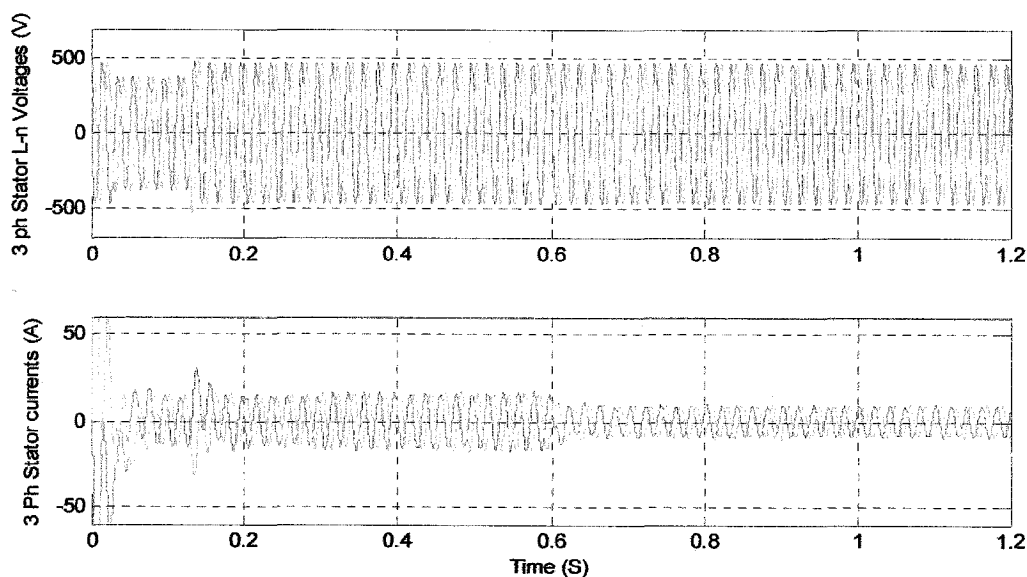


Fig5.45: The 3 Ph stator voltages (ph-n) and ph currents for both sub and super synchronous mode of operation of DFIG using MATRIX converter topology for the rotor circuit.

In figs 5.45 the 3-ph stator line to neutral voltages and line currents are shown, these waveforms are for both sub synchronous and super synchronous mode of operations of DFIG, from time 0 sec to 0.6 sec the DFIG runs in sub synchronous mode and from 0.6 sec to 1.2 sec it runs in super synchronous mode.

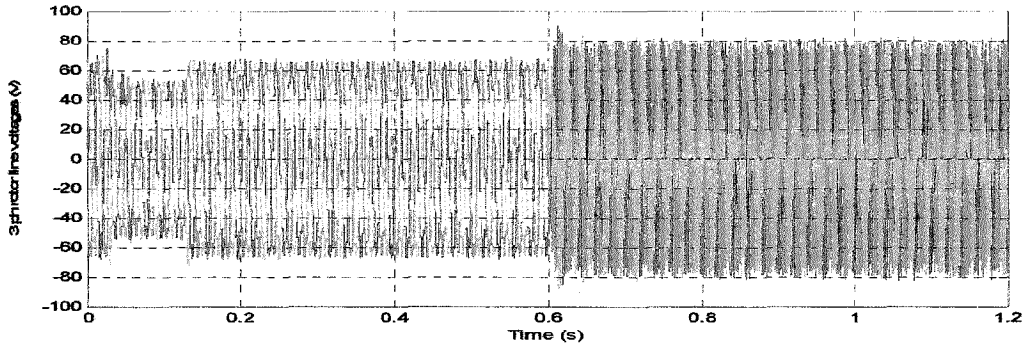


Fig5.46: 3 ph rotor line voltages at the grid side end of Matrix converter for DFIG operating both in sub and super synchronous modes.

In fig 5.46 the 3-ph rotor line to line voltages at the grid side end of the Matrix converter are shown, these waveforms are simulated for both sub synchronous mode and super synchronous mode of operations of DFIG. We can observe from the waveform that the shape is not maintained same throughout the simulation time. From time 0 sec to 0.6 sec the DFIG runs in sub synchronous mode and from 0.6 sec to 1.2 sec it runs in super synchronous mode. We can observe that grid side input is sinusoidal in sub synchronous mode and grid side output is square wave in super synchronous mode. But the frequency of both the wave forms is at 50Hz

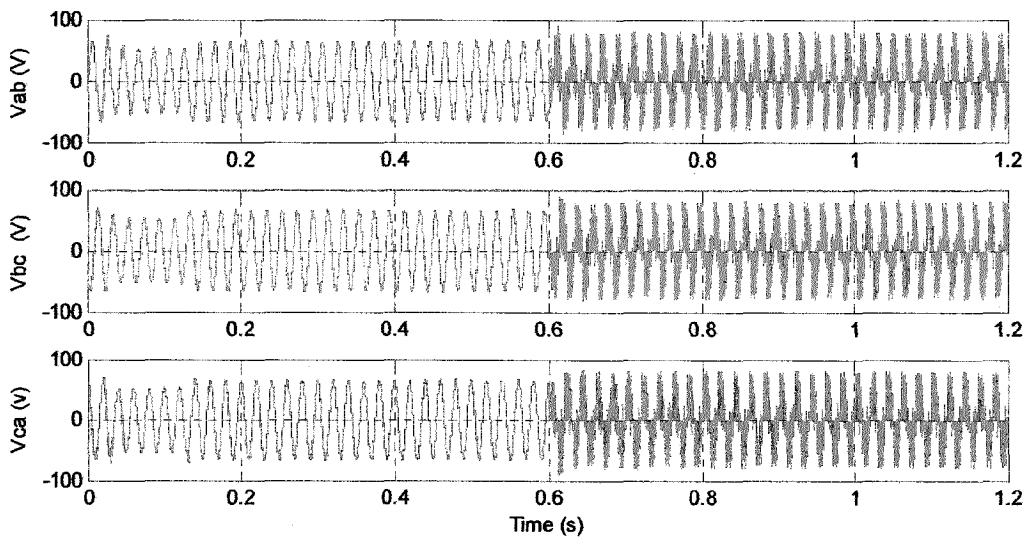


Fig5.47: single ph L-L rotor voltage wave forms at the grid side end of the converter for both the sub and super synchronous modes of operation of DFIG using MATRIX converter topology for rotor circuit.

In fig 5.47 the single ph rotor line to line voltages at the grid side end of the Matrix converter are shown, these waveforms are simulated for both sub synchronous mode and super synchronous mode of operations of DFIG. We can observe from the waveform that the shape is not maintained same throughout the simulation time. From time 0 sec to 0.6 sec the DFIG runs in sub synchronous mode and from 0.6 sec to 1.2 sec it runs in super synchronous mode. We can observe that grid side input is sinusoidal in sub synchronous mode and grid side output is square wave in super synchronous mode. But the frequency of both the wave forms is at 50Hz

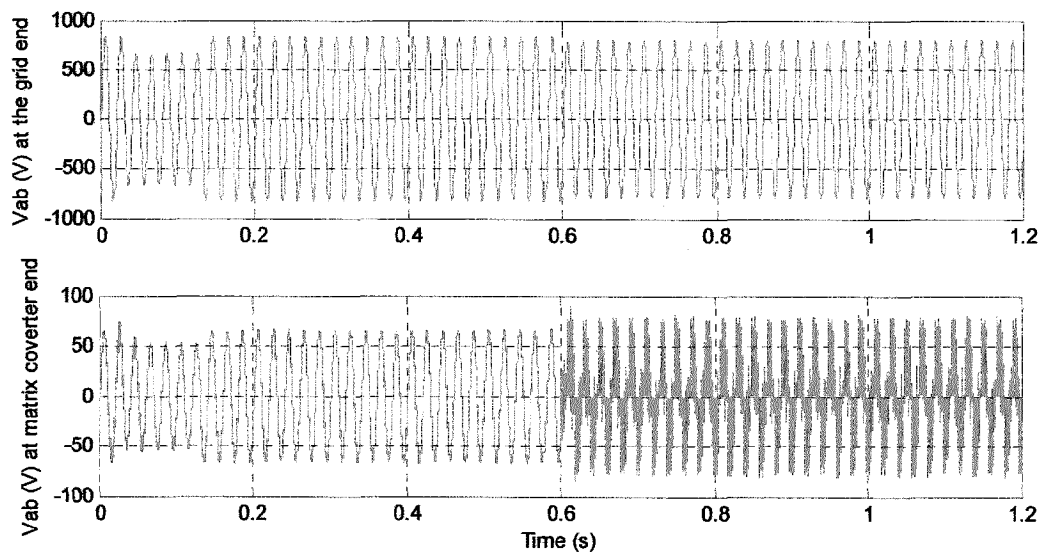


Fig5.48: The comparison of the rotor line voltages before and after T/F for both sub and super synchronous modes of operation

In fig48 the lower wave form is single ph line to line voltage at the grid side end of the Matrix converter and the upper waveform is single ph line to line voltage at the grid. The DFIG operates in sub synchronous mode from 0 sec to 0.6 sec and from 0.6 sec to 1.2 sec it operates in super synchronous mode.

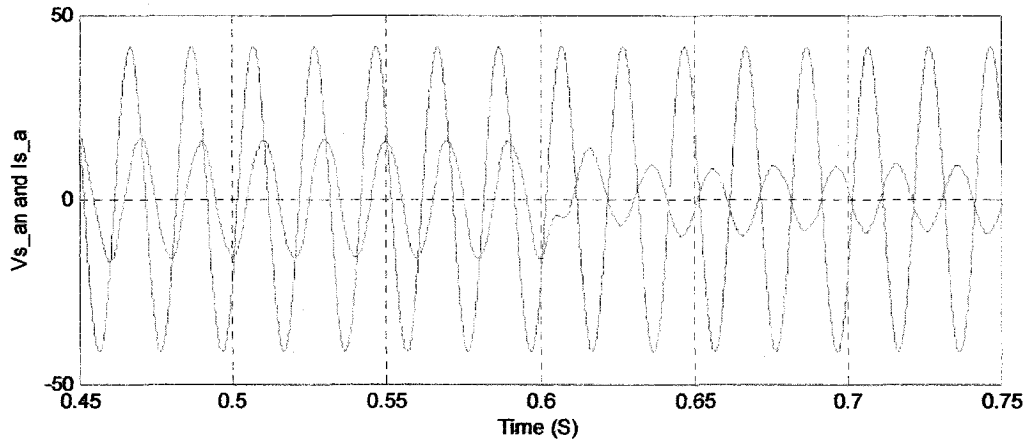


Fig5.49: The expanded wave form of stator voltage (Ph-n) and ph-current (magnitude adjusted for visibility) for both the sub and super synchronous modes of operation.

In fig5.49 the voltage and current wave forms of the stator are shown. The magnitudes of them are adjusted to see them on the same scale. From the wave form it clear that the net power is flowing from the stator to grid, but the amount of power flowing differs in the two following cases i.e, From time 0 sec to 0.6 sec the DFIG operates in sub synchronous mode and from 0.6 sec to 1.2 sec it operates in super synchronous mode.

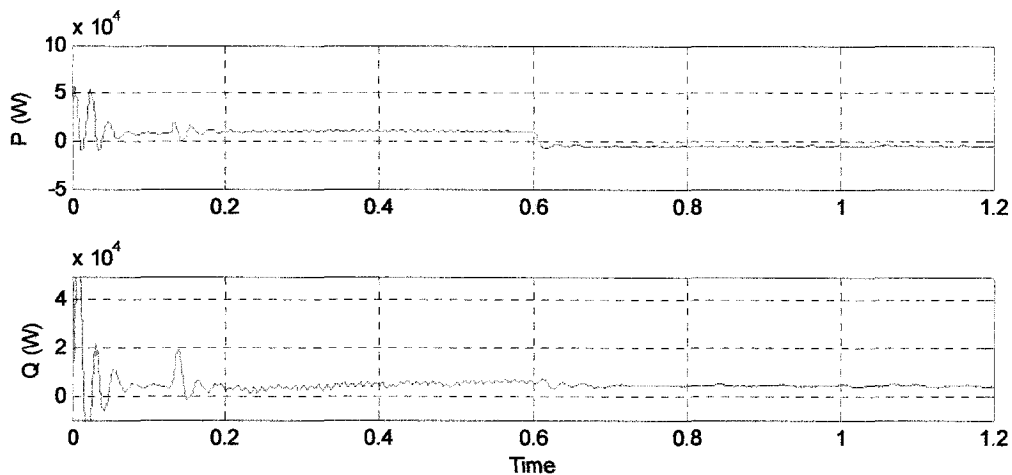


Fig5.50: The wave forms of real and reactive power of the DFIG (using MATRIX converter topology) for both sub and super synchronous modes of operation.

In fig 5.50 the simulated wave forms of real and reactive powers obtained from stator voltages and currents are shown. These waveforms are simulated for both sub synchronous mode and super synchronous mode of operations of DFIG, from time 0 sec to 0.6 sec the DFIG operates in sub synchronous mode and from 0.6 sec to 1.2 sec it operates in super synchronous mode.

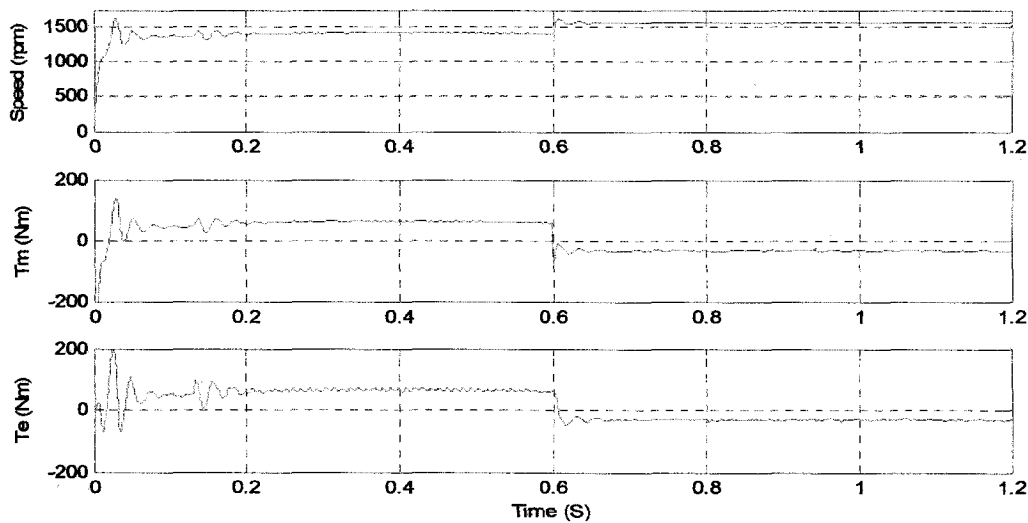


Fig5.51: The simulated wave forms of the speed, T_m and T_e with respect to time for both sub and super synchronous modes of operation of DFIG.

In fig 5.51 the simulated waveforms of speed, input mechanical torque and electromagnetic torque of the DFIG are shown for both sub synchronous and super synchronous mode of operations. From time 0 sec to 0.6 sec the DFIG operates in sub synchronous mode and from 0.6 sec to 1.2 sec it operates in super synchronous mode. We can observe in the top waveform that the speed is below 1500rpm in sub synchronous mode of operation and it is above 1500rpm in super synchronous mode of operation. And the waveforms of T_m and T_e for sub synchronous mode are positive and for super synchronous mode they are negative.

6.1 Conclusions:

Induction machine using as a generator coupled with a wind turbine is an interesting area for the Electrical Engineers, where the controlling of Induction Generator over a wide range of speed is the major concern. The reactive power consumption and harnessing of active power under varying speed are the major concerns to deal with the induction generators; however the development of static power converters has facilitated the control of the variable speed induction generators.

In the present work both Cage rotor and wound rotor induction generators are considered.

For a Squirrel Cage Induction machine to run as SEIG needs a variable reactive power to sustain the excitation and to maintain a constant terminal voltage level. In order to do this a fixed capacitor or a mechanically switched capacitor is not a feasible option. So, in the present work, a FUZZY Logic controller based FC-TCR (in delta connection) is modeled in SIMULINK to sustain the process of self excitation and terminal voltage regulation of SEIG for the variable R-load and RL-load ($\cos\phi=0.8$), which can vary from no load to full load. The FUZZY controller is designed to control the delay firing angle ' α ' of FC-TCR circuit by taking inputs as 'error in terminal voltage' and 'change in line currents'. This system is modeled for a constant speed application. The simulated performance waveforms of SEIG are analyzed for the developed model and results are found to be satisfactory.

Further, considering WRIG's, the Converter topologies to interface the rotor circuit with the grid is the major concerns to deal with the Converter topologies. So, the converter topologies for the rotor circuit of the DFIG are discussed and the same are modeled in simulink. The AC/DC/AC back to back IGBT converter topology for the rotor circuit is modeled. In this GSC is controlled by SVM technique and RSC is controlled by sinusoidal PWM technique. And the MATRIX converter

topology is also modeled and controlled by using SVM technique. The stator of the DFIG is connected to the grid and the rotor is integrated with the grid via these converter setups and a coupling Transformer. The machine is operated in both sub and super synchronous modes of speeds and ensures that the power flow via converter setup is bi-directional. The wave forms for all the voltages and currents and the machine performance characteristics, and the power flow indications are plotted in the SIMULINK and results are found to be satisfactory.

6.2 Future Scope:

The real time implementation of FC-TCR circuit, generation of delay firing pulses for it in real time is also an interesting work to extend, And also design of controller for controlling the delay firing pulses, as to control the capacitive reactance continuously, in turn to maintain a constant terminal voltage for load variations and speed variations within the generating range of SEIG.

Further, the real time implementation of converter topologies and controlling strategies for same is also an alluring area to extend the present work. And also making power factor unity in case of DFIG will extend the present work in developing active filters. The same work on DFIG can be extended in developing a controller for variable prime mover such that the DFIG can operate in both sub and super synchronous modes.

Appendix

FC-TCR design:

$$C=38.5\mu\text{F} \quad \text{and} \quad L = 0.34\text{H}$$

Fixed Capacitor:

$$C=38.5\mu\text{F}$$

Prime mover design for SEIG:

$$T_m = -A + (B * \omega_m)$$

$$A=578 \quad B=3.5$$

Filter Design:

$$C=5 \mu\text{F} \quad \text{and} \quad R=5 \text{ ohm}$$

Prime mover design for DFIG:

$$T_m = -A + (B * \omega_m)$$

$$A= 470 \ 590 \ \text{and} \ 620 \quad B=3.6$$

REFERENCES

Journals and conferences:

- [1] Lahcene Quazene and George McPherson " Analysis of The Isolated Induction Generator", IEEE Trans. on Power Apparatus and Systems, Vol.PAS-102, No.8, pp.2793-2798, August, 1983.
- [2] N.H.Malik and S.E.Haque "Steady-state Analysis and Performance of An Isolated Self-Excited Induction Generator", IEEE Trans. on Energy Conversion, Vol.EC-1, No.3 pp.134-139, September, 1986.
- [3] A.K.Aljabri and A.I.Alolah, "Capacitance Requirement for Isolated Self- Excited Induction Generator", IEE Proceedings, part B, Vol.137, No.3, pp.154-159, May, 1990.
- [4] L.Shridhar, B.P.Singh and C.S.Jha," A Step Towards Improvements in The Characteristics of Self-Excited Induction Generator", IEEE Trans. On Energy Conversion, Vol.8, No.1, pp.40-46, March, 1993.
- [5] S.P.Singh, M.P.Jain and Bhim Singh, "A New Technique for Analysis of Self-Excited Induction Generator", Electric Machine and Power Systems, Vol.23, pp.647-656, 1995.
- [6] E.D. Basset and F.M. Potter, Capacitive excitation for induction generator. *AIEE Trans. (Elect. Eng.)* (1935), pp. 540-545.
- [7] C.F. Wagner, Self excitation of induction motors. *AIEE Trans. (Elect. Eng.)* (1939), pp. 47-51
- [8] J.E. Barkle and R.W. Ferguson, Induction generator theory and application. *AIEE Trans. (Elect. Eng.)* (1954), pp. 12-19
- [9] T. Ahmed, K. Nishida, and M. Nakaoka, "Static VAR compensator based voltage regulator of single phase selfexcited induction generator" IEEE Industry Application Conference 2004, vol. 3, Oct. 2004, pp 2069-2076.
- [10] Bhim Singh, S.S. Murthy, and Sushma Gupta, "Modeling and analysis of STATCOM based voltage regulator for selfexcited induction generator with unbalanced loads", in IEEE Conf TENCON 2003, Bangalore, pp. 1109-1114.
- [11] Bhim Singh, S.S. Murthy, and Sushma Gupta "STATCOM based voltage regulator for self excited induction generator feeding nonlinear loads," in IEEE Conf IECON, 2003, USA, pp. 2741-2746.
- [12] Bhim Singh, S.S. Murthy, and Sushma Gupta, "Analysis and design of STATCOM based regulator for self excited induction generator," IEEE Trans. on Energy Conversion, vol. 19, no. 4, pp. 783-790, Dec. 2004.
- [13] Bhim Singh, S.S. Murthy, and Sushma Gupta, "STATCOM based voltage regulator for self excited induction generator feeding nonlinear loads," IEEE Trans. on Industrial Electronics, vol. 53,no. 5, pp 1437-1452, Oct. 2006.

- [14]Tarek Ahmed, Osamu Noro and Mutsuo Nakaoka: "PI Closed-Loop Feedback Terminal Voltage Control Scheme based on Static VAR Compensator for Three Phase Self-Excited Induction Generator", *IEEJ Trans. PE*, Vol. 124, No. 4, pp.569-581 (2004)
- [15]LEONHARD, W.: 'Control of electrical drives' (Springer Verlag, 1985)
- [16]SMITH, G.A., and MIGIM, K.A.: 'Wind-energy recovery by a static Scherbius induction generator', *IEE Proc. C*, 1981,
- [17] R. C. Bansal, "Three-Phase Self-Excited Induction Generators: An Overview" *IEEE TRANSACTIONS ON ENERGY CONVERSION*, VOL. 20, NO. 2, JUNE 2005
- [18] S. M. Salameh and L. F. Kazda, "Analysis of the steady state performance of the double output induction generators," *IEEE Trans. EnergyConvers.*, vol. EC-1, pp. 26-32, 1986.
- [19]R. S. Pena, G.M.Asher, and J. C. Clare, "A doubly fed induction generator using back-to-back PWM converters supplying an isolated load from a variable speed wind turbine," *Inst. Electr. Eng. Proc.-Elect. Power Appl.*, vol. 143, no. 5, pp. 380-387, Sep. 1996.
- [20]G. Saccomando and J. Svensson, "Control and operation of grid-connected voltage source converter under grid disturbances in variable- speed wind turbines," in *Proc European Wind Energy Conf.*, Copenhagen, Denmark, Jul. 2001.
- [21]Yamamoto, M., Motoyoshi, O. (1991). *Active and reactive power control for doubly-fed wound rotor induction generator*, *IEEE Transactions on Power Electronics* Vol. 6. No. 4 pp. 624-629.
- [23]M.B.Mohamed, M.Jemli, M.Gossa, K.Jemli, "Doubly Fed Induction Generator (DFIG) in wind turbine. Modelling and power flow control", *IEEE International Conference on Industrial Technology (ICIT)*, December 2004, Vol.2, pages 580
- [24]K. Ghedamsi, D. Aouzellag and E.M. Berkouk, Control of wind generator associated to a flywheel energy storage system, *Renew Energy J* **33** (2008), pp. 2145-2156
- [25]M. Venturini, "A new sine wave in sine wave out conversion technique which eliminates reactive elements," *Proc. of POWERCON 7*, E3, 1980, pp. 1-15
- [26]M. Venturini and A. Alisina, "The generalized transformer: A new bidirectional sinusoidal waveform frequency converter with continuously adjustable input power factor," *Proc. of IEEE PESC80*, 1980, pp. 242-252.
- [27]H. W. Van der Broeck and H. C. Skudelny, "Analysis and realization of a pulse width modulator based on voltage space vectors," *IEEE Trans. Industry applications*, Vol 24 jan-feb 1988.
- [28]Guo Yougui, Zhu Jianlin and Deng Cheng, "Three Modulation Modes of SVM for AC-AC Matrix Converter"., *IEEE Conference on Robotics, Automation and Mechatronics (RAM08)*, IEEE Press, Sept. 2008, pp.382-386, doi: 10.1109/RAMECH.2008.4681466.

- [29]S.Muller , M.Deicke And Rik W.De Doncker , “Doubly Fed Induction Generator System For Wind Turbines” , IEEE Industrial Applications Magazine. May/June 2002, pp. 26-33.
- [30]J. A. Baroudi ,V . Dinavahi and A. M. Knight , “A Review Of Power Converter Topologies For Wind Generators ”, Electrical Machines And Drives, 2005 IEEE Conference, pp 458 – 465.
- [31]P. Wheeler, J. Rodriguez, J. Clare, L. Empringham and A. Weinstein, “Matrix Converters: A technology review”, *IEEE Transactions on industrial Electronics*, 49, pp. 276-288, 2002b
- [32]L. Huber and D. Borojevic, “Space vector modulated three-phase to three-phase Matrix converter with input power factor correction”, *IEEE Trans. on Industrial Electronics*, 31, pp. 1234-1246, 1995.
- [33]Domenico Casadei, Giovanni Serra, Angelo Tani, and Luca Zarri, “Matrix Converter Modulation Strategies: A New General Approach Based on Space-Vector Representation of the Switch State,” *IEEE Transactions on Industrial Electronics*, vol. 49, no. 2, April 2002, pp. 370-381
- [30] Deepak Saini “Performance evaluation of variable speed self excited induction generator” A project report of Master of technology.
- [31] S. S. Murthy, O. P. Malik, and A.K.Tandon, “Analysis of selfexcited induction generators,” *Proc. IEE*, vol. 129, pt. C, no. 6, 1982, pp. 260-265.
- [33]M. S. Vicatos and J. A. Teqopoulos, “Steady state analysis of a doubly-fed induction generator under synchronous operation,” *IEEE Trans. Energy Convers.*, vol. 4, no. 3, pp. 495–501, Sep. 1989.
- [34]S.P. Singh, B. Singh and M.P. Jain, “Performance characteristics and optimal utilization of a cage machine as capacitor excited induction generator”, *IEEE Trans. on EC*, Vol. 5, No. 4, 1990, pp. 679-685
- [35]A. K. Al-Jabri and A.I. Alolah, “Limits on the performance of the three-phase self-excited induction generators”, *IEEE Trans. on EC*, Vol. 5, No. 2, 1990, pp. 350-356.
- [37]R. C. Bansal, T. S. Bhatti, and D. P. Kothari, “A bibliographical survey on induction generators for application of nonconventional energy systems,” *IEEE Trans. Energy Convers.*, vol. 18, no. 3, pp. 433–439, Sep. 2003.
- [39]M. Ors, “Voltage control of a self-excited induction generator,” in *Proc. IEEE Int. Conf. Automation, Quality and Testing, Robotics*, Cluj-Napoca, Romania, Vol. 3, pp. 281-286, May 22-25, 2008.
- [40]P. Wheeler, J. Rodriguez, J. Clare, L. Empringham and A. Weinstein, “Matrix Converters: A technology review”, *IEEE Transactions on industrial Electronics*, 49, pp. 276-288, 2002b.
- [41]L. Huber, D. Borojevic and N. Burany, “Voltage Space vector based PWM control of forced commutated cycloconverters”, in *proc. IEEE IECON’89*, 1989, pp. 106-111.

BOOKS and Materials:

- [42]Macro Matteini. “Control Techniques for Matrix Converter adjustable speed drive.” Phd thesis, 1998-2001,
- [43]Dheeraj Kumar Palwalia “Analysis and Control of standalone Generator” Phd thesis Oct 2009, IITR.
- [44]Mukund R. Patel “Wind and Solar Power Systems”, CRC Press

- [45]Thomas Ackermann “Wind Power in Power Systems”, Royal Institute of Technology Stockholm, Sweden, John Wiley & Sons, Ltd,
- [46]N. G. Hingorani and L. Gyugyi, *Understanding FACTS*, IEEE Press, Indian Edition 2001. Mohamed E. El-Hawary,
- [47]R.Mohan Mathur, Rajiv K. Varma THYRISTOR-BASEDFACTS CONTROLLERS FOR ELECTRICAL TRANSMISSION SYSTEMS. *Series Editor. IEEE press*
- [48]Bose.B.K, “*Modern power electronics and AC Drives*”, Prentice Hall, 2002.
- [49]Muhammad H,Rashid, “*Power Electronics Circuits, Devices and Applications*” , Pearson Eductaion, third Edition,2004.
- [50]Matlab 7.6.0 (R2008a) and Simulink, 2008 version.
- [51]Abir Chatterjee, “Performance Investigation of Matrix Converter Fed Induction Motor Drive” dissertation thesis, june 2009 IITR

Papers selected for Conferences

[1]Tirakala Upendra, S.P.Singh, S.Ghatak Choudhuri. "FC-TCR based Voltage Regulation of SEIG". International Conference on Electrical Power and Energy Systems.2010